JAERI-M
84-085

REPORT OF THE JOINT SEMINAR ON HEAVY-ION NUCLEAR PHYSICS AND NUCLEAR CHEMISTRY IN THE ENERGY REGION OF TANDEM ACCELERATORS

May 1984

Department of Physics

日 本 原 子 力 研 究 所
Japan Atomic Energy Research Institute

JAERI-M レポートは，日本原子力研究所が不定期に公刊している研究報告書です。
入手の問合わせは，日本原子力研究所技術情報部情報資料課（〒319—11 茨城県那珂郡東海村）あて，お申しこしください。なお，このほかに財団法人原子力弘済会資料センター（〒319—11 茨城県那珂郡東海村日本原子力研究所内）で複写による実費頒布をおこなっております。

JAERI-M reports are issued irregularly.
Inquiries about availability of the reports should be addressed to Information Section, Division of Technical Information, Japan Atomic Energy Research Institute, Tokai-mura, Naka-gun, Ibaraki-ken 319—11, Japan.

編集兼発行　日本原子力研究所
印　　刷　日立高速印刷株式会社

JAERI-M 84-085

Report of the Joint Seminar on Heavy-Ion Nuclear Physics and Nuclear Chemistry in the Energy Region of Tandem Accelerators

Department of Physics

Tokai Research Establishment, JAERI

(Received April 16, 1984)

A meeting of the joint seminar on Heavy-Ion Nuclear Physics and Nuclear Chemistry in the Energy Region of Tandem Accelerators was held at the Tokai Research Establishment of the JAERI, for three days from January 9 to 11, 1984.

In the seminar, about 50 nuclear physicists and nuclear chemists of JAERI and other Institutes participated, and 30 papers were presented. These include general reviews and topical subjects which have been developed intensively in recent years, as well as the new results obtained by using the JAERI tandem accelerator. This report is a collection of the papers presented to the seminar.

Organizing Committee

K. Harada (chairman)	Japan Atomic Energy Research Institute
N. Shikazono	"
E. Takekoshi	"
A. Iwamoto	"
S. Baba	"
S. Kubono	Institute for Nuclear Study, The University of Tokyo
T. Nomura	The Institute of Physical and Chemical Research
T. Kishimoto	The University of Tsukuba

Keywords: Heavy Ion, Tandem Accelerator, Nuclear Physics, Nuclear Structure, Nuclear Chemistry

The organizing committee would like to thank all participants for their assistance and cooperation in making the seminar so successful and fruitful.

JAERI－M 84－085

タンデム領域の重イオン核物理・核化学の研究会報告書

日本原子力研究所東海研究所物理部

（１９８４年４月１６日受理）

1984年１月９日から11日の３日間，タンデム領域の重イオン核物理・核化学の研究会が日本原子力研究所東海研究所において開催された。

研究会には日本原子力研究所及び所外の研究所，大学の核物理，核化学部門の約50人が参加し，30の研究報告が発表された。これらの報告書には最近集中的に研究開発されたテーマのレビュとトピックス，そしてJAERIタンデム加速器により得られた新しい結果が含まれている。

この報告書は研究会で発表された研究報告をまとめたものである。

研究会世話人

原田吉之助（日本原子力研究所）
鹿園　直基（　〃　）
竹腰　英子（　〃　）
岩本　　昭（　〃　）
馬場　澄子（　〃　）
久保野　茂（東京大学原子核研究所）
野村　　亨（理化学研究所）
岸本　照夫（筑波大学）

研究会の世話人一同は，盛大で成果の多い研究会に出来たことを参加者一同に感謝致します。

CONTENTS

SESSION I. NUCLEAR REACTION (Jan. 9, Monday, 1984)

I.1 Status of the JAERI Tandem Accelerator 1
Michio Maruyama

I.2 Molecular Orbital Formation in the System of Nucleon and Core-Nuclei 5
B. Imanishi and W.von Oertzen

I.3 Spin Alignment and Resonances in Inelastic Scattering between Light Nuclei 9
Norihisa Kato

I.4 Study of Competition between Fusion-Fission and -Evaporation in Heavy Ion Reaction 12
T. Nakagawa, S.M. Lee, K. Furuno, W. Yokota, Y. Fukuchi, T. Komatsubara, S. Kinouchi, Y. Nagashima, J. Shimizu, T. Mikumo, J.C. Adloff, D. Disdier, A. Kamili, G. Rudolf, and F. Scheibling

I.5 On the Competition between Fusion-Fission and Fusion-Evaporation in Heavy-Ion Reactions 16
T. Matsuse

I.6 Heavy-Ion Fusion and Nuclear Level Density 18
Masahisa Ohta, Koichi Hatogai, Sueji Okai and Yasuhisa Abe

I.7 Measurements of the Spin Alignment in the $^{12}C + ^{12}C$ Inelastic Scattering via γ Recoil 20
Yasuharu Sugiyama, Naomoto Shikazono, Yoshiaki Tomita, Hiroshi Ikezoe, Kenzo Nagano, Eiko Takekoshi, Shigeru Kubono, Masahiko Tanaka and Michiro Sugitani

I.8 Possible Quasi-Molecular Band in ^{32}S 23
Shigeru Kubono

I.9 Effect of the Exit Channel Distorting Potential in the $^{19}F + ^{12}C$ Inelastic Scattering 27
Toshiki Tachikawa

I.10 Spin Polarization in $(^{14}N,\alpha)$ Reaction 30
K. Ieki

I.11 Coincidence Measurement between Evaporation Residues and Light Particles Produced in $^{16}O + ^{40}Ca$ Reaction 32
Hiroshi Ikezoe

I.12 Breakup Effects of $^{6,7}_{2}$Li on the Elastic and Inelastic Scatterings from $^{12}_{6}$C 42
Kenji Katori, Tadashi Shimoda, Tomokazu Fukuda, Susumu Shimoura, Atsushi Sakaguchi, Tamiho Yamagata, Masayoshi Tanaka, Hiroshi Ogata, Noriaki Takahashi, Yukinori Sakuragi and Masayasu Kamimura

I.13 Fusion and Deep Inelastic Collision in the Systems of $^{37}_{17}$Cl + $^{27}_{13}$Al and $^{37}_{17}$Cl + $^{48}_{22}$Ti below 200 MeV 46
K. Ideno

SESSION II. NUCLEAR STRUCTURE AND NUCLEAR CHEMISTRY
(Jan. 10, Tuesday, 1984)

II.1 High-Spin States (Theoretical) 49
Yoshifumi R. Shimizu and Kenichi Matuyanagi

II.2 Experimental Studies of High-Spin States 53
Y. Gono

II.3 Heavy Elements and Superheavy Elements 57
Ichiro Fujiwara, Shin-ich Ichikawa, Nobuo Shinohara, Shigekazu Usuda, Toshio Suzuki, Hiroshi Okashita, Toshiaki Sekine, Takayoshi Horiguchi, Yoshikazu Yoshizawa, and Seiichi Shibata

II.4 Symmetric Fission in Relatively Light-Mass Reaction Systems . 61
H. Nakahara, Y.Nagame, K. Sueki, M. Yanokura and I. Kohno

II.5 Incomplete Fusion in the ^{12}C + ^{93}Nb Reaction 65
Toshiaki Sekine, Sumiko Baba, Kentaro Hata and Shin-ichi Ichikawa

II.6 Stability of Unstable Nuclei 69
Kengo Ogawa

II.7 Multiple Coulomb Excitation of Odd-Mass Nuclei 71
Takashi Inamura

II.8 In-Beam Gamma-Ray Spectroscopy through Heavy-Ion-Induced Fusic Reaction 75
Mitsuhiko Ishii and Akiyasu Makishima

II.9 Deformed Ground Band States in $^{152}_{66}$Dy$_{86}$ 77
Y. Nagai

II.10 Nuclear Spectroscopy of Radioisotopes Produced by Heavy-Ion Reactions 79
T. Tamura

II.11 Difference between Renormalization Factors for Unique First Forbidden AXIAL-β Transition and Those for Analogous M2-γ Transitions 82
Hiroyasu Ejiri

II.12 Nuclear-Spin Polarization of Heavy Ions Produced by Tilted Foils and Detected by Coulomb Excitation 87
Kenzo Sugimoto

SESSION III. RELATED TOPICS (Jan. 11, Wednesday, 1984)

III.1 Refinement of Brink Model --- Application to Massive Transfers --- 91
Atsushi Ichimura and Munetake Ichimura

III.2 TDHF Calculations of Heavy-Ion Collisions 96
Shuhei Yamaji

III.3 Preequilibrium Light Particle Emission in ^{14}N Induced Reactions 99
Tomokazu Fukuda

III.4 Pre-Equilibrium Light Particle Emission in Heavy Ion Induced Reactions 102
Koji Niita

III.5 Evidence for Lower Angular-Momentum Cutoff in Heavy-Ion Fusion Reactions 104
T. Nomura

The speakers in papers of collaboration are denoted by underlines (___).

SESSION I. NUCLEAR REACTION

(Jan. 9, Monday, 1984)

Chairmans

Shiro Yoshida
Tohoku University

Seigo Kato
Yamagata University

Teruo Suehiro
Tohoku Institute of Thechnology

Hiroshi Taketani
Tokyo Institute of Technology

I.1 Status of The JAERI Tandem Accelerator

Michio Maruyama

Department of Physics, Japan Atomic Energy Research Institute,
Tokai, Ibaraki, Japan

Introduction

The scheduled operation of the JAERI tandem accelerator for heavy ion experiments started on September 1, 1982 and has been continued for 16 months on the basis of 120 hours a week. This report describes some examples of the performances and the present status of the accelerator. Experience of the continuous operation in the first one year is also presented.

Available Ion Species

The center terminal of the 350KV negative ion injector houses three different negative ion sources, NEC direct extraction duoplasmatron source, Heinicke-Penning source, and Hiconex sputter-cone source. We have extracted reasonable amount of negative ions of 69 elements from these ion sources and already tried to accelerate 25 kinds of them to date. They are now usable for experiments. The extracted and accelerated ions shown in the periodic table of fig.1.

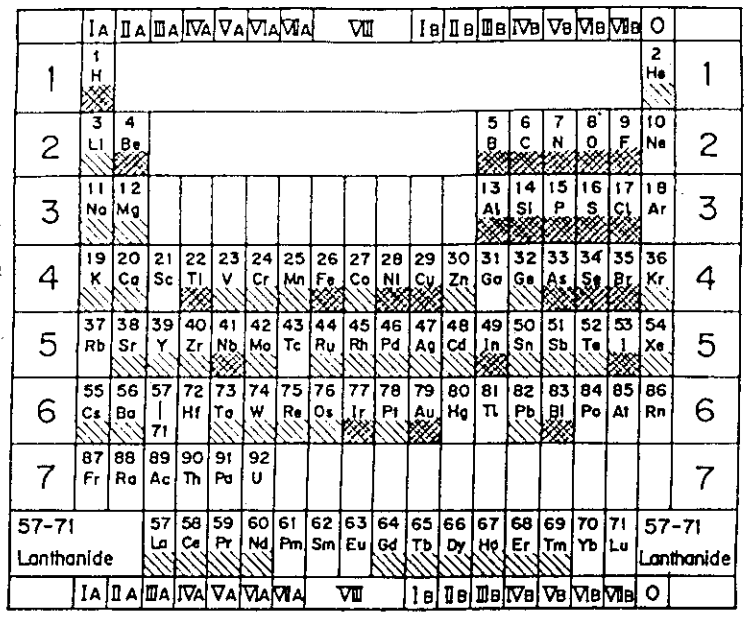

Fig.1. Periodic table showing the extracted (hatched) and accelerated(doubly hatched) ions.

It is impossible to produce negative ions of noble gas elements except for helium, because they don't have positive electron affinity. Minehara and Abe[1] of our laboratory extracted KrF^- and XeF^- from the Heinicke- Penning source by using KrF_2 and XeF_2 gases. Now they are trying to accelerate them by the tandem accelerator.

Ion Beam Performances

Table 1 presents some examples of ion beam performances observed after the analysing magnet. In the cource of these performances we got a strong impression that the folded beam line of tandem accelerators is excellent configuration to accelerate heavy ions because of the high selectivity of

charge states by the 180° terminal magnet. The current values seemed to be limited by performance of the ion sources and loading of the accelerating tube was very small.

In order to demonstrate the beam transmission through the accelerator, ion beam currents observed along the beam line are shown in fig.2. The steep decreasing after the electron stripper is caused by dispersion of positive charge states and multiple scattering by the stripper carbon foil of 10μg/cm^2. For hydrogen ions these effects are very small, so the transmission is very good.

Table 1 Ion Beam Performance

Ion (Continuous)	Terminal Voltage (MV)	Energy (MeV)	Current (pμA)	Pulse Width (ns, FWHM)
H^+	18	36	5	
$^{12}C^{5+}$	14	84	0.2	
$^{16}O^{6+}$	16	112	0.35	
$^{28}Si^{8+}$	13	117	0.025	
$^{35}Cl^{9+}$	18	180	0.53	
$^{58}Ni^{10+}$	13	143	0.02	
$^{63}Cu^{10+}$	13	143	0.03	
$^{81}Br^{10+}$	13	143	0.012	
$^{127}I^{7+}$	18	144	0.54	
(Pulse, 1MHz)				
H^+	13	13	4000(peak)	0.6
	18	18	1100(peak)	0.9
$^{127}I^{8+}$	18	162	12(peak)	1.9

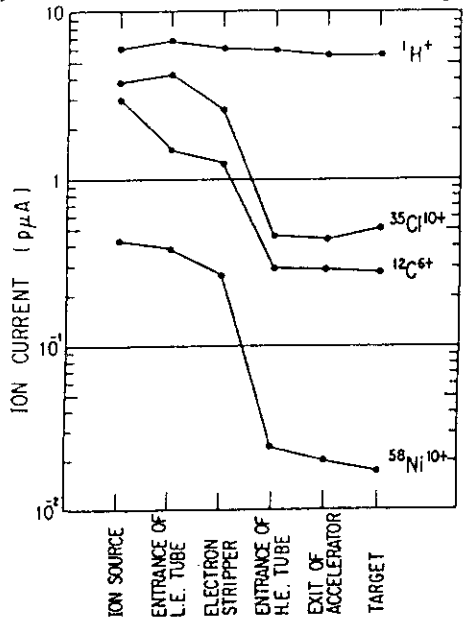

Fig.2. Beam current along the beam line.

Beam Pulsing

The outside and in-terminal beam pulsing systems also worked fairly reliably. The result of the pulsed H^+ beam at 18MV in table 1 was obtained with the in-terminal ion source and pulsing system. This is believed to be the world highest terminal voltage in performances of single ended electrostatic accelerators. Figure 3 shows a typical pulse shape of hydrogen beam produced by the outside pulsing system in the vertical low energy beam line at the terminal voltage of 17.5MV. The time spectrum was obtainen by observing γ-rays from Ta target bombarded by 35MeV hydrogen ions with two plastic scintillators.

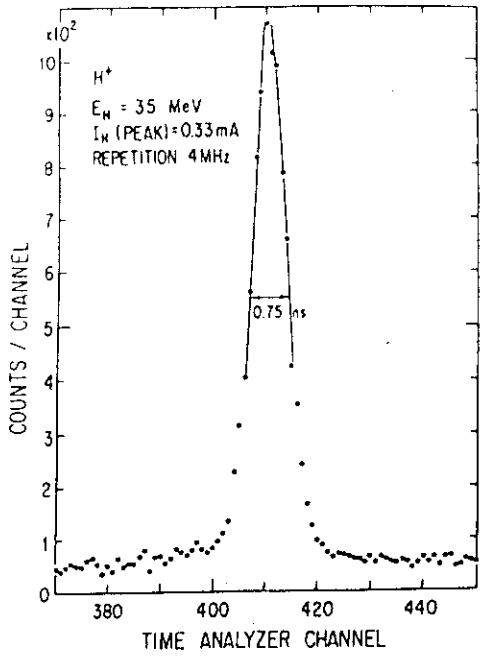

Fig.3. Time spectrum of pulsed hydrogen beam.

Charge Exchange

JAERI type longe-lived carbon foils[2] $10\mu g/cm^2$ thick have been used as the electron strippers. Table 2 describes consumption of the foils in the first foil exchanger at the exit of the low energy accelerating tube. During one year from September, 1982, eighteen foils were used for H, D, B, C, O, Cl, Ni, Br and a little bit of other ions. Eight foils of them were broken and the others still usable. Figure 4 shows a profile of No. 240 foil Which withstood irradiation of D, O, and Cl ions for 249 hours. The irradiated area seems to get very thin.

Table 2 Consumption of Carbon Stripper Foils for One Year

Foil	Irradiated Time(hours)	Ion Dosage (pμA·hours)	Injected Ion	Status
240	249	187.3	D,C,O,Cl	O(usable)
239	150	88.4	H,B,C,O,Al,S,Fe	X(broken)
236	35	10	Cl,Ni	X
235	200	58.6	Cl,Ni	O
234	148	98.6	C,Cl,Ni	X
233	39	11.1	Cl	O
229	38	47,8	Cl	X
228	385	289.8	C,O,F,Cl,Ni,Pt	X
226	61.5	89.5	D,O,Cl,Br	X
225	24	24.2	H,D	O
224	163	227.5	D,C,O,Cl	O
222	99	83	H,D,Cl,Ni	O
213	21.5	24.1	O	O
212	47	3.7	C,Cl,Ni	O
211	321	100.5	D,B,C,O,Cl,Ni	O
210	127	72	D,O,F,Cl,Kr	O
209	177	85.6	O,S,Cl	?
208	108	58.6	C,O,Cl	X

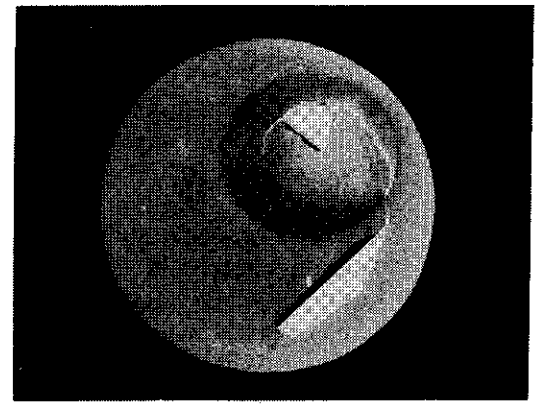

Fig.4. No.240 foil. Diameters of the holder opening and the irradiated area are 10 and 5mm, respectively. Only triangle break in the irradiated area was found when taken out.

Use of the second foil stripper on the high energy accelerating tube in the upper dead section was tried to get higher energies for ^{58}Ni ions and the results are described below. Ion energies increased by about 40%. There

Terminal voltage	Injected current	Charge state after 1st stripper	2nd stripper	Transmitted current	Ion energy
15.0 MV	450 nA	11	18	3.1 pnA	248 MeV
14.2	170	12	19	1.6	249

seems not to be essential difficulty in the charge balance and the ion optics.

Since the lifetimes of the foils are enough long and each foil exchanger can hold 240 foils, we have not been forced to open the accelerator vessel for recharging new foils since July, 1982.

Summary of Operation

The first continuous operation for experiments was performed for about 4 months in fall of 1981 prior to the acceptance of the accelerator and the scheduled operation has been regularly continued since September, 1982. The accelerator runs for 5 days every week on 24 hours basis. The following are

summary of the scheduled operation from September 1, 1982 to September 2,1983.

1)Time distribution by terminal voltage

17—18MV	2days	1.4%	11—12MV	2days	1.4%
16—17	15	10.3	10—11	5	3.4
15—16	31	21.4	9—10	7	4.8
14—15	39	26.9	8— 9	1	0.7
13—14	30	20.7	7— 8	1	0.7
12—13	11	7.6	3— 4	1	0.7

2)Time distribution by type of projectile

H	3days	2.1%	Cl	44days	30.6%
D	16	11.1	Ni	15	10.4
B	1	0.7	Br	1	0.7
C	23	16.0	Others	8	5.5
O	33	22.9	(P,Pt,Au etc. for test)		

3)Time distribution by type of activity

Operation for research		145days	40%
Atomic and solid state physics	16		
Radiation effects in materials	19		
Nuclear chemistry	23		
Nuclear physics	57		
Fast neutron physics	17		
Accelerator development	13		
Voltage conditioning		29	8
Scheduled maintenance (3 openings)		71	19
Unscheduled maintenance(4 openings)		29	8
Unused time		93	25

References

1) E. Minehara and S. Abe, Nucl. Instr. and Meth. 190(1981) 215 and 212 (1983) 533.

2) S. Takeuchi, C. Kobayashi, Y. Satoh, T. Yoshida, E. Takekoshi, and M. Maruyama, Nucl. Instr. and Meth. 158(1979) 333.

S. Takeuchi and E. Takekoshi, Japan Atomic Energy Research Institute JAERI-M 9322(1981).

S. Takeuchi and S. Kanazawa, Nucl. Instr. and Meth. 197(1982) 267 and 206(1983) 331.

I.2 Molecular Orbital Formation in the System of Nucleon and Core-Nuclei

B. Imanishi* and W. von Oertzen**

*INS, University of Tokyo, **HMI and Freie Universität Berlin

In this present study we discuss adiabatic molecular orbital formation[1-4] with particle-core model through an analysis of the system of $^{12}C+^{13}C$. This system is expected to show strong CRC effects due to the molecular orbital formation of the valence nucleon in $^{13}C^{(*)}$(gr.,$1/2^-$; 3.086MeV,$1/2^+$; 3.854MeV,$5/2^+$). The reasons are the following:

i) As the system involves two identical core nuclei, ^{12}C's, the transfer and direct interactions work additively on the wave functions in the total system with plus parity.

ii) The close vicinity of the 1p1/2, and sd orbitals gives favourable conditions for a parity mixing of orbitals, similar to the s-p hybridization effect in atomic physics.[5]

To see the effect of the multiple interactions between different channels, we investigate the Born series expansion in powers of the following off-diagonal-channel interaction ΔU;

$$(\Delta U)_{ij} = (V_{ij}+K^t_{ij})(1-\delta_{ij}) \ , \qquad (1)$$

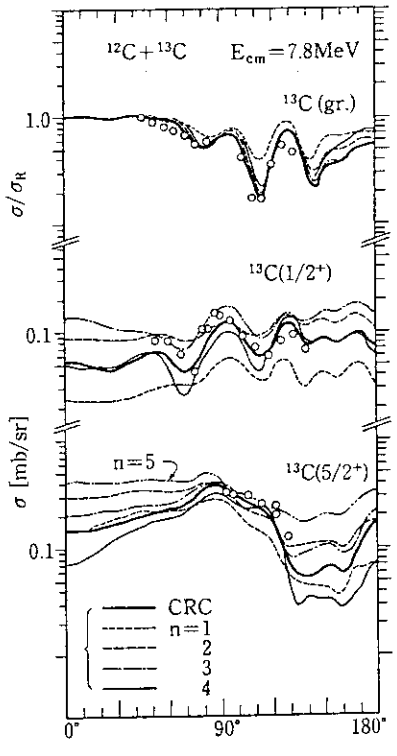

Fig. 1

with the use of the distorting potential U^0 ($(U^0)_{ij} = (U_{CC}+V_{ii}+K^t_{ii})\delta_{ij}$). The operator U_{CC} represents the core-core optical potential and is diagonal with respect to channel indices. The operators V and K^t are the interactions for direct and transfer processes, respectively.

In fig. 1 the strong divergences of the series of the differential cross sections $\sigma(n)$ (n=1,2,$\cdots$) (slim lines) are shown at the energy of E_{cm} = 7.8 MeV. The calculations include up to the n-th order of multiple interactions (see fig. 2).

We divide the coupling interaction ΔU into two parts; the one $\Delta\bar{U}$ responsible for the hybridization between p1/2 and s-d channels, and the other $\Delta\hat{U}$ responsible for the reorientation of the 1d5/2 orbitals;

$$\Delta U = \Delta\bar{U} + \Delta\hat{U} \ , \tag{2}$$

The CRC effects due to the interaction $\Delta\hat{U}$ alone are tested with the use of the series of the partial cross sections $\hat{\sigma}_{5/2}(n)$ (n=1,2,$\cdots$) going to $^{13}C^{*}(5/2^{+})+^{12}C$ channel. Similarly, we estimate the CRC effects due to the interaction $\Delta\bar{U}$ alone. The schematic diagrams for the expansion series are given in fig. 2. Both the series of the cross sections, $\hat{\sigma}_{5/2}(n)$ and $\bar{\sigma}_{5/2}(n)$ (n=1,2,$\cdots$), showed convergence except only for the case for $J^{\Pi} = 5/2^{+}$ at E_{cm} = 7.8MeV. This means that complex operation of $\Delta\hat{U}$ and $\Delta\bar{U}$ causes the divergence, which is expressed by the following expansion of the T-matrix elements T_{j1} ($j \geq 2$);

$$T_{j1} = \sum_{m=0}^{\infty} \langle \hat{\underset{\sim}{u}}_{j}^{(-)}, (\Delta\bar{U}g)^{m}\Delta\bar{U}\ \hat{\underset{\sim}{u}}_{1}^{(+)} \rangle \ , \tag{3}$$

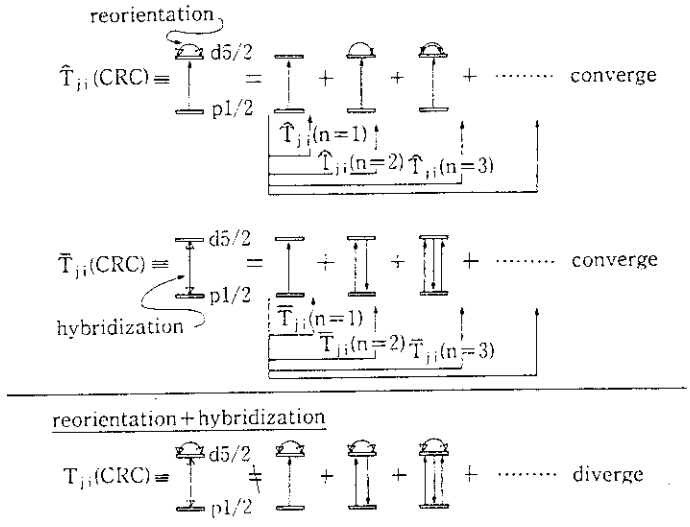

Fig. 2

where the wave functions $\hat{\underset{\sim}{u}}_{i}^{(+)}$ as well as Green's function $\hat{g}$ are generated by the potential $(U^{0}+\Delta U)$. The physical meanings of the divergence are the followings:

i) First, the reorientations of 1d5/2 orbitals occur, which are included in the wave function $\hat{\underset{\sim}{u}}$ and Green's function $\hat{g}$ in eq. (3). In this situation the density distribution of the valence nucleon extends along the axis joining the centres of the core nuclei.

ii) Second, the mixing due to $\Delta\bar{U}$ is so strong between the 1p1/2 and the "reoriented" 1d5/2 channels that the series diverges. This mixing causes extremely biased density distribution (called hybridization) of the valence nucleon as is shown in fig. 5.

We see in the calculations that the transfer interactions play an essential role in the strong multiple interaction scheme due to the hybridization. However, it should be noted that the direct interaction gives non-negligible effects in the hybridization, since the direct

interaction contributes additively to the transfer interaction in the system of Π = plus (gerade system), an effect which is caused by the identity of the cores.

In the discussion of the adiabatic approach we introduce the base functions[6] $\phi^{JM\Pi}_{n\ell jK}$ employed in the CRC method in the helicity representation. The "rotating" molecular orbital (RMO) is expressed with the base functions mentioned above:

$$\phi^{JM\Pi}_{p} = \sum_{K} \sum_{n\ell j} \phi^{JM\Pi}_{n\ell jK} \cdot A^{J\Pi}_{n\ell jK,p(r)} \quad . \tag{4}$$

The transformation coefficients $A^{JM\Pi}_{n\ell jK,p(r)}$ are obtained by the diagonalization for the interaction of angular part of the relative motion - Corioli's K-mixing term, and the direct- and transfer interactions in the CRC coupled equation. Adiabatic potentials $\mathcal{V}^{J\Pi}_{p}(r)$, are obtained as the eigenvalues of the diagonalization at each point of r. If the coupling interactions with the RMO representation are small perturbation, Φ_p is good base function describing the scattering process.

Fig. 3 shows the S-matrix elements between α = 1 and 2 and α = 1 and 3 (α=1,2,3$\Rightarrow$($n\ell jK$)=(1p1/2,K=1/2),(2s1/2,K=1/2),(1d5/2,K=1/2)) with the calculations of CRC, 1st-order perturbation in the CRC representation (PWR 1-step) and 1st-order perturbation in the RMO representation (ADB 1-step). At low incident energies ADB 1-step calculation is much better approximation of the exact calculation (CRC) than the PWR 1-step calculation. As well, elastic scattering was well described at low incident energies only with the adiabatic potential.

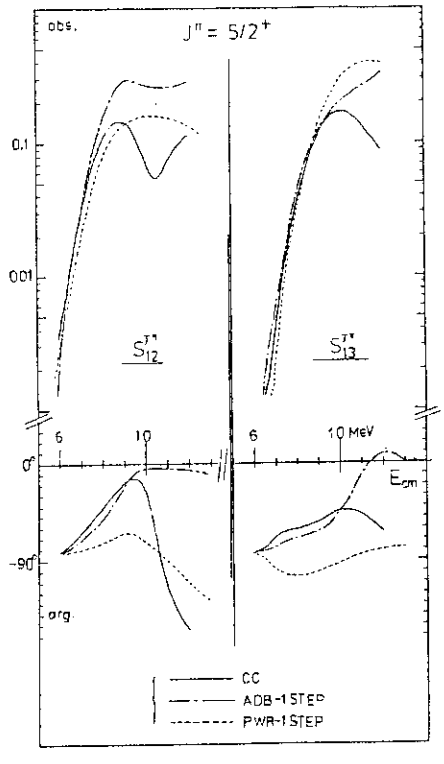

Fig. 3

In fig. 4 each α-component of the RMO wave function of p=1 and J^{Π} = 5/2$^+$ is drawn as a function of the relative distance r. In the region of the distance from 9fm to 2fm a state with the components of α = 1, 2 and 3, each of which belongs to the same K-quantum number of 1/2, is formed and each α-component changes rather smooth-

ly with the change of the distance. At the distances r > 2 fm the RMO states $\Phi_p^{J\Pi=+}$ of p=1 define intrinsic molecular orbitals in the rotating frame, because the RMO states belong to a pure K-quantum number.

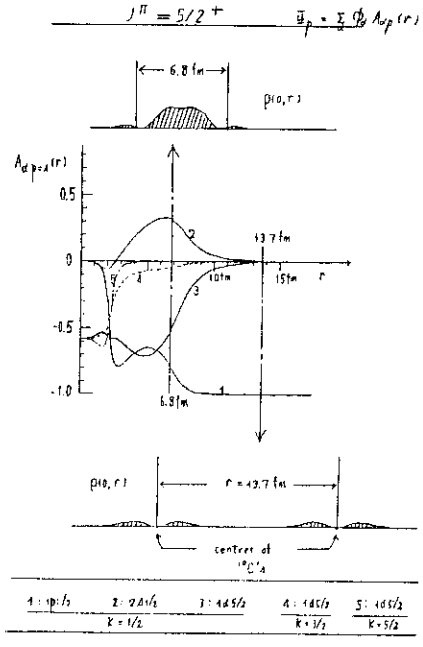

Fig. 4

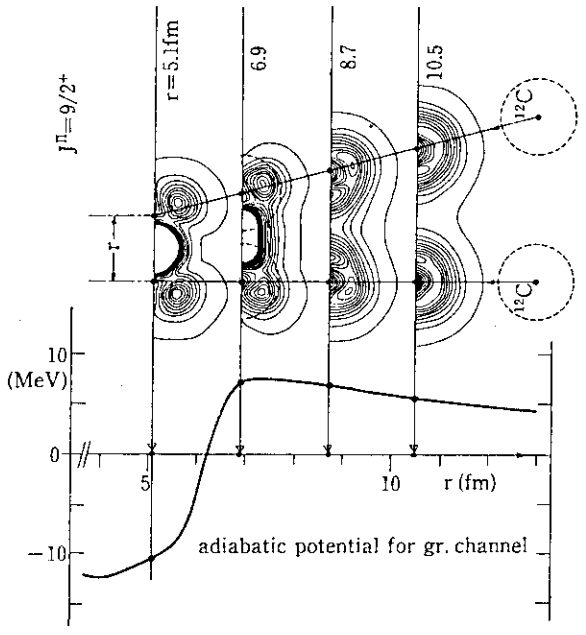

Fig. 5

In fig. 5 examples of the density distributions,[8]

$$\rho_p^{J\Pi}(xz,r) \equiv \sum_\sigma \int d\hat{r} \left| \Phi_p^{JM\Pi} \right|^2 , \qquad (5)$$

for the state of p=1 are drawn along the line of the Z-axis joining the centres of two ^{12}C nuclei. In the figure the linear chain structure, ^{12}C-n-^{12}C is observed. Such a charateristic configuration is formed due to the hybridization.

References

1. F. Becker et al., Nucl. Phys. A221 (1974) 475.
2. J. Y. Park, W. Scheid and W. Greiner, Phys. Rev. C20 (1979) 188, C25 (1982) 1902.
3. B. Imanishi and W. von Oertzen, Phys. Lett. 87B (1979) 188.
4. W. von Oertzen, B. Imanishi, H. G. Bohlen, W. Trei and H. Voit, Phys. Lett. 93B (1980) 21.
5. L. Pauling, The Nature of the Cemical Bond (Cornell Univ. Press, 1960).
6. W. von Oertzen and B. Imanishi, Proc. on Symp. on Resonances in Heavy Ion Reactions ed. K. A. Eberhard (Springer-Verlag, Bad Honnef, 1981) Lecture Notes in Physiccs 156, p.388.

I.3 Spin Alignment and Resonances in Inelastic Scattering between Light Nuclei

Norihisa Kato

Department of Physics,Faculty of Science,Kyushu University

In the excitation functions of the inelastic scattering between light nuclei like ^{12}C and ^{16}O, pronounced gross and intermediate structures have been observed in the energy region from $E_{cm} \cong 18$ to 30 MeV [1][2]. So far many studies have been reported to explain these structures from various theoretical bases[3][4]. At present it is basically understood that the prominent intermediate structures are caused by the coupling of the entrance channel to specific doorway states。 In most of the models the inelastic excitations to the low-lying states (e。g。 2^+state(4。44MeV),3^-state(6.13MeV)) are thought to be the most important channels to couple with the entrance one. Almost models predict the specific coupling scheme of the relative orbital angular momentum between outgoing partners and the intrinsic spin of the residual state。 Since these coupling schemes are directly connected to the magnetic substate population of the residual state, measurement of the spin alignment of the residual state is expected to be a crucial test of the proposed models.

The purpose of the present report is to show the results of the experimental investigations of the magnetic substate population in the $^{12}C+^{16}O(3^-)$ and $^{12}C(2^+)+^{12}C(2^+)$ inelastic channels, and to clarify the nature of the resonant structures by blief qualitative discussions.

1) $^{12}C+^{16}O(3^-)$ single inelastic excitation.

In the excitation function of this system, prominent intermediate structures of several hundred keV width have been observed in the energy region around E_{cm}= 20 MeV. We have investigates the spin

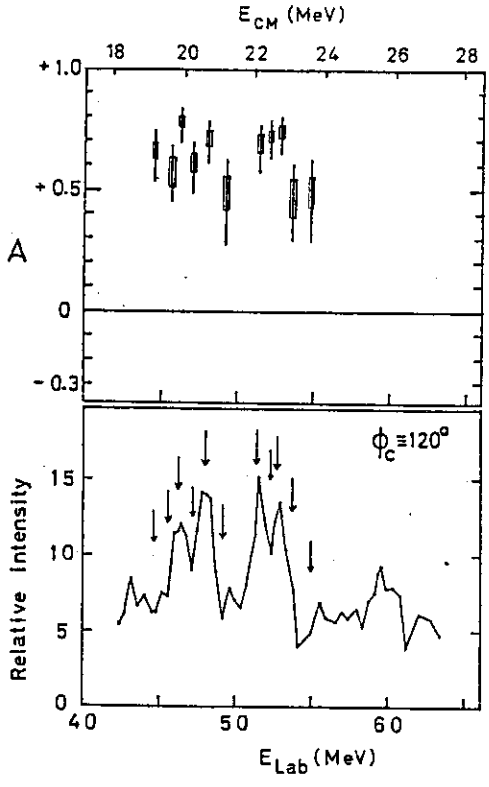

fig.1

alignment of the residual state at energies properly selected on- and off-resonances[5]. When the quantization axis is chosen along the direction perpendicular to the reaction plane, only the substates with ± 3 and ± 1 can participate in the reaction process according to Bohr's theorem. By the particle-gamma angular correlation method, we extracted the spin alignment defined as $A=(P_{\pm 3}-P_{\pm 1})/\sum_m P_m$.

In fig.1, angle averaged spin alignments (upper panel) are compared with the inelastic scattering excitation function. The arrows in the lower panel indicate the energies where the spin alignments were measured. As shown in fig.1, the values of the spin alignment A are positive at all energies and those at on resonance energies E_{cm} = 19.7, 20.5, 22.0 and 22.6 MeV are larger than those at off-resonance energies. These results, which show the enhancement of the population of $m=\pm 3$ substates especially on the resonances, indicate that the dominance of the aligned configuration between angular momentum and the intrinsic spin of the residual state play an important role in the reaction process. Recently it is reported that this experimental feature is qualitatively reproduced by the band crossing model[6].

In fig.2 the contributions of the $m=\pm 3$ and ± 1 components to the angular distributions are shown with those of the summed cross sections(solid lines without data points). It is clearly indicated that only the $m=\pm 3$ components increase on the resonances and those of $m=\pm 1$ stay almost constant at all energies. Additionally we can get more regular dependence of the differential cross sections for each component than those for summed ones and then the assignments of the resonant angular momentum may be possible even from the

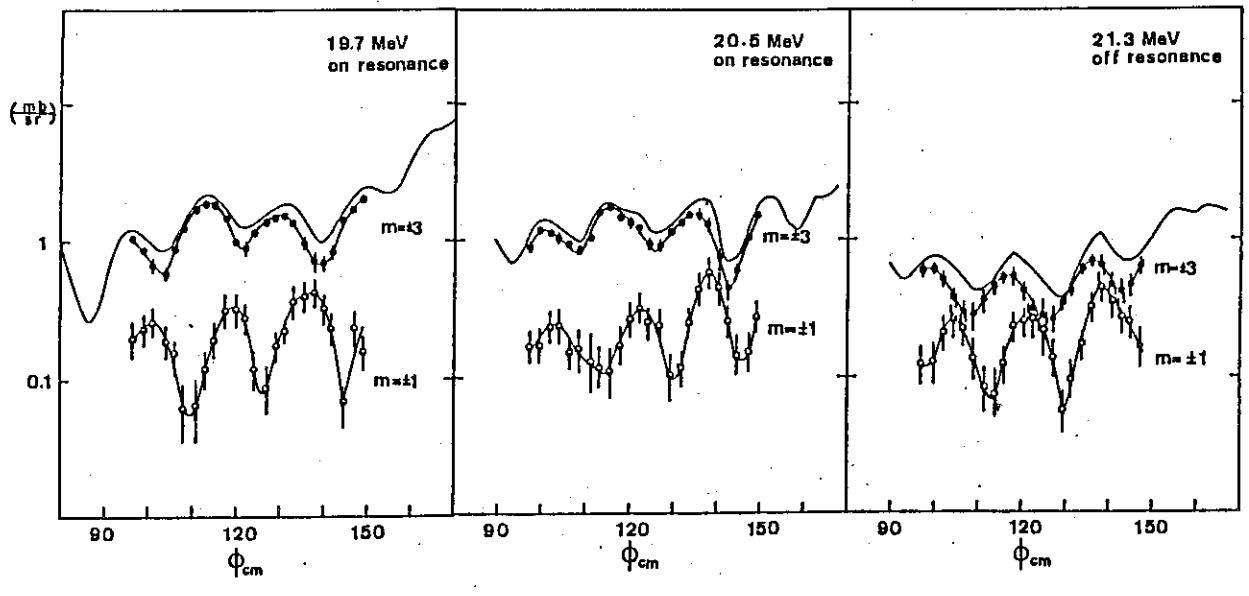

fig.2

inelastic scattering data.

2) $^{12}C(2^+)+^{12}C(2^+)$ mutual excitation.

In mutual excitation the magnetic substate population in the residual states $(|m_1|, |m_2|)$ of each nucleus is limited only to the following four combinations (2,2),(2,0),(0,0) and (1,1) according to Bohr's theorem. Angular distributions of the spin alignments were measured at seven energies around the resonance structure at E_{cm}=25 MeV using the Heidelberg crystal ball spectrometer[7]. Correlated increase of the spin alignments with the excitation functions of the cross sections was observed at resonance energies. This result indicates that the aligned configuration dominates again on the resonance. In fig.3 the angular distributions of the spin alignments and the populations of each substate component are shown. Components of the aligned configuration (2,2) are given in the middle panels, and the solid, dotted and dashed lines in the lower panels correspond to the population of the components (2,0),(0,0) and (1,1), respectively. The above experimental features are in contrast with the results obtained for the single excitation $^{12}C+^{12}C(2^+)$ case, where the enhancements of the aligned configurations were not clear at resonance energies[8].

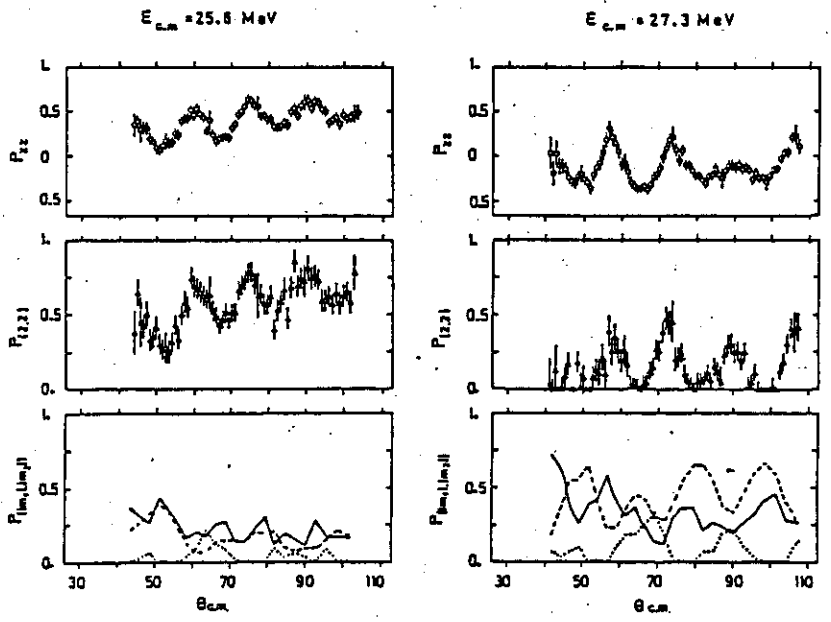

fig.3

References;

[1] R.E.Malmin et al., Phys.Rev.C18(1978)163.

[2] T.M.Cormier et al., Phys.Rev.Lett.38(1977)940.

[3] H.J.Fink et al., Nucl.Phys.A188(1972)259.

[4] Y.Abe et al., Prog.Theor.Phys.Suppl.68(1980)303.

[5] N.Kato et al., Phys.Lett.120B(1983)314.

[6] T.Tazawa et al., RIFP(Kyoto)-493(1983).

[7] D.Konnerth et al., to be published in Nukleonika.

[10] W.Trombik et al., preprint(1983).

I.4 STUDY OF COMPETITION BETWEEN FUSION-FISSION AND -EVAPORATION IN HEAVY ION REACTION

T.Nakagawa*, S.M.Lee*, K.Furuno*, W.Yokota*, Y.Fukuchi*, T.Komatsubara*
S.Kinouchi*, Y.Nagashima*, J.Schimizu*, T.Mikumo*, J.C.Adloff**,
D.Disdier**, A.Kamili**, G.Rudolf** and F.Scheibling**

* Institut of Physics, University of Tsukuba, Ibaraki, Japan

** Centre de Recherches Nucleaires, Strasbourg, France

In heavy ion reaction for Light-Heavy system, The total reaction cross section is nearly equal to fusion cross section and there are two different decay modes ; fusion-fission and fusion-evaporation. Recently we reported the existance of constant critical angular momentum J_{ER} in compound nucleus for which the dominant regions of evaporation- and fission-decay can be clearly distinguished.[1)2)] Using J_{ER} and J_{cr}, fusion,fusion-evaporation and fusion-fission cross section can be given by

$$\sigma_f = \sigma_{f-f} + \sigma_{f-er} = (\pi\hbar^2/2\mu E_{CM}) \times (J_{cr} + 1)^2 \quad (1)$$

If $J_{cr} \leq J_{ER}$

$$\sigma_{f-er} = (\pi\hbar^2/2\mu E_{CM}) \times (J_{cr} + 1)^2 \quad (2)$$

$$\sigma_{f-f} = 0 \quad (3)$$

If $J_{cr} \geq J_{ER}$

$$\sigma_{f-er} = (\pi\hbar^2/2\mu E_{CM}) \times (J_{ER} + 1)^2 \quad (4)$$

$$\sigma_{f-f} = (\pi\hbar^2/2\mu E_{CM}) \times ((J_{cr} + 1)^2 - (J_{ER} + 1)^2) \quad (5)$$

where σ_f, σ_{f-f} and σ_{f-er} are fusion, fusion-fission and fusion-evaporation cross sections respectively.

For studying the compound nucleus effect for J_{ER} and its isotope dependence, we have measured fusion-fission and fusion-evaporation cross sections for the system of $^{16}O + ^{170,174}Yb$ and $^{32}S + ^{144,154}Sm$.

The beam of ^{16}O in energy range 70-88MeV were porduced by 12UD peretron tandem accelerator of University of Tsukuba. The beam of ^{16}O in energy range 100-140MeV and the beam of ^{32}S in energy range 140-200MeV were produced by the up-graded MP tandem accelerator of Strasbourg C.R.N.

For measurments of fusion-evaporation cross sections, we used T.O.F method with the time resolution of Δt=2ns made by pulsed beam, which was enough to distinguish evaporation residues from the elastic tails. 8 silicon detectoes were placed at 30cm from the target to measure evaporation residues. The thin target (about 50μg/cm^{2}evaporated on 20μg/cm^2 C) were used to minimize

multiple scattering effect and energy loss in target. In order to measure fusion-fission cross sections, 8 angle ΔE-E counter telescopes was used where the ionization chamber was used as ΔE counter and silicon detectors as E counter.

Fig.1 shows the excitation function of fusion, fusion-fission and fusion-evaporation cross sections as a function of $1/E_{CM}$. It clearly shows that fusion-evaporation cross section is proportional to $1/E_{CM}$ above the fission threshold energy. Fig.2 shows J_{ER} and J_{cr} for the system of $^{16}O + ^{170}Yb$ and $^{32}S + ^{154}Sm$ which lead to same compoud nucleus ^{186}Pt. Comparing the experm-ental fusion-evaporation cross section and eq.(4), we obtained the values of J_{ER} as indicated in table 1. From these results, it is clarified that J_{ER} is strongly dependent on the nature of compound nucleus and is influenced quite sensitively by numbers of neutron. J_{ER} of various compound nucleus are shown in fig.3 as a function of Z^2/A, where Z and A are charge and mass number of compound nucleus. In fig.3, it seems that J_{ER} decreases rapidly above $Z^2/A=30$.

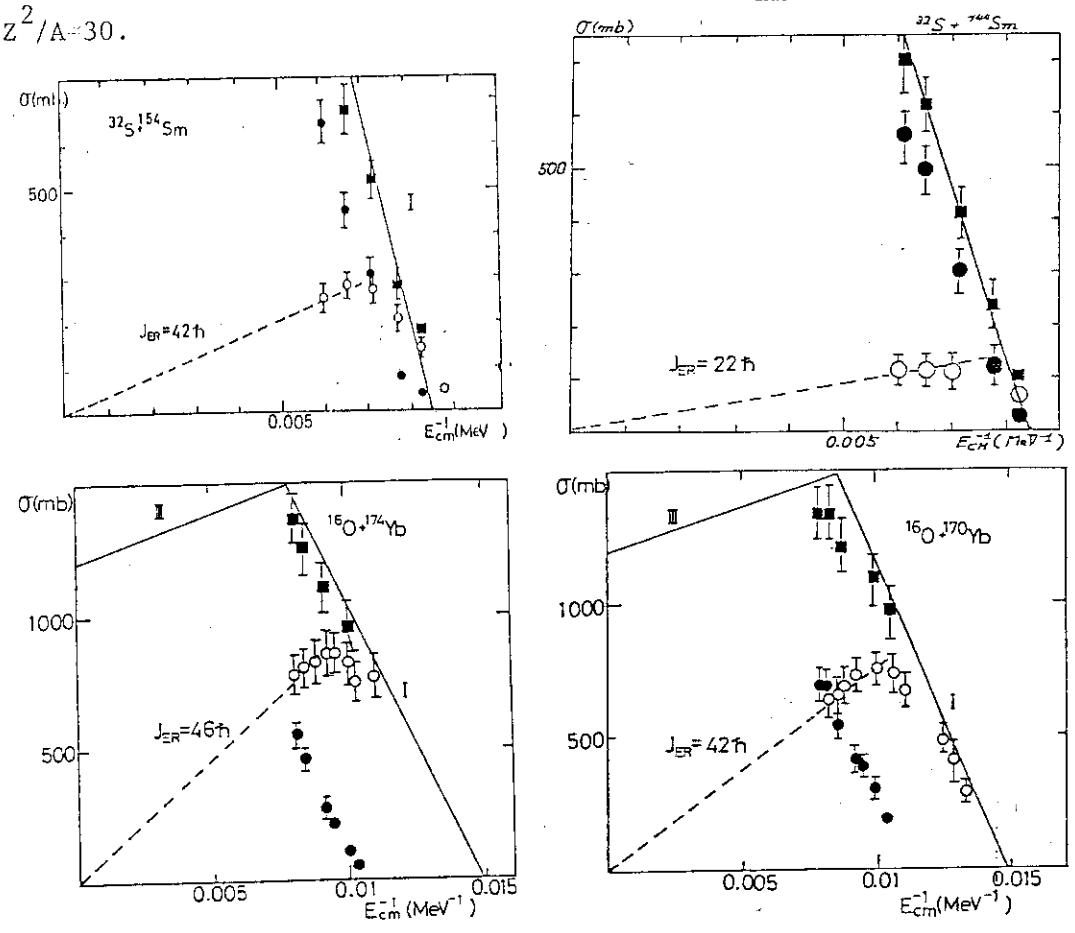

Fig.1 The excitation function of fusion-fission and fusion-evaporation cross section as a function of $1/E_{CM}$ for $^{16}O+^{170,174}Yb$ and $^{32}S+^{154,144}Sm$

○ :experimental $\sigma_{f\text{-}er}$, ● :experimental $\sigma_{f\text{-}f}$, ■ :experimental σ_f

—— : the theoritical σ_f in Region I[3] and RegionIII[4].

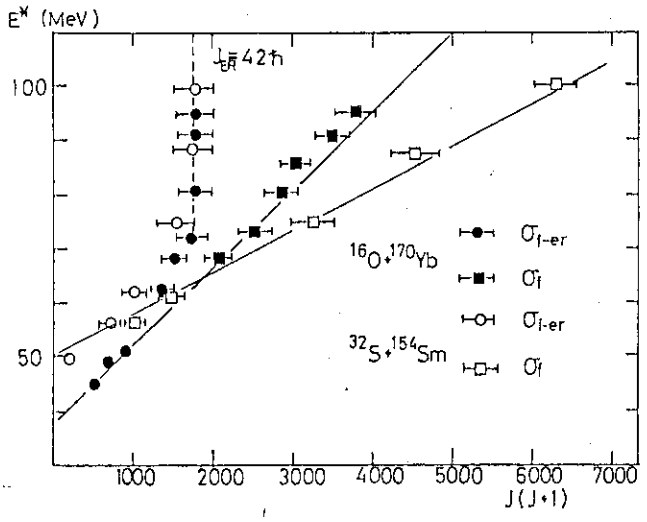

Fig.2 J_{ER} and J_{cr} in the plane of E^* and J(J+1) for the system of $^{16}O + ^{170}Yb$ and $^{32}S + ^{154}Sm$ which lead to the same compound nucleus

● and ■ are experimental J_{ER} and J_{cr} for $^{16}O + ^{170}Yb$

○ and □ are experimental J_{ER} and J_{cr} for $^{32}S + ^{154}Sm$

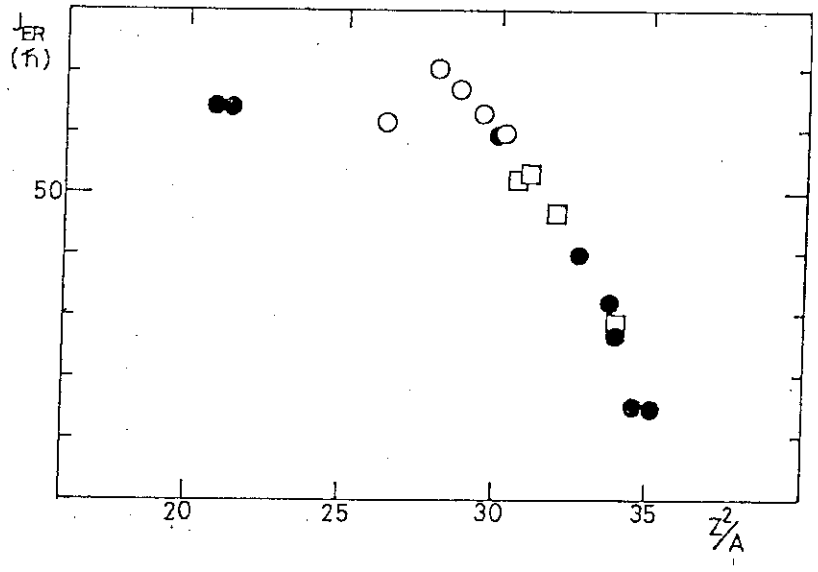

Fig.3 J_{ER} of various compound nucleus as a function of Z^2/A

● are experimental J_{ER} from σ_{f-f} and σ_{f-er}

○ are experimental J_{ER} from σ_{f-er}

□ are extracted J_{ER} from σ_{f-f} and theoritical σ_f [3)4)]

Table 1

system	compound nucleus	$J_{ER}(\hbar)$
$^{16}O + ^{174}Yb$	^{190}Pt	46
$^{16}O + ^{170}Yb$	^{186}Pt	42
$^{32}S + ^{154}Sm$	^{186}Pt	42
$^{32}S + ^{144}Sm$	^{176}Pt	22

References

1) S.M.Lee, T.Nakagawa and T.Matsuse, Contributed paper to the "Conference on Nuclear Physics with Heavy Ion", April 14-16, 1983, Stony Brook

2) T.Nakagawa et al, Contribution paper to the "International Conference on Nuclear Physics" (Florence, 1983)

3) S.M.Lee, T.Nakagawa and W.galster, Contribution paper to the Int. Conf. on Nucleus-Nucleus Collisions (Michigan,1982)

4) T.Matsuse, A.Arima and S.M.Lee, Phys. Rev. C26(1982)2338

I.5 On the competition between fusion-fission and fusion-evaporation in heavy-ion reactions.*)

T. Matsuse

Department of Physics, University of Tokyo, Tokyo, 113, JAPAN

Recently we have showed that the energy independent critical angular momentum J_{er} in fusion-evaporation cross section may exist in highly excited energy region and the J_{er} has the very interesting compound nucleus dependence. A possible interpretation for the existence of J_{er} is to be discussed in terms of the competition between fusion-fission and fusion-evaporation. The essential point of the existence of J_{er} has been presented by T. NAKAGAWA in this symposium.[1)]

In order to reproduce the essential quantities of fusion-fission and J_{er}, we adopted Hauser-Feshbach method to the fission part. All avairable two-body decaying nucleus pairs are taken into account and the effect of excitation of fission fragment pairs is included in the phase-space calculation.

The most difficult problem in this extended Hauser-Feshbach method is to determine the transmission coefficient between fission fragments. We parametrized the transmission coefficient so as to reproduce the observed mass and kinetic energy distributions. The very preliminary calculated results are presented in this report.

In order to make clear the physical meaning of the observed J_{er}, at first we investigate the effect of multi-chance fission through the neutron evaporation.

In the case of $^{19}F+^{181}Ta$ system, the contribution of multichance fission is shown in table I. We can see that the effect is very large in this system. In the lighter system, for example $^{32}S+^{76}Ge$ system, the multi-chance effect is negligible small.

Although the physical picture is very different from that of RLDM, this result is very consistent with that of other calculation [2].

As a result of our calculation, in the heavier system ($A_{cn} \gtrsim 180$), the effect of multi-change fission becomes very large. Then the deduced J_{er} from experimental cross section does not correspond to the first chance fission in our model. Furthermore it is expected that more wide domain of

*) This work has been performed under the collaboration with S. M. LEE and T. NAKAGAWA.

angular momentum than that expected from experimental result may contribute to the fully equilibriated compound nucleus formation as we discussed in Ref.[3].

The calculated J_{er} for the several systems are shown in table II. The values J_{er} in parenthesis indicates the calculated J_{er} included multi-chance fission effect, the other values show the first chance contribution only. From these results our approach by the use of extended Hauser-Feshbach method is very promising for understanding the competition between fusion-fission and fusion-evaporation induced heavy-ion reactions.

MULTI-CHANCE FISSION

$^{32}S + ^{76}Ge \rightarrow ^{108}Cd$ E_L=200 MeV E^*=130.7 MeV

N	$\sigma_{f.f}^{(N)}$(mb)	$\sum_N \sigma_{f.f}^{(N)}$(mb)	$-J_{ev}$
1	391.7	391.7	65
2	22.0	413.9	↓
3	5.8	419.7	↓
4	0.9	420.6	64

$^{37}Cl + ^{141}Pr \rightarrow ^{176}Os$ E_L=200 MeV E^*=87.0 MeV

N	$\sigma_{f.f}^{(N)}$(mb)	$\sum_N \sigma_{f.f}^{(N)}$(mb)	J_{ev}
1	362.2	362.2	41
2	32.9	395.1	↓
3	9.9	405.5	↓
4	4.6	409.6	↓
5	4.5	414.1	↓
6	0.3	414.3	36

$^{19}F + ^{181}Ta \rightarrow ^{200}Pb$ E_L=125 MeV E^*=89.0 MeV

N	$\sigma_{f.f}^{(N)}$(mb)	$\sum_N \sigma_{f.f}^{(N)}$(mb)	J_{ev}
1	2.3	2.3	58
2	40.3	42.6	↓
3	101.4	144.0	↓
4	112.6	256.6	↓
5	174.4	431.0	↓
6	116.5	547.5	↓
7	17.0	564.5	↓
8	77.2	641.7	↓
9	24.0	665.7	38

TABLE I.

$A_1 + A_2$	A_{cN}	E^*(MeV)	J_{ev}	$J_{ev}^{(obs)}$
$^{32}S + ^{76}Ge$	^{108}Cd	130.7	65 (64)	65
$^{35}Cl + ^{62}Ni$	^{97}Rh	114.6	64 (63)	64
$^{35}Cl + ^{116}Sn$	^{151}Ho	96.5	67	62
$^{35}Cl + ^{141}Pr$	^{178}Os	71.0	40 (36)	39
$^{32}S + ^{124}Sn$	^{156}Dy	115.9	72	71
$^{32}S + ^{120}Sn$	^{152}Dy	110.9	71	67
$^{32}S + ^{116}Sn$	^{148}Dy	106.9	69	64
$^{32}S + ^{112}Sn$	^{144}Dy	96.4	63	60
$^{64}Ni + ^{124}Sn$	^{188}Pt	80.0	52	47
$^{64}Ni + ^{118}Sn$	^{182}Pt	71.0	40	32
$^{64}Ni + ^{112}Sn$	^{176}Pt	63.0	28	21
$^{16}O + ^{174}Yb$	^{190}Pt	113.0	61 (41)	46
$^{16}O + ^{170}Yb$	^{186}Pt	155.0	55 (40)	42
$^{30}Si + ^{170}Er$	^{200}Pb	77.6	56 (32)	32
$^{28}Si + ^{170}Er$	^{198}Pb	81.6	53 (29)	26
$^{28}Si + ^{167}Er$	^{195}Pb	75.8	42 (22)	19
$^{28}Si + ^{164}Er$	^{192}Pb	71.5	29 (16)	19

TABLE II.

References

1) T. Nakagawa, report in this symposium.

2) D. J. Hinde, et al., Nucl. Phys., A385 (1982) 109

3) T. Matsuse, A. Arima and S. M. Lee, Proc. XXI intern. Winter Meeting on Nuclear Physics, Bormio, Italy, (1983) 640

I.6 Heavy Ion Fusion and Nuclear Level Density

Masahisa Ohta*, Koichi Hatogai*, Sueji Okai* and Yasuhisa Abe**

*Department of Physics, Konan University, **Research Institute for Fundamental Physics, Kyoto University

Fusion process, as nuclei involved are composite particles, has recently disclosed its many-body nature in many aspects[1]. At the beginning, the notations used in this note are defined with brief comment. σ_{CF} is referred to as the complete fusion and defined to be the cross section for the process via the compound nucleus (mass number A), which composes of all constituents of projectile (A_1) and target (A_2): $A=A_1+A_2$. Incomplete fusion cross section σ_{IF} is distinguished from σ_{CF} as processes via another compound nuclei $A < A_1+A_2$. Under σ_{ER}, we understand the sum of σ_{CF} and σ_{IF}.

Experimentally, σ_{CF} is the cross section characterized by the full linear momentum transfer: Incident particle imparts all its linear momentum to the compound nucleus A ($=A_1+A_2$). One of the important problem in this case is to answer the qestion: Is it always possible to form the compound nucleus without any limitation on the excitation energy ? There is no evidence to support it in the affirmative way, but it is supposed implicitly to be the case, since σ_{ER} is assumed tending to zero as bombarding energy increases infinitely.

In this note, we will show from the theoretical consideration that the compound nucleus can not be formed beyond an upper bound on the excitation energy. Compound nucleus has a finite size in the configuration space and thus the wave function is limited within this region. With this in mind, the state density of the compound nucleus is calculated to show that there is a certain excitation energy beyond which we can not confine a set of nucleons to the finite region. Finiteness of the nucleus, on the other hand, means that for the respective excitation energy the angular momentum of the nucleus has the maximum value, which is identified to be the critical angular momentum for fusion.

Finiteness of nuclei is realized by making all nucleons occupied in the bound states available in the single particle potential. There are only a finite number of bound states in the potential with finite range. It is well known in the statistical mechanics[2] that as far as states available for nucleons is finite, the nuclear temperature defined by $T = (dS/dE)^{-1}$

increases from zero to infinity as E starts from zero to a certain excitation energy E_H. Here, S is the entropy and E is the excitation energy. As E becomes still larger than E_H, the temperature suddenly changes its sign (negative infinity) and then tends eventually to minus zero at the excitation energy E_M. Thus, the finite nucleus can not accomodate anymore excitation energy greater than E_M.

What is emphasized here is that there is an upper bound on the excitation energy of the compound nucleus. However, both E_M and E_H are not the least upper bound which we want to know, because the compound nucleus is treated as an isolated system and do not contain any components of open channels. As one method to get the bound, it is suggested to calculate the transition probability between the states of the compound nucleus and the degenerate states of open channels. Tentatively, we calculated the neutron decay width of the compound nuclear state. It turns out that we have a certain excitation energy E_L, almost idependent of angular momentum of the compound nucleus, for the lifetime assumed to be 10^{-22}sec. The energy E_L is always less than a half of E_H for nuclei $A < 100$.

For the excitation energies higher than E_L, the compound nucleus should decay so fast that the complete fusion is no more of useful concept. In an incident energy giveing rise such a highly excited compound nuclear state, another compound nucleus formed by incomplete fusion remains still a long-lived system. Then, the procedure mentioned above is applied to the system to obtain the critical angular momentum for fusion.

Finally, it is pointed that observed value of σ_{ER}^{obs} is approximately equal to calculated one of σ_{CF}^{cal} for the compound nucleus A ($=A_1+A_2$) even for large bombarding energy partly leading to incomplete fusion. In other words, some parts of σ_{CF}^{cal} are really σ_{CF}^{obs}, while the remaining part is attributed to σ_{IF}^{obs}. This last statement is based on the approximate relation $\sigma_{CF}^{cal} \fallingdotseq \sigma_{IF}^{cal}$ which is easily proved using Eqs. (2) and (3) in Ref. 3.

References:

1) R.Vandenbosch, Paper presented at Conference on Nuclear Physics with Heavy Ions (Stony Brook, New York, April 14-16, 1983)
2) M.Toda and R.Kubo (eds.), Statistical Physics (Foundation of Modern Physics Vol.6) (Iwanami, Tokyo, 1972, in Japanese) p.42
3) H.Lehr et al., Lecture note in phsics Vol.117 edited by W.von Oertzen (Springer-Verlag, 1980) p.354

I.7 Measurements of the spin alignment in the $^{12}C+^{12}C$ inelastic scattering via γ recoil

Yasuharu Sugiyama*, Naomoto Shikazono*, Yoshiaki Tomita*, Hiroshi Ikezoe*, Kenzo Nagano*, Eiko Takekoshi*, Shigeru Kubono**, Masahiko Tanaka** and Michiro Sugitani**

*Department of Physics, Tokai Research Establishment, JAERI,
**Institute for Nuclear Study, University of Tokyo

It is known in experiments with heavy ions that γ-decay in flight of an excited nucleus broadens a line width in the momentum spectrum of the outgoing nucleus, reflecting the Doppler shift of the emitted γ-rays[1]. The shape of the line is determined by angular distributions of the γ-rays, which have characteristic patterns for different m substates. Characteristic line shapes were observed in the momentum spectrum and the m substate population was deduced by unfolding the line shapes, when a high momentum resolution was achieved for the particle spectrum like as ^{12}C or ^{16}O[1]. Some formulas were presented for deducing the substate population from the line shapes[1]. The z axis was taken to be the direction of scattering angle θ_b of laboratory system with which an excited heavy ion left the reaction region. The orientation of the nucleus produced in the reaction was specified by the components $\rho_{mm'}$ of the nuclear density matrix, where substate m or m′ was quantized with respect to the z axis. In these formulas, however, in addition to the diagonal matrix element non-diagonal matrix elements became important and affected the line shapes for large kinematic factor $k(=dp/p/d\theta)$. These made the analysis for obtaining the substate populations of excited nucleus complicated and less accurate. We introduced here a new z axis which was chosen to point into the direction of $\theta_b+\tan^{-1}k$ in the reaction plane. By taking this z axis , the line shapes are definded only by the diagonal density matrix elements and the substate population can be extracted precisely from the line shapes. This analysis was applied to the single and mutual excitations of the 2^+ state of ^{12}C in the $^{12}C+^{12}C$ inelastic scattering which was carried out at JAERI tandem

Van de Graaf by using a newly constructed heavy ion magnetic spectrograph[2]. The spectrograph, named ENMA, has a characteristic feature that a kinematic momentum shift k is compensated from k=-0.7 to 2.0, so that a high momentum resolution is achieved for a wide range of k[2]. Fig.1 shows a spectrum of the inelastically scattered ^{12}C for the Q-value of -4.44MeV. The kinematic broadening (ΔE=1.96MeV) due to a large horizontal acceptance angle is compensated well and the line shape broadened by γ emission in flight is clearly observed in addition to the sharp peak. The m substate populations of the single and mutual excitations of the 2^+ state were derived from those line shapes. Some typical examples are shown in Fig.2. Angular distributions of m substate populations are presented in Fig.3. It was found that the substate populations of the single excitation were characterized by angular oscillations which increased in frequency with bombarding energy, while such oscillations were not observed for the substate populations of the mutual excitation.

References

1) H.G.Bohlen et al.,Phys. Rev. Lett. 37 (1976) 195 ; H.G.Bohlen and W.von Oertzen, Z.Physik A285 (1978) 371

2) Y.Sugiyama, N.Shikazono H.Ikezoe and H.Ikegami, Nucl. Instr. and Meth. 187 (1981) 25 ; Y.Sugiyama, N.Shikazono, T.Sato and H.Ikegami, Nucl.Instr. and Meth.215(1983) 17 ;Y.Sugiyama, N.Shikazono, T.Sato, T.Takayama and H.Ikegami, JAERI-M 9358 (1981) ; M.Sawada, Y.Sugiyama and E.Takekoshi, JAERI-M 83-014 (1983)

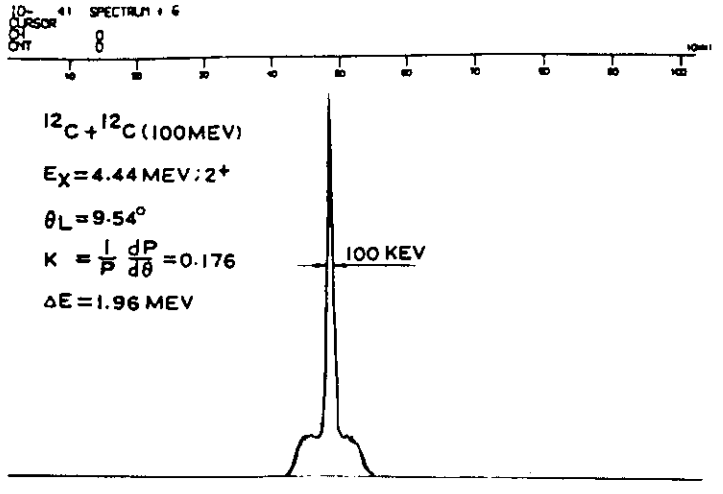

Fig.1 A spectrum of inelastically scattered ^{12}C for the Q-value of -4.44MeV

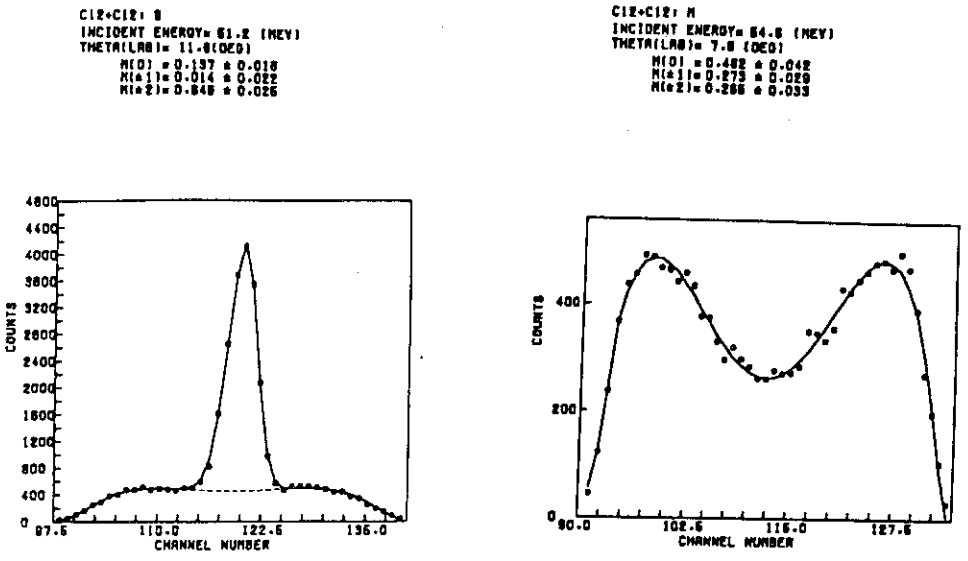

Fig.2 Characteristic line shapes of the single (left) and mutual (right) excitations and obtained m substate populations

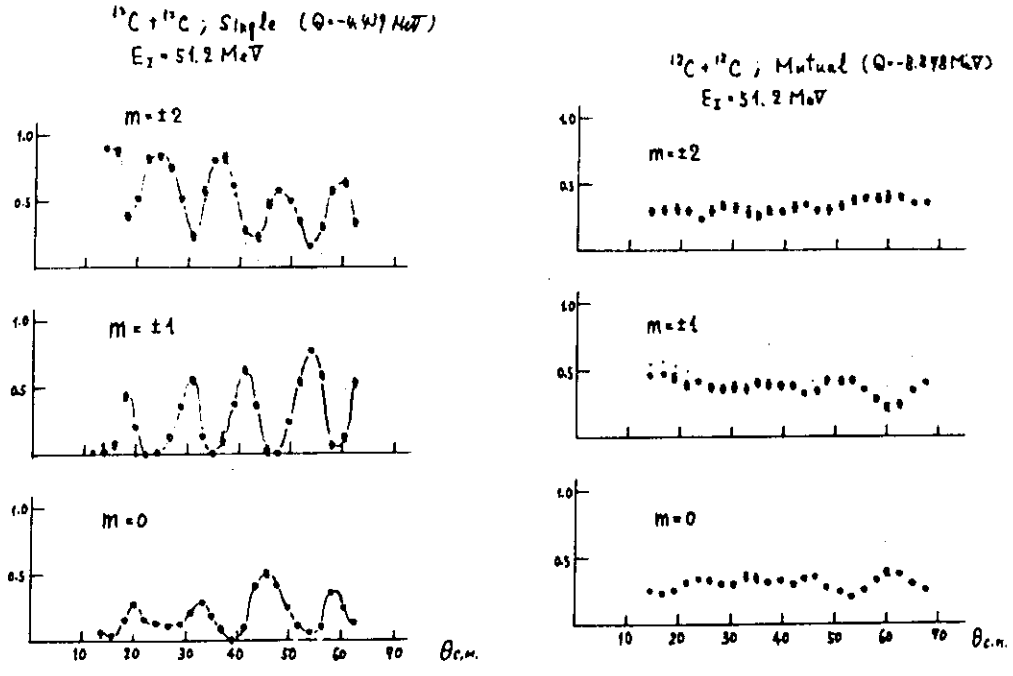

Fig.3 Angular distributions of m substate populations for the single (left) and mutual(right) excitations

I.8 Possible Quasi-Molecular Band in ^{32}S**

Shigeru Kubono

Institute for Nuclear Study, University of Tokyo,
Tanashi, Tokyo, 188 Japan

Highly excited states of ^{32}S have received a great attention from several theoretical approaches[1-6], which all predict cluster states or isomeric states with di-nuclear configuration of $^{16}O + ^{16}O$. However, little experimental studies have been made on high-lying states at excitation energy of 10 - 20 MeV in ^{32}S. There is no rotational band structure known in ^{32}S. It is known only up to spin 5^- state[7], but not 6^+ states below the $^{16}O + ^{16}O$ threshold. Therefore, it is very interesting to study highly excited high spin states in ^{32}S specifically by using the ^{16}O particle transfer reaction $^{16}O(^{20}Ne,\alpha)^{32}S$.

A 51.9-MeV $^{20}Ne^{4+}$ beam was obtained from the SF-cyclotron of the Institute for Nuclear Study, University of Tokyo. The target is a self-supporting Ta_2O_5 foil of 30 and 10 $\mu g/cm^2$. Singles α-spectra were obtained at 0° by using a QDD-type magnetic spectrograph[8] and a position-sensitive gas proportional counter[9] placed on the focal plane. A plastic scintillator placed behind the gas counter was used to get a fast timing signal for the coincidence and the time-of-flight measurements. Other experimental setups are the same as used previously for the study of ^{28}Si[10].

In the excitation energy range of 11 - 16 MeV, there are about 12 states excited clearly through the $(^{20}Ne,\alpha)$ reactions. Typical angular correlation functions obtained for the reaction $^{16}O(^{20}Ne,\alpha)^{32}S^*(\alpha)^{28}Si(g.s.)$ are shown in Fig. 1 together with the best fit curves of $a + bx|P_L(\cos\theta)|^2$. Previously, there had been no spin assignments for these states. The values of Γ_{α_0} are also derived from α_0 branching ratios and total widths (Γ). Since $\theta^2_{\alpha_0}$ is, in principle, proportional to the α-spectrroscopic factors,

this value provides a test if two states belong to the same band or not.

Some states which have similar α-reduced widths were connected by dotted lines in Fig. 2, and they seem to follow straight lines in the figure. Clearly, there are three possible positive parity bands with a large moment of inertia, the rotational constatnt $k = \hbar^2/2\mathcal{I} = 91 - 109$ keV, and also a negative parity band in between with a similar moment of inertia and with roughly the same α-reduced widths (connected with dashed lines in Fig. 2) similar to those of the lowest positive band. This large k value is quite close to k = 91 keV of $^{16}O + ^{16}O$ quasi-molecular band calculated with a microscopic α-cluster model by Schultheis and Schultheis[5]. However, these possible bands seem to be quite different from the band predicted by Ragnarsson et al.[6] in a sence of the moment of inertia. In the case of Schultheis and Schultheis, the band head energy and the k value have been adjusted simultaneously with a same multiplication factor. Therefore, if the band head energy is set to a lower value, for example 7.5 MeV, with their way, the k value becomes smaller, and the band predicted become similar to that of Ragnarsson et al. On the other hand, the band predicted by Ragnarsson et al.[6] has also a large parentage of $^{16}O + ^{16}O$ configuration. Thus, these two calculations predict very similar bands. One puzzling fact is why there are three bands with roughly the same k values but with completely different α-reduced widths within an energy range of about 1.5 MeV. Since the highest positive parity band has very small α-reduced widths and the energies are close to the $^{16}O + ^{16}O$ threshold, it could be the shape isomeric state of $^{16}O + ^{16}O$. And an interesting question is what the origin for the positive and negative parallel bands is. One possibility is that these two bands are of well developed α-cluster states and form an inversion doublet.[11] However, the moments of inertia are too large for α-cluster states as shown by the dashed line for the rigid rotor of $\alpha + ^{28}Si$ in Fig.2. This could be an interesting question to be solved theoretically.

** This work is made in collaboration with K. Morita, M. H. Tanaka, H. Utsunomiya, S. Kato, M. Sugitani, J. Schimizu, T. Tachikawa, and N. Takahashi.

References :

1) T. Ando, K. Ikeda, and A. Tosaki-Suzuki, Prog. Theor. Phys. 64, 1608 (1980)
2) D. Baye and G. Reidemeister, Nucl. Phys. A258, 157 (1976)
3) P. G. Zint and U. Mosel, Phys. Rev. C14, 1488 (1976)
4) S. J. Krieger and C. Y. Wong, Phys. Rev. Lett. 28, 690 (1972)
5) H. Schultheis and R. Schultheis, Phys. Rev. C25, 2126 (1982)
6) I. Ragnarsson, S. Aberg and R. K. Sheline, Physica Scripta 24, 215 (1981)
7) F. Haas, et al., Phys. Rev. C (1983)
8) S. Kato, T. Hasegawa and M. Tanaka, Nucl. Instr. Meth. 154, 19 (1078)
9) M. H. Tanaka, S. Kubono and S. Kato, Nucl. Instr. Meth. 195, 509 (1982)
10) S. Kubono, et al., Phys. Lett. 103B, 320 (1981)
19) K. Ikeda, private communication

Fig. 1 α-α angular correlation functions for the states deneoted. The lines are the best fit curves with a function of $a + bx|P_L(\cos\theta)|$.

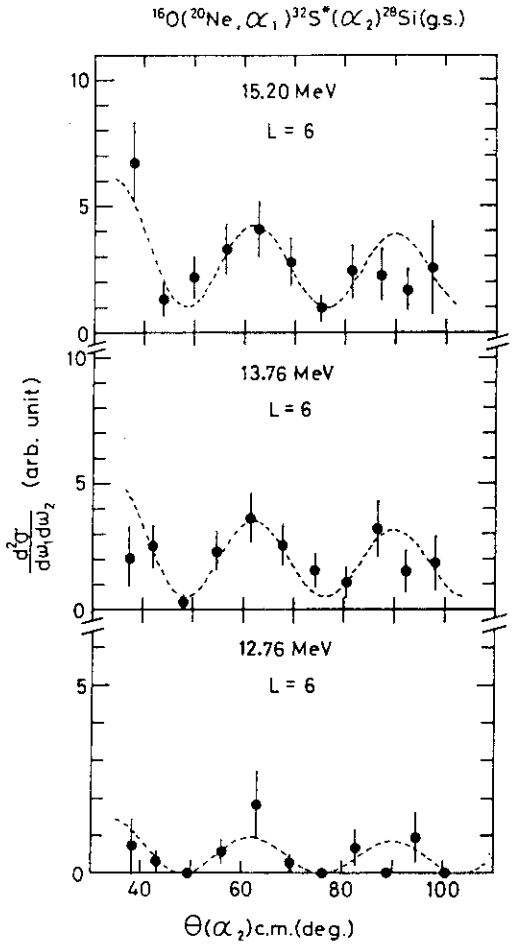

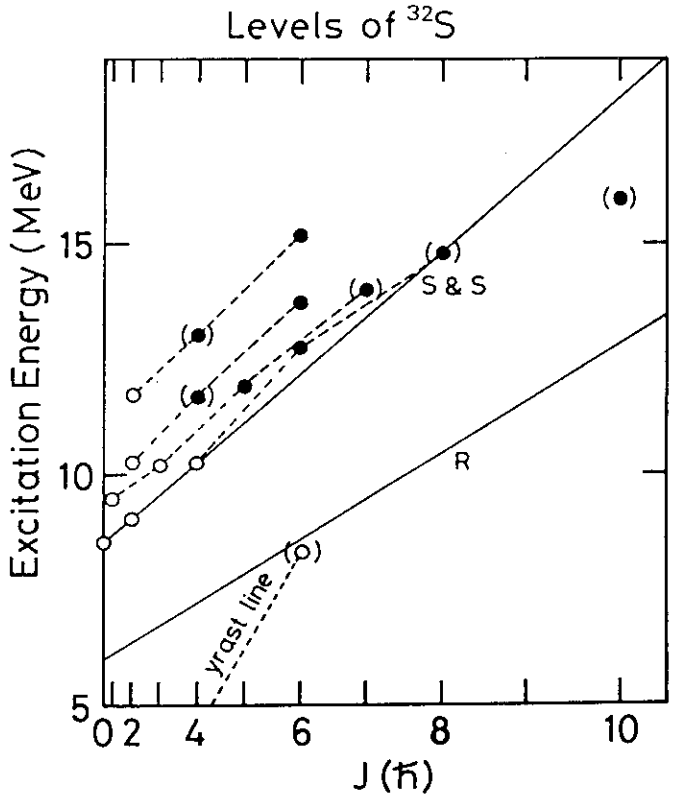

Fig. 2 Excitation energies and the spins determined in the present experiment (closed circles) together with the states known previously (open circles)[7] and possible quasi molecular bands (dashd lines), and some theoretical predictions (solid lines)[5, 6] as denoted.

I.9 Effect of the exit channel distorting potential in the $^{19}F + ^{12}C$ inelastic scattering

Toshiki Tachikawa

Department of Physics, Faculty of Science, Kyushu University

Recently the angular distributions for the elastic ($1/2^+$) and inelastic ($5/2^+$,$3/2^+$) scattering of ^{12}C from ^{19}F have been measured with the 30, 40[1], 50 and 60 MeV ^{12}C beams from the Kyushu University tandem accelerator. The data show a remarkable feature, i.e. the oscillations of the transitions to the $5/2^+$ and $3/2^+$ states are almost in phase with those of the elastic scattering. And this phase anomaly has not been able to be reproduced with the DWBA calculations using collective model form factors.

One of the possible origins may be a channel coupling effect. However, the full L=2 CC calculations among the three states ($1/2^+$, $5/2^+$ and $3/2^+$) can not improve the fit. The purpose of the present study is to make a calculation including the coupling effects which can not be incorporated or might have not yet been considered correctly. Especially we are interested in the coupling of the 2^+ state in ^{12}C. According to the study of Kubo and Hodgson[2], we have tried to obtain a DWBA exit channel distorting potential which reproduces the oscillations of the data. In the calculations the entrance potential is the same as the elastic optical potential (e.g. "D40-A" for 40 MeV, see table 1.) and the exit channel potential has been searched (The form factor is also the 1st derivative of the elastic potential.). The search of the exit channel potentials has been done only for the $5/2^+$ transition and the calculations of the $3/2^+$ transition have been made simply using the searched potentials.

The results are shown in fig. 1 and the deduced potential parameters are listed in table 1. The calculations give excellent fits to both the $5/2^+$ and $3/2^+$ data at all energies. The modified exit channel potentials (denoted by "AB") have much deeper real depths than the elastic optical potential at the nuclear surface (see fig. 2) and this variation is essential to shift the phase of the oscillations. As shown also in table 1, the nuclear deformation lengths $(\beta_2 R)_N$ are 1.2-1.7 times larger than the Coulomb deformation length $(\beta_2 R)_C$= 1.27 fm (from the Coulomb excitatin analysis). For the 2^+ transition of ^{12}C the modified potential ("D40-AB2") have a slightly shallower depth than the elastic one and the calculation using the potential "D40-AB" can not explain the data at all.

The large discrepancy between real parts of the entrance and exit cha-

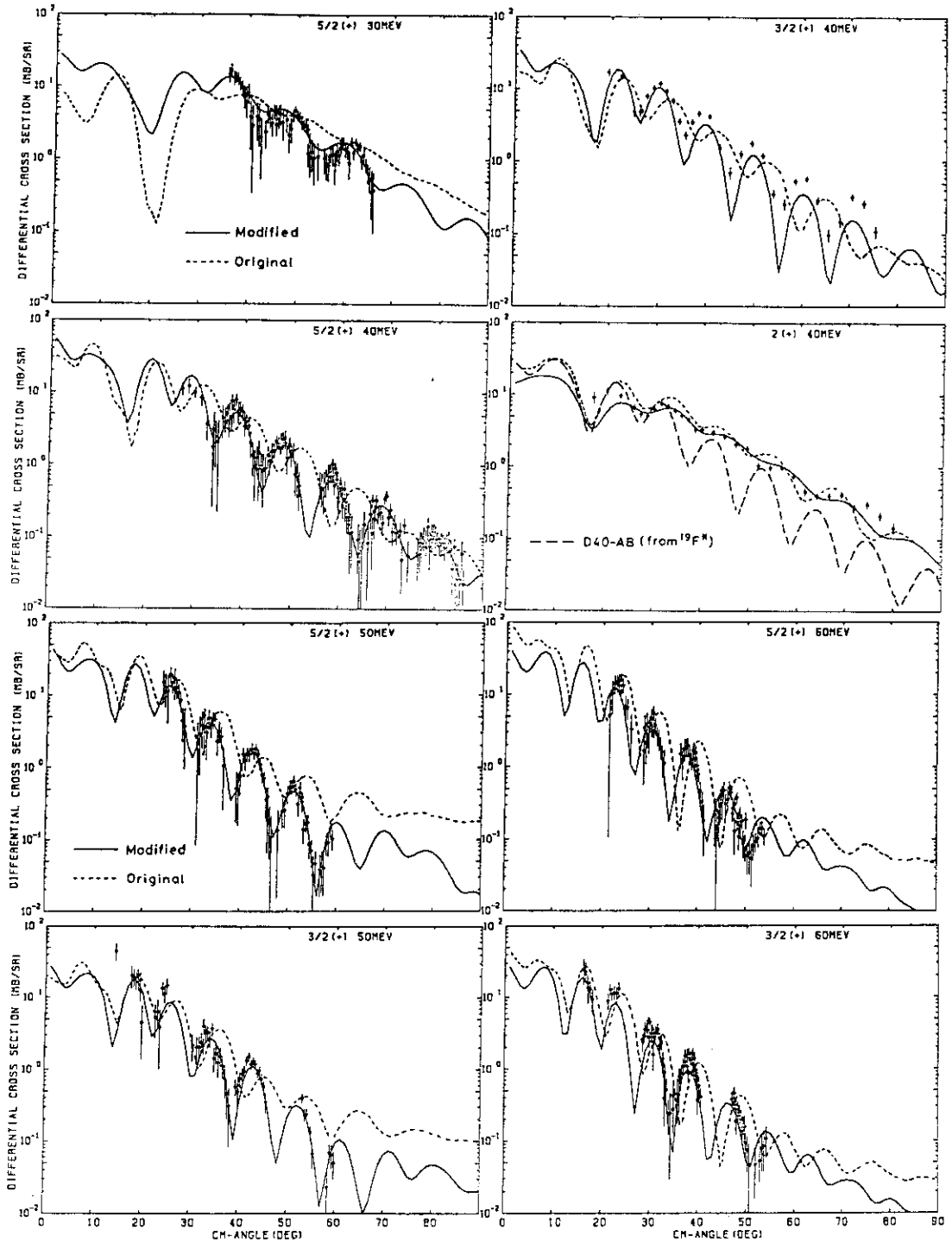

Fig. 1. DWBA calculations using the modified potentials (solid lines) and the original elastic optical potentials (dashed lines) as the exit channel distorting potentials.

nnel potentials is a contrast to the result for the $^{40}Ca + ^{16}O$ system[2),3)], where only an imaginary part is required to be modified. Our result agrees with the analysis of the $^{154}Sm(\alpha,\alpha')$ data[4)]. However, the present exit channel distorting potential can not reproduce the data at all when it is used as a CC potential. Another problem is what (including the elastic optical

potentials and the modified exit channel potentials) should be used for the form factors. The $(\beta_2 R)_N$ values are much influenced by this choice. (If the exit channel potential is used, too small value (0.85 fm for 40 MeV) is needed.)

Table 1. Optical Potentials for modified DWBA** calculations

SET	V_R (MeV)	r_{0R} (fm)	a_R (fm)	W_I (MeV)	r_{0I} (fm)	a_I (fm)	$(\beta_2 R)_N$ (fm)
D40-A	286.7	0.862	0.654	22.6	1.030	0.819	1.58
D30-AB	352.6	0.962	0.696	41.8	1.096	0.388	2.10
D40-AB	310.6	0.997	0.684	37.8	0.811	0.704	2.16
D50-AB	296.9	1.008	0.668	12.8	1.350	0.350	1.64
D60-AB	310.6	0.997	0.684	79.4	1.169	0.436	1.53
D40-AB2*	327.4	0.824	0.597	26.0	1.081	0.467	0.98

**) $T_{fi} = \langle \phi_f^{(-)} | V | \phi_i^{(+)} \rangle$

(AB) (A) (A)

*) $^{12}C^*(2^+)$ at $E(^{12}C)$=40 MeV

Finally it is found that 2^+ coupling does not seem to be effective to improve the fit. Indeed there is no rule that the two potentials, "D40-AB" and "D40-AB2", must be equal. Exact CC calculations including the 2^+ coupling are required to solve this problem.

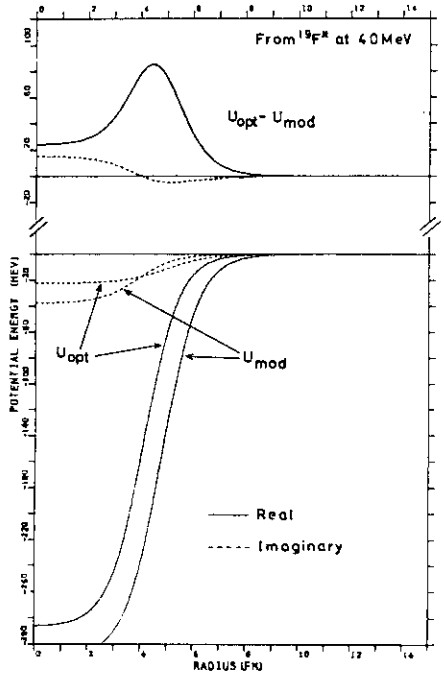

Fig. 2. Modified exit channel distorting potential U_{mod}(D40-AB) with the elastic optical potential U_{opt}(D40-A). The upper curves show the difference between them.

References

1) T.Tachikawa, K.Anai, H.Fujita, N.Kato, K.Kimura, Y.Nakajima and T.Sugimitsu: Genshikaku-Kenkyu 27 (1983) 43.

2) K.-I.Kubo and P.E.Hodgson: Nuclear Phys. A336 (1981) 320

3) K.E.Rehm, W.Henning, J.R.Erskine and D.G. Kovar: Phys.Rev.Letters 40 (1978) 1479

4) A.J.Baltz, N.K.Glendenning, S.K.Kauffmann and K.Pruess: Nuclear Phys. A327 (1979) 221

I.10 Spin Polarization in (^{14}N,α) reaction

K. Ieki

Department of Physics, Tokyo Institute of Technology

In recent years, several measurements[1-3] of spin polarization have been made in heavy ion dissipative reactions, providing valuable information for reaction mechanisms. In this work, we study spin polarization of residual nuclei in (^{14}N,α) reactions by measuring circular polarization of emitted γ ray. In such light heavy ion induced reactions, energetic light particles(p,α,...) are known to be emitted strongly in forward directions. Systematic study of spin polarization will bring a new sight for fast light particle emission phenomena.

Self supporting foils of ^{159}Tb, ^{181}Ta, ^{93}Nb, ^{nat}Ni, whose thicknesses are 3.4, 4.3, 4.3 and 2.7 mg/cm^2 respectively, were bombarded with 115 MeV ^{14}N beam from the RIKEN cyclotron. The experimental method used was essentially the same as that of Trautmann et al[4]. Gamma ray circular polarization was measured using two identical sets of forward scattering type polarimeters, in which γ rays were Compton scattered on the surface of iron magnet and detected in 6"ϕx6" NaI detector. The polarimeters were placed at both sides of the normal directions to the reaction plane. Ejected particles were detected with two sets of counter telescopes consisting of 50 μm and 1500 μm Si-solid state detectors. They were placed at symmetric angles with respect to the beam axis.

In fig. 1, the polarization spectra vs energy E_α of ejected α particle detected at 30° are shown for various targets. For lighter targets(^{nat}Ni, ^{93}Nb), polarization values P_z are small and shows rather flat distributions. These results are qualitatively consistent with a simple picture that nucleons are transfered in multi step process, reducing P_z value significantly. On the contrary, the results for heavier targets(^{159}Tb, ^{181}Ta) show a quite different feature. P_z values are mainly negative and depend on E_α.

P_z values for θ=20°, 30°, 40°, 50° in ^{159}Tb(^{14}N,α) reactions at 115 MeV are shown in a form of a contour plot(fig.2). This figure clearly shows a dip structure of the negative P_z located at beam velocity energy and grazing angle for this reaction. These facts are characteristic for peripheral type reactions and suggest a contribution of direct-type process, in which a massive cluster(^{10}B) may be transfered to the target, in addition

to the multistep process.

This work was performed in collaboration with M.Ishihara, T.Inamura, S.Kohmoto(RIKEN), H.Utsunomiya(MSU), K.Sueki(Tokyo Metropolitan Univ.) and H.Kudo(Niigata Univ.).

references

1) K.Sugimoto et al., Phys. Rev. Lett. 39 (1977) 323.

2) W.Trautmann et al., Phys. Rev. Lett. 39 (1977) 1062.

3) T.Sugitate et al., Nucl. Phys. A388 (1982) 402.

4) W.Trautmann et al., Nucl. Inst. Meth. 184 (1981) 449.

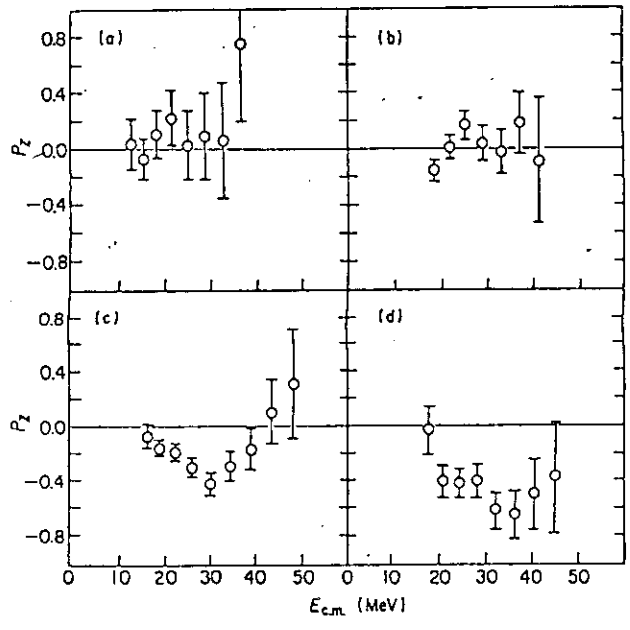

fig.1 P_z vs E for ^{14}N-induced reactions at 30°: (a) ^{nat}Ni, (b) ^{93}Nb, (c) ^{159}Tb, (d) ^{181}Ta.

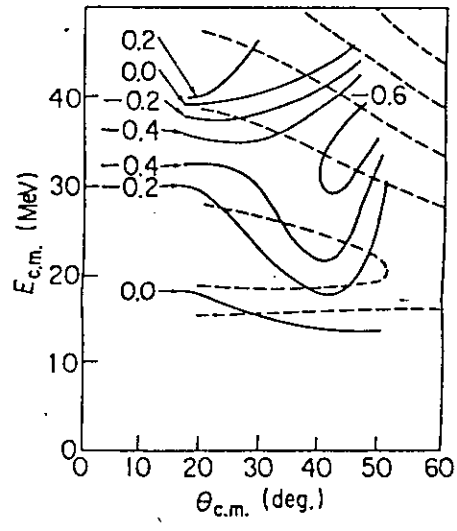

fig.2 Contour plots of P_z(solid line) and yield (dashed line, log scale) for $^{159}Tb(^{14}N,\alpha)$ reaction. P_z is plotted in 0.2 step.

I.11 Coincidence Measurement Between Evaporation Residues and Light Particles Produced in $^{16}O+^{40}Ca$ Reaction

Hiroshi Ikezoe
Division of Physics, Tokai Research Establishment, JAERI

1. Introduction

The incomplete fusion processes where full linear momentum has not been transfered to the compound nucleus have been observed at higher bombarding energies(E>8-10 MeV/A).[1] These processes are experimentally characterized by a velocity deficit of the fusion residues or too large a folding angle of the fusion-fission fragments.[2,3] The phenomenological studies such as velocity measurements of evaporation redidues or the target-projectile dependence on the linear momentum transfer,have been performed.[4] Since experimental distinguishing of the incomplete fusion processes from the complete fusion processes is difficult, the detail of the reaction mechanism giving rise to the incomplete fusion process is not well understood. In the present study the velocity(or energy) spectra of both the evaporation residues and the light particles detected in coincidence were measured with the motivation of better understanding the reaction mechanism.

2. Experimental Procedure

Coincidence measurement of the evaporation residues with the light particles were performed for the reaction $^{16}O+^{40}Ca$ using beams of ^{16}O 157 MeV from the Argonne National Laboratory Superconducting Lineac. The masses and the velocities of the evaporation residues were measured at $\theta_{lab}=9°$ using a channelplate/Si detector time-of-flight telescope with the flight path of 1.1m. The velocity versus mass spectrum obtained is shown in Fig.1. The light particles were identified and their energy spectra measured in six triple Si detector telescopes located at $\theta_{lab}=+58.6°,+28°,-15°,-25°,-40°,-70°$, where the negative angles indicate angles on the opposite side of the beam from the time-of-flight telescope. During the coincidence

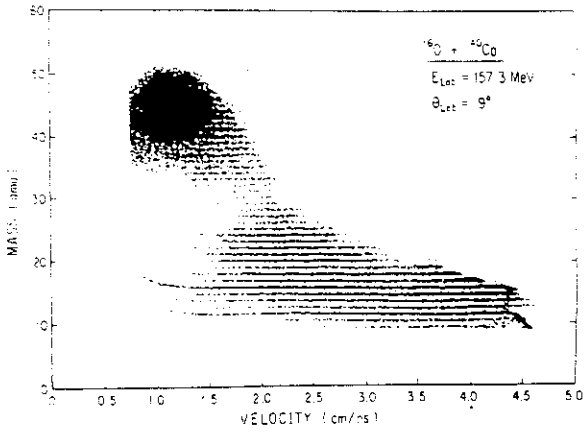

Fig.1 Velocity-mass spectrum of the reaction products from 157 MeV ^{16}O on ^{40}Ca at 9°.

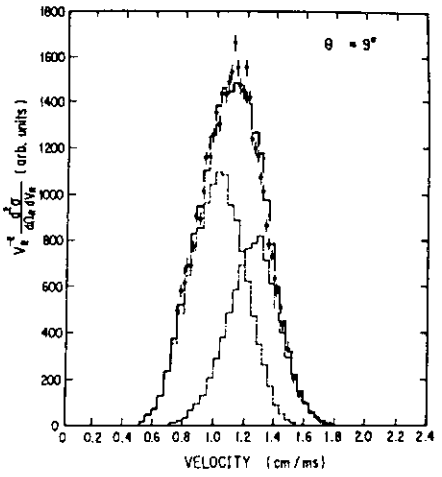

Fig.2 Summed spectrum of single residues (mass≥40) compared with LILITA calculations; $^{16}O+^{40}Ca$(dash-dotted line) and $^{12}C+^{40}Ca$(dashed line). The solid line is the sum of the two calculations.

experiment the velocities of the singles evaporation residues were also recorded. The residue velocities were corrected for the thickness of the target and the carbon foil of the channel plate detector. However the velocity corrections due to the plazma delays in the Si detector was not performed and only taken into account in the error estimation.

3. Experimental Results

The singles evaporation residues $V_R^{-2}d^2\sigma/d\Omega_R dV_R$ of the mass number from 40 to 52 have the average velocity centroid 9.4 $\pm\frac{1}{3}$ % lower than the value $V_c\cos\theta_{lab}$ of the complete fusion, consistent with the results of Chan et al.,[5] where V_c is the velocity of the center of mass system. The summed spectrum(Fig.2) of the singles residue masses from 40 to 50 was compared with the statistical model calculation using the program code LILITA.[6] In order to avoid the ambiguity of the calculation due to the unknown complete fusion cross section, the three different fusion cross sections(500,830,1100 mb) were assumed as a input parameter. Since besides the velocity deficit the observed width of the velocity spectrum was larger than those of the calculations, we considered that the observed velocity

spectrum has an extra compoment besides the statistical evaporation compoment. If the LILITA predictions are normalized to reproduce the higher velocity side of the observed velocity spectrum and subtructed from the data, a Gaussian shape compoment is obtained, whose velocity centroid is about 18% lower than the $V_c\cos\theta_{lab}$. The position of the velocity centroid of the extra compoment does not depend on the assumed values of the fusion cross section. If one assumes that the fast α particles with the beam velocity escape from the projectiles toward the forward direction before the thermal equilibrium is reached and the rest of the projectile and the target fuse together with smaller linear momentum 12/16 of the initial one, the velocity centroid of such fused system would be 19% lower than the $V_c\cos\theta_{lab}$. Therefore the extra compoment may correspond to the evaporation residues from an incompletely fused system where the beam velocity α particles are emitted before fusion. In order to confirm this possibility, the simulation calculation of the $^{12}C+^{40}Ca$ fusion reaction using the LILITA was performed, assuming that ^{16}O projectiles break up into ^{12}C and α and then ^{12}C fuse together with the ^{40}Ca target. In this calculation, the same incident energy per nucleon(9.8 MeV/A) as those of beams and the angular momentum window of ℓ=29-34$\hbar$ were assumed.Figure 2 shows the fitting of the data with the two LILITA calculations (the $^{16}O+^{40}Ca$ fusion and the $^{12}C+^{40}Ca$ fusion), where only relative normarization was changed to reproduce the data. From this analysis, the relative yield of the incomplete fusion reaction was estimated to be 35-50% of the total fusion yield at the θ_{lab}=9°, where the uncertainty mainly comes from the plazma delay in the Si detector(less than 3% of the $V_c\cos\theta_{lab}$).

The proton energy spectra in coincidence with the evaporation residues are shown in Fig.3 together with the LILITA predictions, where the fusion cross section 830mb was assumed. There is no higher energy component and their spectrum shapes can be reproduced by the predictions except the most probable energies. The fact that the most probable energies are smaller than those calculated has been also found by Gonthier et al. in the ^{16}O(310MeV)+Ti reaction.[7] Although it is not obvious wheter or not this smaller most probable energies are caused by the proton evaporations from the incompletely fused system, the protons

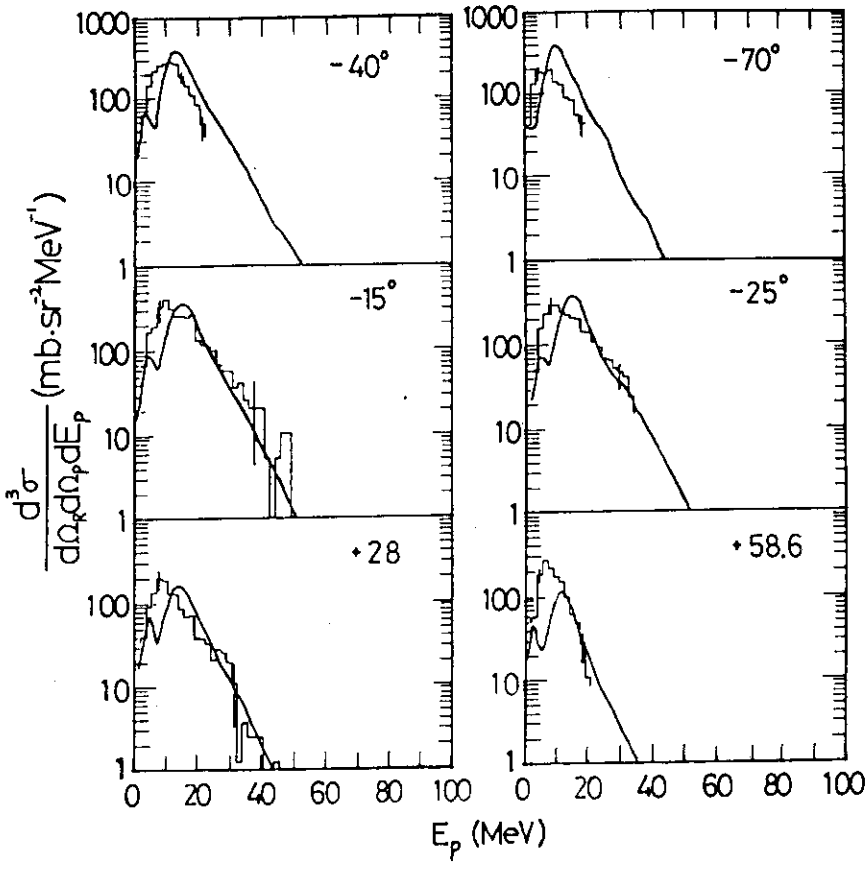

Fig.3 Proton energy spectra detected in coincidence with evaporation residues(mass≥40) observed at 9° in the reaction of 157 MeV ^{16}O with ^{40}Ca. Error bars represent the statistical errors.

are seemed to be mainly evaporated from the statistically equilibrated compound nucleus.

The velocity shift of the evaporation residues spectra $V_R^{-2}d^3\sigma/d\Omega_R d\Omega_P dV_R$ in coincidence with proton are plotted in Fig.4a as a function of the proton detection angles. The measured centroids have the middle values between the complete fusion and the incomplete fusion calculations. If the velocity centroid predicted for the $^{16}O+^{40}Ca$ fusion reaction are shifted toward lower velocity with the amount of 9.4% which is shown as the dotted line in Fig.5a, the measured velocity centroids can be reproduced. Therefore this result, together with the evaporation like character of the proton energy spectra, suggests that the protons are statistically evaporated from a

slow moving source whose velocity is about 9.4% lower compared with that of the completely fused system. The value 9.4% is also the velocity centroid shift of the singles evaporation residues. Thus the statistical evaporations from both the complete fusion reaction and the incomplete fusion reaction can be ascribed to the particle evaporation from the 9.4% slow moving source.

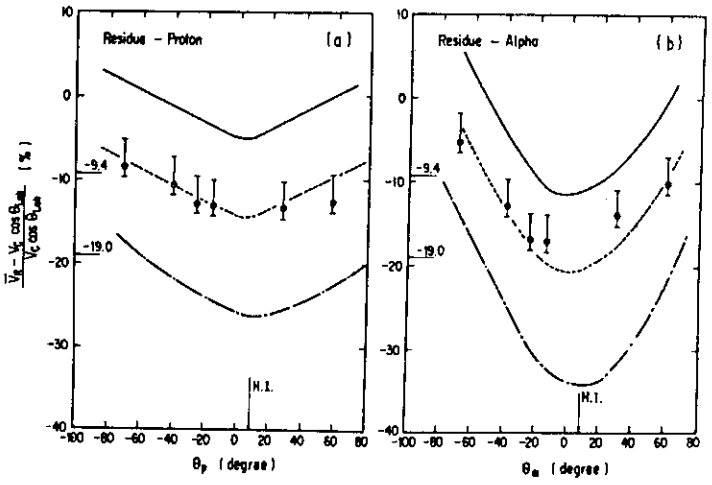

Fig.4 Velocity shifts of evaporation residues (mass≥40) detected in coincidence with (a) proton and (b) alpha together with LILITA calculations ; $^{16}O+^{40}Ca$(solid lines) and $^{12}C+^{40}Ca$(dash-dotted lines). The dashed lines are the 9.4% shifted ones from the solid lines.

Alpha energy spectra in coincidence with the evaporation residues(40≤A≤52) are shown in Fig.5 together with the LILITA predictions. The energy spectra have higher energy components at θ_{lab}=-15° and -25° compared with the predictions. Especially at the θ_{lab}=-25°, the higher energy component is peaked around the beam velocity α ($E_\alpha \cong 40$MeV). On the other hand at the backward angles and at the positive angles, no such higher energy component was observed and the spectrum shapes are almost similar to the predictions. Almost the same results were obtained by Gonthier et al.[7], where non-statistical evaporation components in coincidence with α are mainly concentrated at the forward angles, opposite side of the time-of-flight telescope.

The velocity centroids of the evaporation residue velocity spectra $V_R^{-2}d^3\sigma/d\Omega_R d\Omega_\alpha dV_R$ in coincidence with α particles are shown in Fig.4b. The measured velocity centroids are lower than the LILITA prediction for the $^{16}O+^{40}Ca$ fusion reaction and can be reproduced by the 9.4% shifted line from the prediction as discussed for the proton case. This fact, together with the evaporation like character of the α energy spectra at the backward angles (θ_{lab}=-40°,-70°) and

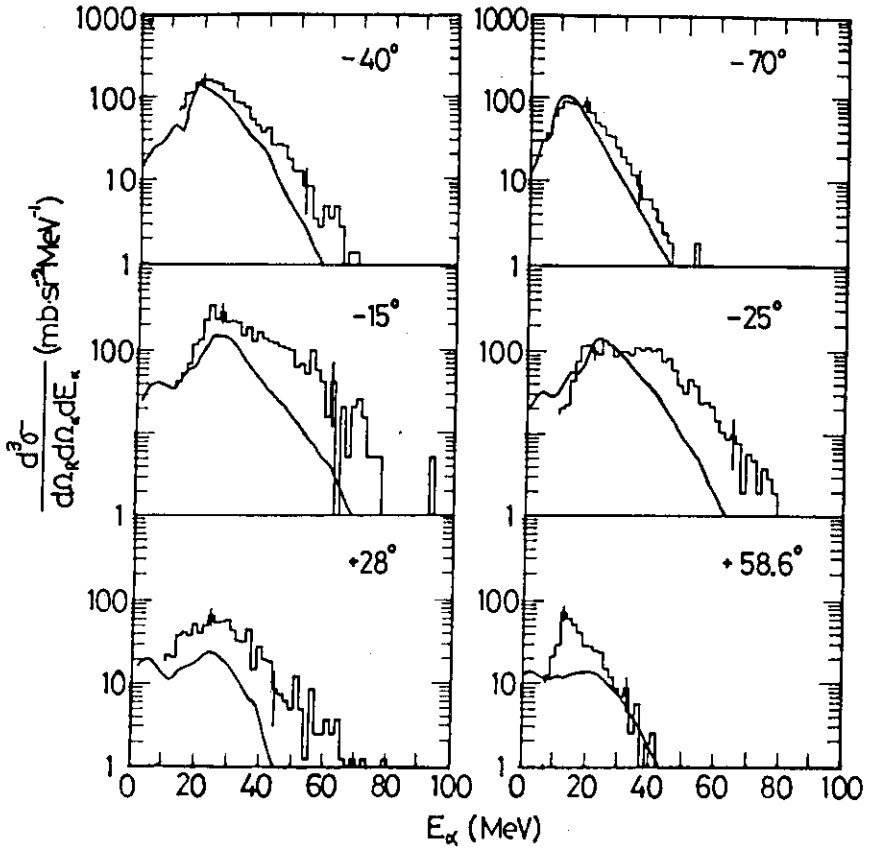

Fig.5 Alpha energy spectra detected in coincidence with evaporation residues(mass≥40) observed at 9° in the reactions of 157 MeV ^{16}O with ^{40}Ca. Error bars represent the statistical errors.

at the positive angles, suggests that the α particles emitted at these angles in coincidence with the evaporation residues come from the statistical evaporation from the 9.4% slow moving source. On the other hand, the α particles emitted at the forward angles(θ_{lab}=-15° and -25°) have non-statistical component or the beam velocity component in addition to the statistical evaporations. The velocity centroids of the evaporation residues in coincidence with these components should shift with the amount of 19%, if these α particles are emitted with the beam velocity from the projectiles or the pre-equilibrium stage of the compound nucleus. Since the velocity spectra of the evaporation residues in coincidence with the lower portion of the α energy spectra would have the velocity centroid indicated by the 9.4% shifted line in Fig.5b, two

velocity centroids, one corresponds to the evaporation residues in coincidence with the beam velocity α and the other in coincidence with the statistical component of the lower energy α, would coincide each other. In order to make sure that the lower and the higher energy components of the α energy spectra give rise to the same velocity deficit in the evaporation residues, the energy gates E_α<30MEV and E_α>30MEV were put on the α energy spectra and the velocity centroids of the evaporation residues in coincidence with these gates were examined. The velocity centroid gated by the E_α>30MEV was only 1∿2% lower than those gated by the E_α<30MEV, although the LILITA calculations predict the large kinematic velocity shift of 7∿8% between the velocity spectra gated by the same conditions at forward directions.

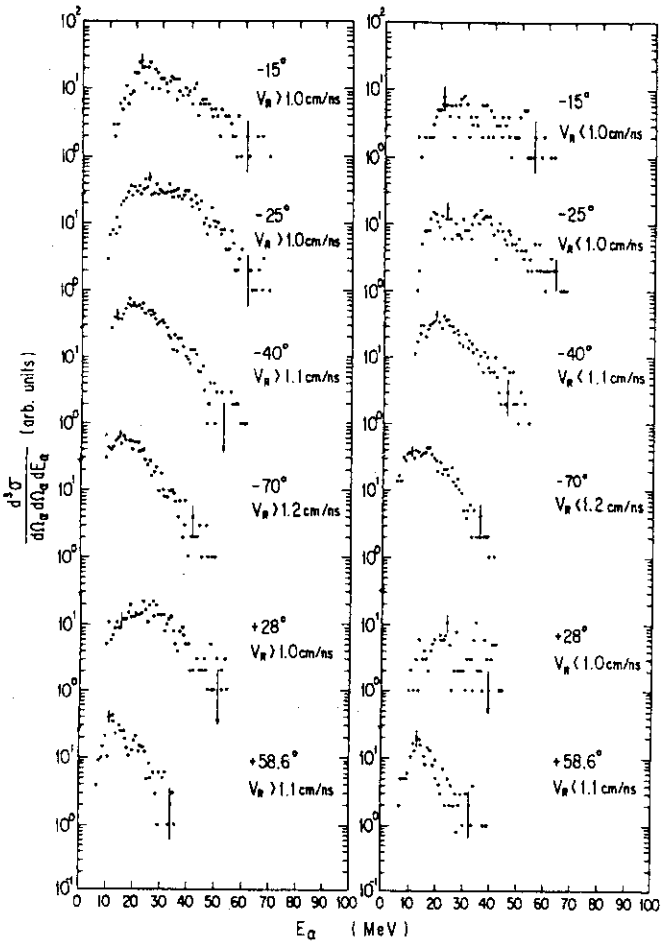

Fig.6 Alpha energy spectra gated by the velocities V_R of the evaporation residues (mass≥40).

The gates were also put on the evaporation residue velocity spectra to examine the α energy spectra. If the lower velocity portions of the evaporation residue spectra are mainly contributed from the incomplete fusion processes, the α energy spectra gated by the lower portions of the residue velocities would have relatively large yield of the beam velocity components compared with the yield of the lower energy

portions at the forward angles. They would have almost the same shapes as the ungated spectra at the backward angles and at the positive angles, because those energy spectra would have only the statistical evaporations from the incomplete and the complete fusion processes and these statistical evaporations would have similar shapes. The gated α energy spectra are shown in Fig.6.

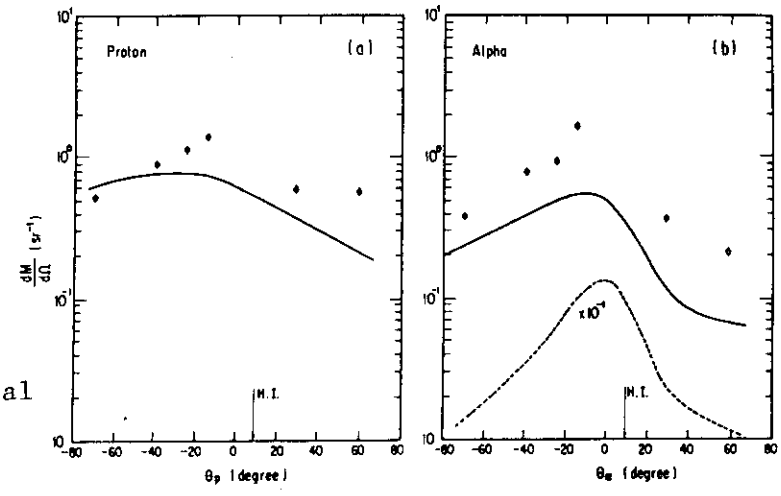

Fig.7 Differencial multiplicities of (a) proton and (b) alpha. The angle of the residue counter is indicated by the arrow (H.I.). The solid lines are the LILITA calculations and the dashed line indicates the yield difference between the data and the calculation.

The α energy spectrum gated by the residue velocity V_R<1.0cm/ns at the θ_{lab}=-25° has the enhanced beam velocity compoment compared to the other spectrum gated by the V_R>1.0cm/ns condition. At the backward angles and at the positive angles, the gated spectra have almost the same shapes as the ungated spectra. These experimental evidences strongly suggest that with certain probability the fast α particles are emitted with the beam velocity at forward directions and then the α particles and proton are statistically evaporated from the incompletely fused systems in addition to the particle evaporations from the completely fused systems.

The differencial multiplicities $dM/d\Omega_\alpha$ and $dM/d\Omega_p$ for the α particles and proton are shown in Fig.7 together with the LILITA calculations. The $dM/d\Omega_\alpha$(or $dM/d\Omega_p$) was defined as the ratio of the coincidence cross section to the singles evaporation residues cross section at the θ_{lab}=9°. The $dM/d\Omega_p$ has the same magnitude as the prediction at the backward angles. At the forward angles and at the positive angles the discrepancy between the data and the prediction becomes large. The α differencial multiplicity is almost twice as large

as those of the prediction. Especially at the forward angles, the discrepancy becomes more larger. The yield difference of the $dM/d\Omega_\alpha$ between the data and the prediction is forward peaked(a dotted line in Fig.7). This result is consistent with the forward peaking angular distribution of the α particles concerning to the incomplete fusion processes and also consistent with the large yield of the incomplete fusion component observed in the singles evaporation residues spectrum.

4. Summary

We have studied the incomplete fusion processes of the $^{16}O+^{40}Ca$ reaction by detecting the evaporation residues in coincidence with the light particles. The velocity spectrum of the singles evaporation residues have velocity deficit of $9.4\pm\frac{1}{3}$% compared with the completely fused system and this imply that the spectrum consists of the two components, one is the incomplete fusion processes and the other the complete fusion processes. The direct evidence of the incomplete fusion processes were observed in the α energy spectra in coincidence with the evaporation residues, which have the non-statistical compoment or the beam velocity compoment at the forward angles and the statistical character at the backward and the positive angles. The proton spectra are almost similar to the statistical model prediction and can be ascribed to the statistical evaporation from the 9.4% slow moving source in consequence of the sizable probability of the incomplete fusion processes. The evaporation residues velocity spectra in coincidence with the light particles can be consistently explained by taking into account the fast α particle emission following the fusion evaporation processes.

The experimental work has been performed in collaboration with D.G.Kovar, G.Rosner, G.Stephans, E.Ungricht, and B.Wilkins(ANL), and C.Maguire, Z.Kui, W.C.Ma, S.Robinson, D.Watson, and G.Word(Vanderbilt Univ.), and T.C.Awes, and G.Young(ORNL). The author wish to acknowledge the operation staff of the Argonne National Laboratory Tandem-Lineac.

References:

1. H.Morgenstern, W.Bohne, K.Grabisch, D.G.Kovar, and H.Lehr, Phys. Letts. 113B, 463 (1982).
2. B.B.Back, K.L.Wolf, A.C.Mignerey, C.K.Gelbke, T.C.Awes, H.Breuer, V.E.Viola,Jr., and P.Dyer, Phys. Rev. C22, 1927 (1980).
3. J.R.Huizenga, J.R.Birkelund, L.E.Tubbs, D.Hilscher, U.Janke, H.Rossner, B.Gebauer, and H.Lehau, Phys. Rev. C28, 1853 (1983).
4. G.Rosner, D.G.Kovar, P.Chowdhury, D.Henderson, H.Ikezoe, R.V.F.Janssens, W.Kuhn, G.S.F.Stephans, B.Wilkins, F.Prosser,Jr., J.Kolata, and J.Hinnefeld, Bulletin of the American Physical Society (1983).
5. Y.Chan, M.Murphy, R.G.Stokstad, I.Tserruya, and S.Wald, Phys. Rev. C27, 447 (1983).
6. J.Gomez del Campo and R.G.Stokstad, Oak Ridge National Laboratory Report, 1977 (unpublished).
7. P.L.Gonthier, H.Ho, M.N.Namboodiri, J.B.Natowitz, L.Adler, S.Simon, K.Hagel, S.Kniffen, and A.Khodai, Nucl. Phys. A411, 289 (1983).

I.12 Breakup Effects of ^{6,7}Li on the Elastic and Inelastic Scatterings from ^{12}C

Kenji Katori, Tadashi Shimoda, Tomokazu Fukuda, Susumu Shimoura*, Atsushi Sakaguchi*, Tamiho Yamagata**, Masayoshi Tanaka***, Hiroshi Ogata+, Noriaki Takahashi++, Yukinori Sakuragi+++ and Masayasu Kamimura+++

Laboratory of Nuclear Studies,Osaka University,*Department of Physics,Kyoto University,**Department of Physics,Konan University,***Kobe Tokiwa Junior College,+Research Center for Nuclear Physics,Osaka University,++College of General Education,Osaka University and +++Department of Physics,Kyushu University.

In their systematic analyses of elastic scattering induced by heavy-ions from Li to O, Satchler and Love pointed out that the usual double-folding model failed to reproduce the angular distributions of ^{6}Li, ^{7}Li and ^{9}Be[1]. Half of the strength was required for the real part of the optical potential to fit data, in contrast to the right prediction for the other ions. Several authors have tried to explain this anomaly of the potentials. Kamimura et al. recently pointed out that this overprediction is due to the breakup effect of ^{6}Li and ^{7}Li projectiles[2]. Nuclear structure of ^{6}Li is different from that of ^{7}Li in many points:(1) quadrupole-moment,(2) breakup threshold energy,(3) properties of excited states and (4) non-resonant parts of unbound states. In lower bombarding energies, observables of elastic scattering for ^{6}Li considerably differ from those for ^{7}Li.

In the present paper, we have measured differential cross sections for elastic and inelastic scatterings of ^{6}Li and ^{7}Li from ^{12}C and analyzed them by using double folding potential and coupled channel method. To investigate stability of normalization factor (N_R) for the bombarding-energy variation and projectile variation, we have chosen the highest bombarding energies as high as 123.5 MeV and 168.8 MeV for ^{6}Li and 131.8 MeV for ^{7}Li[3]. The ^{6,7}Li^{3+} ions were obtained by backbombarding the LiF crystal by Xe and Ar ions and accelerated by the 230 cm AVF cyclotron at Research Center for Nuclear Physics Osaka University. The data are taken by a conventional ΔE-E Si counter telescope and a position-sensitive detector placed at backward angles.

Results and Analyses

Experimental results are shown in Fig.1,2, 3 and 4. Elastic scattering data were analyzed by the double folding potential in which both real and imaginary parts were chosen in the same form and the strengths were independently searched to fit data. The potential used is

$$U(\vec{R})=-(N_R+N_I^i)\int \rho_{ij}^{Li}(\vec{r}_1)\,\rho_{00}^{^{12}C}(\vec{r}_2)\,v_{NN}(\vec{r}_1+\vec{R}-\vec{r}_2)\,d\vec{r}_1\,d\vec{r}_2$$

v_{NN} is an effective nucleon-nucleon interaction (M3Y) and $\rho_{00}^{Li}(\vec{r})$ and $\rho_{00}^{^{12}C}(\vec{r})$ are ^{6}Li-(^{7}Li-) and ^{12}C-density distributions described by the d+α (t+α) and 3α RGM wave functions, respectively[2]. The best fit to experimental cross sections at E= 123.5,168.8 MeV for ^{6}Li and 131.8 MeV for ^{7}Li was attained with the normalization factors of N_R=0.715,0.660 and 0.68, respectively as shown in Fig.1 and 3. The overprediction of the strength of the real part of the potential is clearly noticed by the same factor for both ^{6}Li and ^{7}Li. In order to verify whether this overprediction is attributed to the breakup effect, the coupled-discretized-continuum-channels calculations were performed, which involved resonant- and non-resonant-parts in excited states of ^{6}Li and ^{7}Li properly. Both experimental cross sections for ^{6}Li and ^{7}Li were reproduced with the normalization factor of N_R=1.0 in the quality similar to those in one-channel calculation of double-folding model as shown in Fig.1 and 4. Therefore, it is concluded that the overprediction of the real part of the potential for both ^{6}Li and ^{7}Li needed in the usual double-folding model is due to the breakup effect of projectiles on the elastic channel. It is remarkably noted that in spite of different structures of ^{6}Li and ^{7}Li and different bombarding energies, the normali-

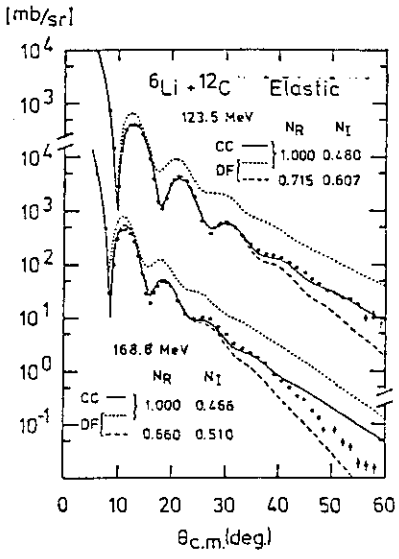

Fig.1. Experimental and calculated cross sections for elastic scattering of ^{6}Li at E=123.5 and 168.8 MeV.

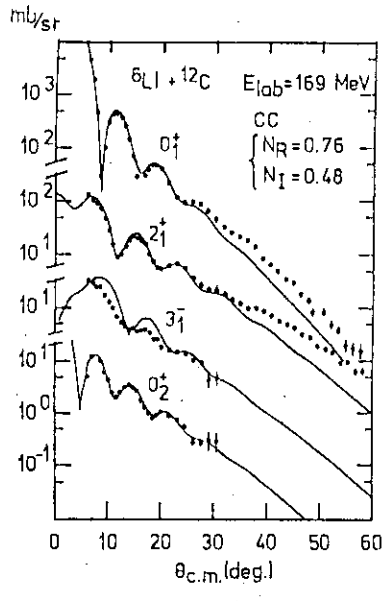

Fig.2(a). Experimental and calculated cross sections for inelastic scatterings of ^{6}Li from ^{12}C at E=168.8 MeV.

zation factors of N_R recover to unity within allowable adjustment of N_I for the imaginary part of the potential.

Inelastic scattering data of ^{6}Li and ^{7}Li from ^{12}C at E=123.5 and 168.8 MeV for ^{6}Li and 131.8 MeV for ^{7}Li were analyzed by folded transition potential calculated in the same procedure as that for the usual double-folding model for the elastic scattering. The transition density distribution for the 2^+(4.44MeV),0_2^+(7.65MeV) and 3_1^-(9.64MeV) states are consistently and uniquely determined in the 3α RGM calculation for ^{12}C[4],which describes the density distribution of the ground state. The differential cross sections were calculated in coupled-channel method between the ground and three excited states of ^{12}C. For simplicity,the potential of the elastic scattering was taken as one-channel double-folding one with the normalization factor of N_R=0.77,0.76 for ^{6}Li and 0.68 for ^{7}Li as indicated in Table I. Angular distributions for the inelastic scattering and the relative yields for the four states are quite well reproduced as shown in Fig.2 and 3. The angular distribution for the 0_2^+(7.65MeV) state which has hardly reproduced well by the usual DWBA calculation is satisfactorily reproduced. It is rather surprising that the enhancement of $\sigma(0_2^+,7.65\text{MeV})/\sigma(2_1^+,4.44\text{MeV})$ by a factor of two in comparison to that for (p,p') and (α,α') scatterings is well described without any adjustable parameters used. This enhancement factor can be explained by the coherent effect which is caused by both a difference of the wave functions between the 2_1^+,4.44MeV state(a bound state) and the 0_2^+,7.65 MeV state(an unbound state) and a distortion of

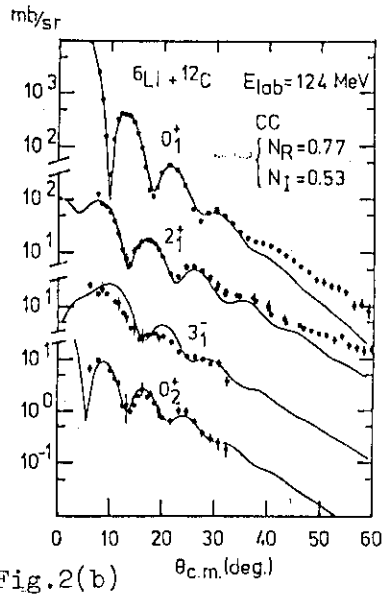

Fig.2(b)

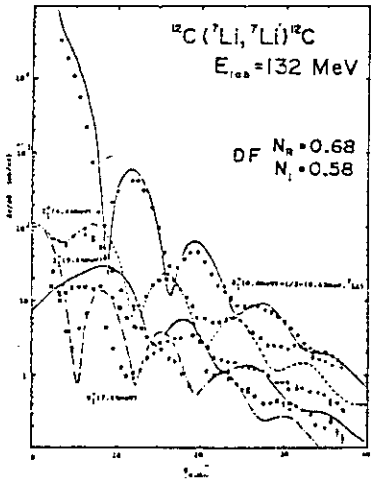

Fig.3. Elastic and Inelastic scatterings of ^{7}Li.

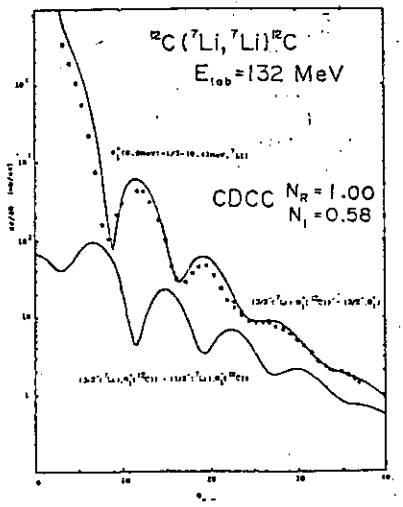

Fig.4. Elastic scattering.

waves at the nuclear surface which are strongly influenced by the breakup.

For the double-folding potential which takes into account the coupled channel effects between three excited states of ^{12}C, the volume integral of the real part of the potential was obtained. These are 259.5 MeV.fm^3 ,256.1 MeV.fm^3 for 123.5 MeV ^6Li and 168.8 MeV ^6Li and 229.0 MeV.fm^3 for 131.8 MeV ^7Li. These values are consistent to those deduced from the A_T-dependence of the optical potential for ^6Li and ^7Li extracted at lower bombarding energies [5]. Those are quite small, compared with the values extended from the projectile mass-dependence of proton,deuteron,^3He and ^4He. It is suggested in the energy region below 75 MeV/A_p that this reduction could reflect the inherent dynamic polarization effect of structured particles,$^{6,7}Li$ on the values of the volume integral per projectile mass.

References

1) G.R.Satchler and W.G.Love, Phys.Report 55 (1979) 183.

2) Y.Sakuragi,M.Yahiro and M.Kamimura, Prog.Theo.Phys. 68 (1982) 322.

3) K.Katori,T.Shimoda,T.Fukuda,S.Shimoura,A.Sakaguchi,T.Yamagata,M.Tanaka, H.Ogata,Y.Sakuragi and M.Kamimura, Proc.of 1983 RCNP Int.Sym.,1983,Osaka. p.635.

4) M.Kamimura, Nucl.Phys.A351 (1981) 456.

5) J.Cook, Nucl.Phys.A388 (1982) 153.

Table I. Normalization factors and volume integrals

123.5 MeV ^6Li(20.6MeV/N)		168.8 MeV ^6Li(28.1MeV/N)		131.8 MeV ^7Li(18.8MeV/N)	
N_R=0.715	N_R=0.770	N_R=0.660	N_R=0.760	N_R=0.680	N_R=0.680
N_I=0.607	N_I=0.530	N_I=0.510	N_I=0.480	N_I=0.580	N_I=0.580
N_R=1.0	259.5MeV.fm^3	N_R=1.0	256.1MeV.fm^3	N_R=1.0	229.0MeV.fm^3
N_I=0.480		N_I=0.466		N_I=0.58	

I.13 Fusion and Deep Inelastic Collision in the Systems of $^{37}Cl + ^{27}Al$ and $^{37}Cl + ^{48}Ti$ below 200 MeV

K. Ideno

Department of Physics, Japan Atomic Energy Research Institute

In the energy region below 200 MeV of ^{37}Cl beams, fusion reaction occupies a dominant part for the system A = 60 - 90. Above 160 MeV other reactions such as deep inelastic collision begin to be important. Using the TANDEM accelerators of JAERI and University of Tsukuba, we measured fusion evaporation residues and deep inelastic fragments for the systems of $^{37}Cl + ^{27}Al$ and $^{37}Cl + ^{48}Ti$. Figs. 1 and 2 show the plots of $\sigma_{E.R.}$ vs $1/E_{c.m.}$ for the two systems. At higher energies of $E_{c.m.} \gtrsim 60$ MeV $\sigma_{E.R.}$ takes a constant value of ~1000 mb. In this energy region observed cross

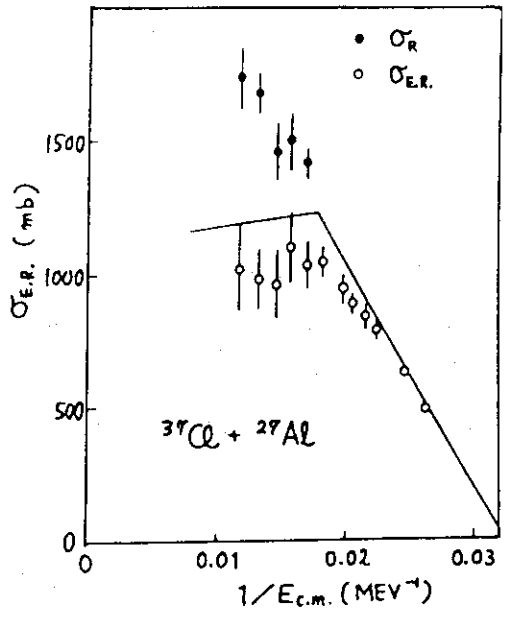

Fig. 1

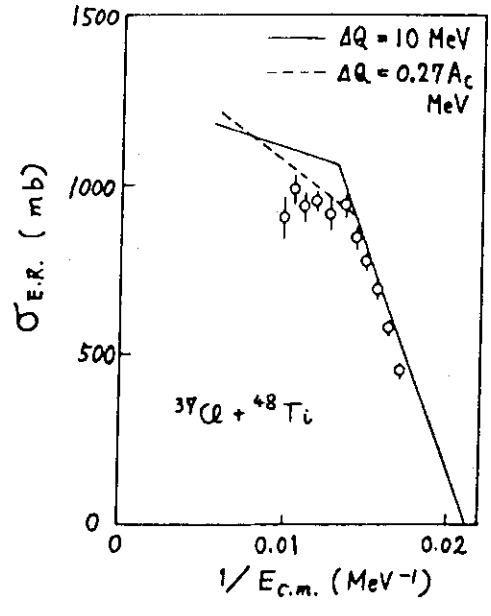

Fig. 2

This report is due to the results of collaboration with S. Hanashima*, S. Takeuchi*, Y. Tomita*, W. Yokota**, Y. Fukuchi**, S. Kinouchi**, T. Komatsubara**, S. M. Lee**, T. Mikumo**, Y. Nagashima**, T. Nakagawa**, M. Ogiwara** and W. Galster***; * JAERI, ** Univ. of Tsukuba, *** Hahn-Meitner Institute.

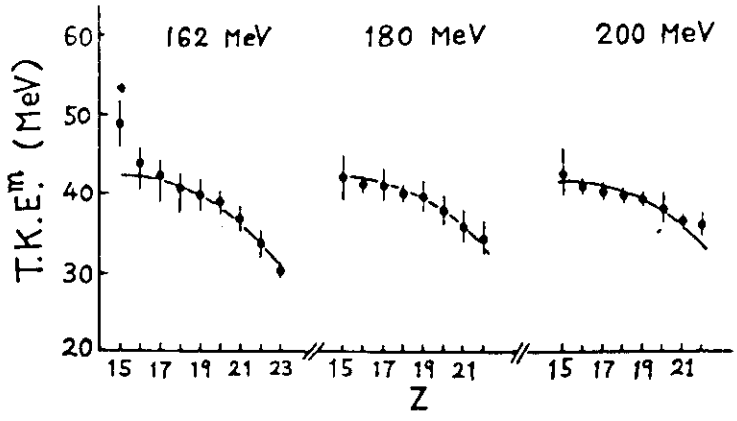

Fig. 3

sections were compared with the predictions of Lee et al.[1] and Civitareze et al.;[2] In the fusion process the energy transferred to the internal excitation of the compound nucleus is constant (ΔQ = 10 MeV) in Ref. 1 while it is proportional to the mass A_c of the compound nucleus in Ref. 2. The difference between the two predictions is small for the system of $^{37}Cl + ^{27}Al$. For the system of $^{37}Cl + ^{48}Ti$ the variable ΔQ model seems to fit better with the experimental values. Deep inelastic fragments at backward angles were analyzed with the assumption of the bianary process.[3,4] The resulted most probable total kinetic energy ($T.K.E.^m$) shows a similar behavior with Z in the energy region between 160 and 200 MeV. Further analyses are in progress.

1) Lee et al., Phys. Rev. Lett. 45 (1980) 165.
2) Civitareze et al., Phys. Lett. B125 (1983) 22.
3) T. M. Cormier et al., Phys. Rev. C14 (1976) 334.
4) P. B. Braun-Munzinger et al., Phys. Rev. Lett. 36 (1976) 849.

SESSION II. NUCLEAR STRUCTURE AND NUCLEAR CHEMISTRY

(Jan. 10, Tuesday, 1984)

Chairmans

Tokihiro Kuroyanagi
Kyushu University

Hiromichi Kamitsubo
Masayasu Ishihara
The Institute of Physical and Chemical Research

Teruo Kishimoto
The University of Tsukuba

II.1 High-Spin States (Theoretical)

Yoshifumi R. Shimizu and Kenichi Matsuyanagi

Department of Physics, Kyoto University, Kyoto 606

In recent years, the rotating shell model (RSM)[1] has become a basis for discussing high-spin yrast spectroscopic data. One of the keys to the success of the RSM is the construction of an orthogonal basis in the rotating frame of reference, called "diabatic quasiparticle representation", which is associated with the rotating deformed potential. In contrast to the "adiabatic representation" which is conventionally adopted in calculations in terms of the constrained Hartree-Bogoliubov method, the use of "diabatic representation" enables us to unambiguously specify individual rotational bands in which internal structures of the quasiparticle state vectors smoothly change as functions of the rotational frequency ω_{rot}. Such an unambiguous specification of the rotating frame is especially important in the band-crossing region in order to avoid the shortcoming[2] of the semiclassical (cranking-model) description of the band-band interactions.

After constructing the diabatic representation with the use of the Tanaka-Suekane method,[3] we have extended the scope of the RSM such that 1) the pairing- and quadrupole-deformation parameters of the reference configurations are selfconsistently determined as functions of ω_{rot}, and 2) the residual interactions between the quasiparticles are explicitly taken into account by means of the RPA in the rotating frame.[4] Our aim is to understand the effects of the alignment of quasiparticle angular momentum on collective properties of the nuclear system in the high-spin yrast region.

Below we present some typical results of theoretical calculation on the problems of 1) microscopic mechanism of the pairing phase transitions, 2) growth of triaxial deformations induced by the aligned quasiparticles, and 3) character-change of the γ-vibrations at high spin.

Figure 1 shows the selfconsistent values of the neutron pairing gaps Δ for several bands in ^{163,164}Er, which indicate that 1) the Δ depends only weakly on ω_{rot} within individual bands, 2) the Δ would decrease stepwise at the band-crossing points along the yrast line, and 3) the Δ would

vanish when four quasiparticles align their angular momenta. The stepwise reduction of Δ caused by the blocking effects of the aligned quasiparticles seems to be the major microscopic mechanism of pairing phase transition from superfluid to normal phases. The recent experimental data[5] for ^{168}Hf seem to indicate an occurrence of the pairing phase transition in the region $I \gtrsim 30$, in agreement with theoretical expectations.

Figure 2 shows the equilibrium deformations (β, γ) of the ground- and Stockholm-bands determined as functions of ω_{rot}. In order to easily perform this type of calculations, we have utilized the semiclassical requirement that average velocity distribution at equilibrium shall be isotropic in the rotating frame. We see in Fig. 2 that 1) incipient triaxial deformations are induced by excitation of the aligned quasiparticles, and 2) the sign of the

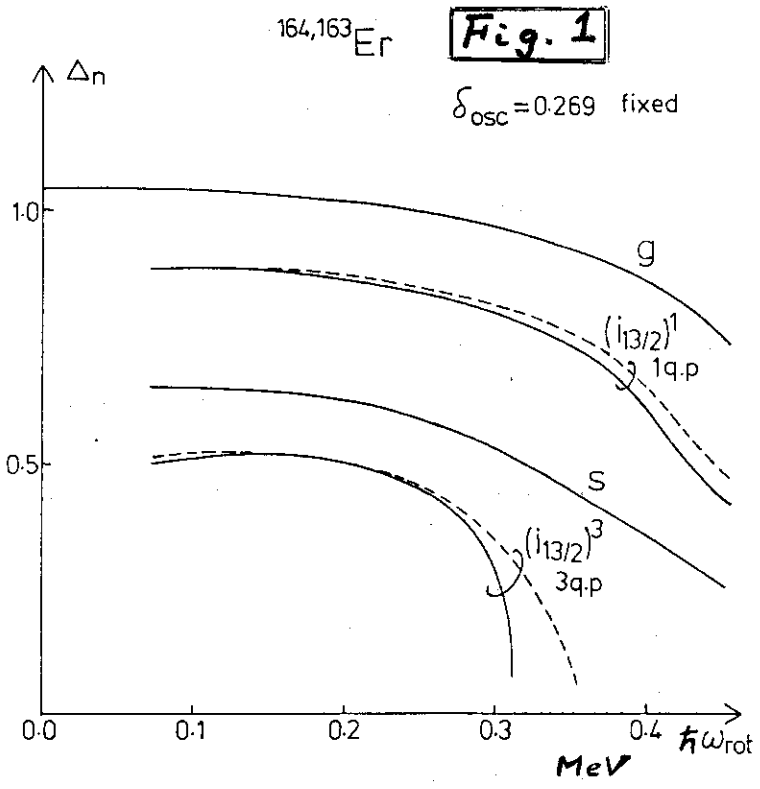

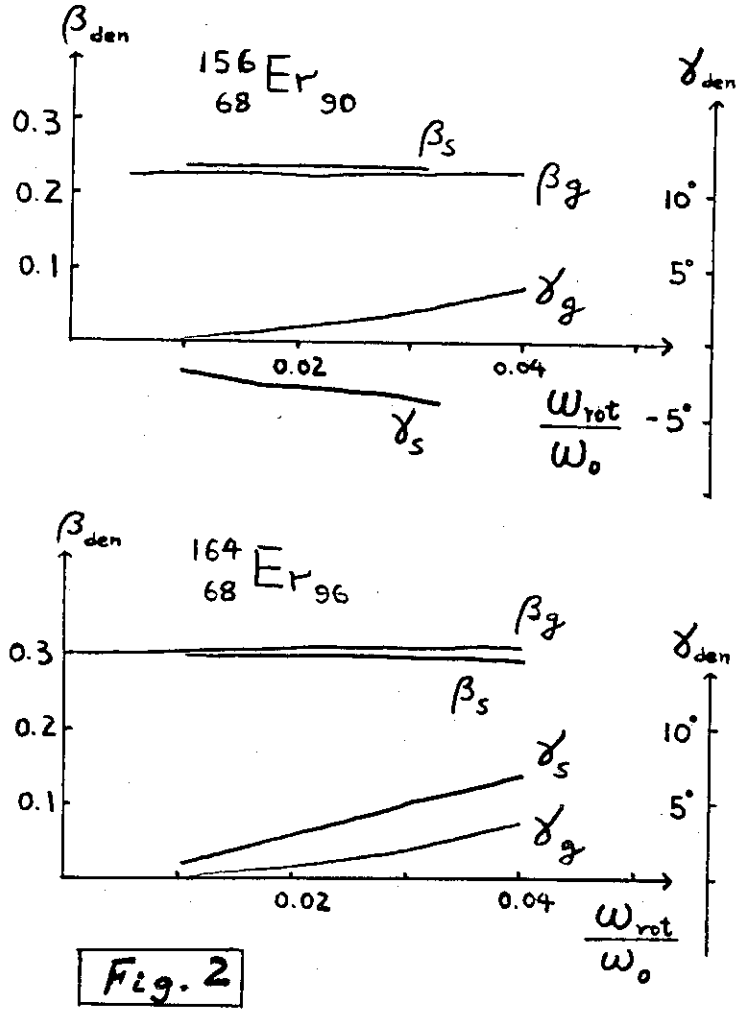

Fig. 2

triaxiality parameter γ of the s-band changes as the neutron number N goes from 90 to 98, sensitively reflecting the character-change of the aligned quasiparticles from particle-like to hole-like.

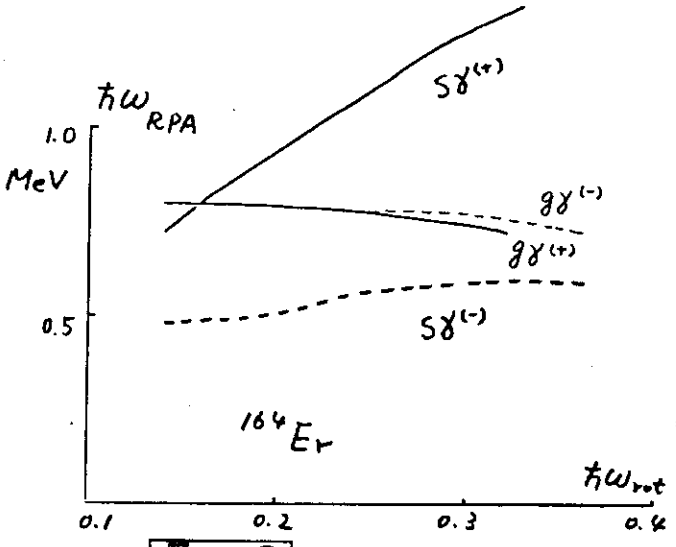

Fig. 3

Figure 3 shows the theoretical excitation energies of the γ-vibrational modes in ^{164}Er. The positive (negative)-signature modes are plotted by the full (broken) lines. These are measured in the uniformly rotating frames associated with the g-band or the s-band. We see that, in contrast to the γ-vibrations created on the g-band (denoted by $g\gamma$), a drastic signature-splitting occures in the γ-vibrations created on the s-band (denoted by $s\gamma$). A detailed analysis of their properties reveals that 1) the positive-signature (even-I) modes tend to loose their identities because of the mixings with the neighboring non-collective quasiparticle states, and 2) the negative-signature (odd-I) modes appear low in energy retaining their collectivities. This latter result may be regarded as an incipient trend of the character change of the negative-signature γ-vibrations toward the wobbling modes of motion, which are expected to be one of the most remarkable features of nuclei with axial-symmetry breaking. Their frequencies may be written as

$$\omega_{wobb} = \omega_{rot}\sqrt{\frac{(\mathcal{J}_x - \mathcal{J}_y)(\mathcal{J}_x - \mathcal{J}_z)}{\mathcal{J}_y \mathcal{J}_z}}$$

The moment of inertia $(\mathcal{J}_x, \mathcal{J}_y, \mathcal{J}_z)$ can be microscopically calculated in terms of the RPA. Figure 4 illustrates a theoretical picture about the dependence of $(\mathcal{J}_x, \mathcal{J}_y, \mathcal{J}_z)$ on the triaxiality parameter γ. We see that the

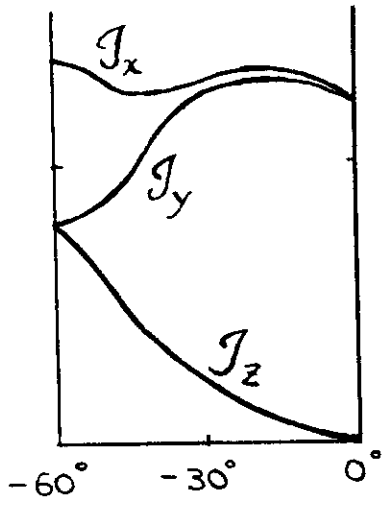

$\delta_{20} = 0.22$
$\Delta_n = \Delta_p = 0.5$ MeV
^{147}Gd, $\hbar\omega_{rot} = 0.3$ MeV

Fig.4

γ-dependence of the calculated moment of inertia changes from the irrotational-fluid-like to rigid-body-like characters, as the equilibrium deformation changes from prolate-like ($\gamma \approx 0°$) to oblate-like ($\gamma \approx -60°$, rotations about the symmetry axis) shapes.

References

1) S. Frauendorf, in Nuclear Physics, edited by C.H. Dasso (North-Holland, 1982), p.111.

2) I. Hamamoto, Nucl. Phys. A271 (1976), 15.

3) Y. Tanaka and S. Suekane, Prog. Theor. Phys. 66 (1981), 1639.

4) Y.R. Shimizu and K. Matsuyanagi, Prog. Theor. Phys. 70 (1983), 144, 319, preprint KUNS 707, and papers in preparation.

5) R. Chapman et al., Phys. Rev. Lett. 51 (1983), 2265.

II.2 Experimental Studies of High-Spin States

Y. Gono
RIKEN, Wako-shi, Saitama 351

Recent progress of the studies of high-spin states by the in-beam γ-ray spectroscopic techniques has been made mainly by the application of multi-detector systems. Among them TESSA of NSF at Daresbury which consists of six large germanium detectors surrounded by the 10"ϕ x 12" NaI(Tl) anti-compton shields has been used most effectively to study the high-spin phenomena in detail[1]. Many rotational bands (including many side bands) in some nuclei in the rare-earth region were observed to high-spin states above the back-bending region. These observations caused new theoretical developments as discussed by Matsuyanagi in this symposium[2]. In this report two new developments made at RIKEN concerning the topics are discussed.

i) RIKEN BGO-ACS (Anti-Compton Shield)

Some groups in this field proposed to construct a TESSA type system by replacing NaI(Tl) scintillators with the newly developed BGO (bismuth germanate) crystals. The BGO scintillator has 2.5 time shorter radiation length than NaI(Tl). This fact assures the smaller size of BGO-ACS than that of NaI(Tl)-ACS with the same efficiency. This compactness results in larger solid angle for each germanium detector.

Such a system which consists of eight sets of BGO-ACS is now being prepared at RIKEN. Dimensions of the BGO-ACS are given in fig.1 which correspond roughly to the 12"ϕ x 12" NaI(Tl) ACS in the γ-ray detection efficiency. The expected compton suppression factor of this system is six. An example of the compton suppressed spectrum of ^{60}Co is shown in fig.2 giving a suppression factor four. Some

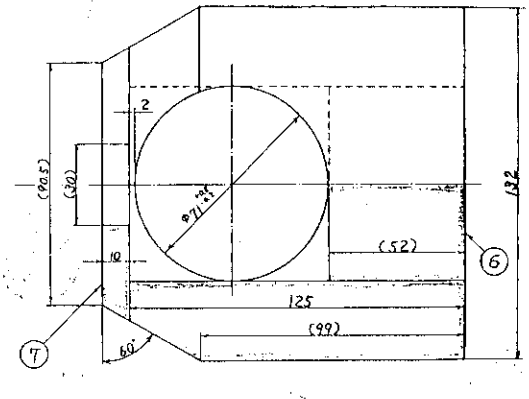

Fig.1 RIKEN BGO-ACS

improvements are expected by solving problems of electronics to pick up about ten times smaller signals of BGO in comparison with that of NaI(Tl). The system is designed to have seven independent segments of BGO which are coupled individually to photomultipliers. This configuration was taken to allow high counting rate for ACS so that the system can be used with a relatively thin collimator in front of the ACS-germanium system. Also it may be expected to use the same BGO's as a multiplicity filter at the same time.

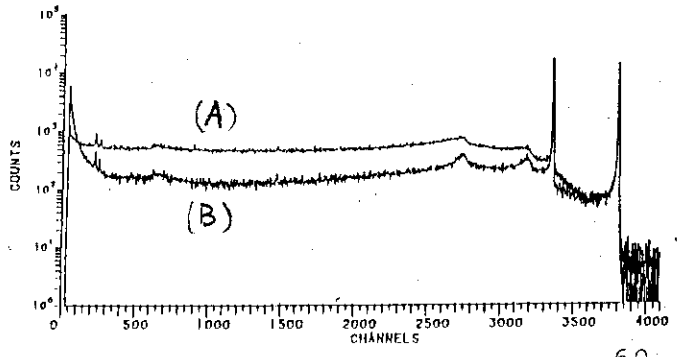

Fig.2 Singles γ-ray spectra of ^{60}Co taken (A)without and (B)with BGO-ACS.

ii) IN-BEAM γ-RAY STUDY WITH ^{210}Pb

Studies of high-spin states in nuclei with atomic number Z 82 and the neutron number N 126 were made by many groups[3-5] both experimentally and theoretically. There are only a few isotopes which are available to use as targets for the in-beam spectroscopy in this mass region. The exotic nuclei in this mass region which have so far been studied by this technique are ^{218}Ra (ref.6) and ^{222}Th (ref.7).

A ^{210}Pb ($T_{1/2}$= 22y) target was prepared by the electro-deposition on ∿100 μg/cm^2 Ni-foil at RIKEN as a target to

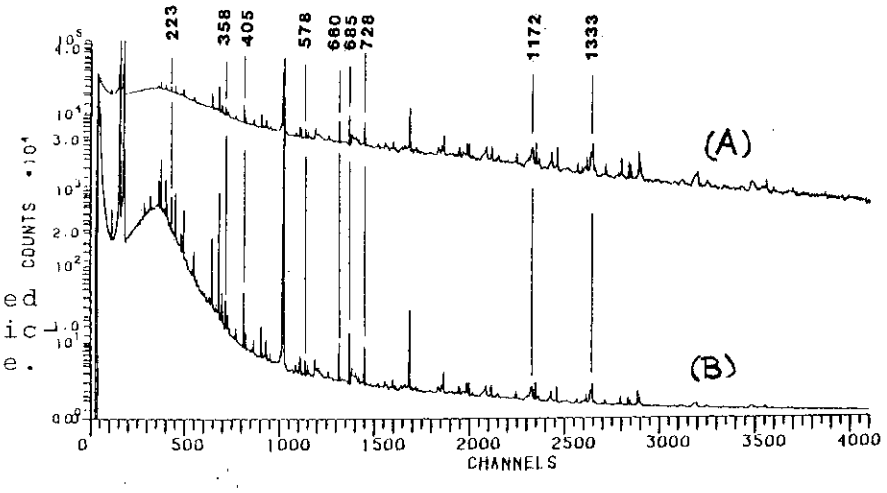

Fig.3 Singles γ-ray spectra from the ^{210}Pb + α reaction at E=30 MeV plotted by (A)logarismic (B)linear-scale.

study the nuclei such as ^{220}Ra, ^{216}Rn, ^{212}Po ,etc.. The first use of this target for the in-beam γ-ray study was made by using the $^{210}Pb(\alpha,2n)^{212}Po$ reaction with the 30 MeV α-beam from the RIKEN cyclotron.

Singles γ-ray spectrum is shown in fig.3. The peak to back-ground ratio is not good as seen in the figure. However it was worthwhile to perform the γγ-coincidence experiments on this reaction. A preliminary result of a level scheme of ^{212}Po which was constructed based on the present experiment is shown in fig.4. The spin values of the levels above the 1477 keV (8^+) state are given tentatively using a systematics of the N=128 isotones[4]. The excited states in ^{212}Po were assigned up to the 2.889 keV state which lies close to the famous α-decaying isomer at E ∿ 2.9 MeV. The yrast level sequence is quite similar to the calculated one in ref.8. However this tentative spin assignment might be inconsistent to the life-time of T=45 s of the 2.905 (16^+) isomer unless the excitation energy of the isomer is much closer to the 2.889 keV. It may be worthwhile to point out that the accuracy of the excitation energy of the isomer[9] is worse than the others since it was deduced from the α-decay energy while the others were from the γ-ray energies.

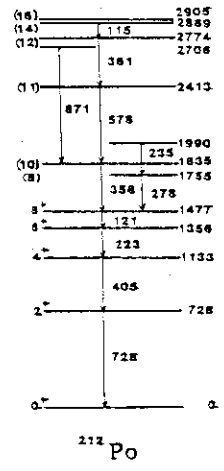

Fig.4 Proposed level scheme of ^{212}Po.

I would like to acknowledge Mr.M.Fukuda for his substantial contribution for the preparation of BGO-ACS system. The auther is also thankful to Prof.I.Fujiwara for the preparation of ^{210}Pb target. The work on ^{212}Po was made mostly by Mr.M.Sugawara.

References:

1) R.Chapman et al., Phys.Rev.Lett. 51(1983)2256
and references therein.
2) K.Matsuyanagi, P.___ in this report.
3) D.Horn et al., Nucl.Phys. A317(1979)520.
4) Y.Itoh et al., Nucl.Phys. A410(1983)156
and references therein.
5) K.Matsuyanagi et al., Nucl.Phys. A307(1978)253.
6) M.Gai et al., Phys.Rev.Lett. 51(1983)646
and references therein.
7) D.Ward et al., Nucl.Phys. A406(1983)591.
8) D.Strottman, Phys.Rev. C20(1979)1150.
9) I.Perlman et al., Phys.Rev. 127(1962)917.

II.3 Heavy Elements and Superheavy Elements

Ichiro Fujiwara*, Shin-ichi Ichikawa**, Nobuo Shinohara**, Shigekazu Usuda**, Toshio Suzuki**, Hiroshi Okashita**, Toshiaki Sekine***, Kentaro Hata***, Takayoshi Horiguchi****, Yashikazu Yoshizawa****, and Seiichi Shibata*****

*Institute of Atomic Energy, Kyoto University, **Department of Chemistry, Japan Atomic Energy Research Institute, ***Department of Radoisotope Production, Japan Atomic Energy Research Institute, ****Department of Physics, Hiroshima University, *****Institute of Nuclear Study, Tokyo University.

Introduction

Many transuranium elements have been produced by accelerator since the first transuranium element neptunium was discovered 44 years ago. All elements up to Z=107 were discovered already [1,2], and production of the 119th element is undertaken now[3]. However, in the case of production of the elements beyond Z=100, the formation cross section is extremely small due to competition between particle evaporation and fission in the excited nuclide. Therefore it is necessary to find most suitable conditions for production of the aimed nuclide. In this lecture, ^{250}Fm and some other nuclides produced by interaction between ^{238}U and ^{16}O using the JAERI Tandem Accelerator and some new nuclides in transuranium region as future program are discussed first. Superheavy element has been in concept with us for 30 years, but is not yet discovered either by accelerators or in nature[4]. However, superheavy element is still an attractive subject for nuclear chemistry. The present situation of research and the possibility of production of the element are discussed next.

Synthesis of Transuranium Nuclides by JAERI Tandem Accelerator

The formation cross sections of ^{250}Fm, ^{246}Cf, ^{242}Cm, ^{238}Np, ^{239}Np, ^{237}U and ^{239}U were obtained by bombardment of ^{238}U with ^{16}O, as shown in Fig. 1. The nuclides were separated chemically after bombardment and measured with α- or γ-spectrometry. The excitation function of $^{238}U(^{16}O, 4n)^{250}Fm$ reaction was investigated by Flerov et al.[5] previously, and our results agree qualitatively with it.

Excitation functions of $^{238}U(^{16}O, 4n)^{250}Fm$ and $^{238}U(^{16}O, \alpha 4n)^{246}Cf$ reactions were computed by ALICE code[6,7], in which a fission barrier 2.25 times as large as that of the liquid drop model was selected. The computed cross sections are also shown in Fig. 1 (dashed lines). The fitness between the computed and the experimental values is good.

The formation of ^{242}Cm is probably from direct reaction such as deep inelastic collision rather than compound reaction. The nuclides of ^{238}Np, ^{239}Np, ^{237}U and ^{239}U seem to be formed by transfer reaction.

In future program, Md nuclides including an unknown nuclide ^{249}Md would be produced by $^{238}U(^{19}F, xn)^{257-x}Md$ reactions. U-241, one of the other unknown nuclides, would be prodeced by transfer reactions of ^{238}U with ^{18}O or ^{37}Cl.

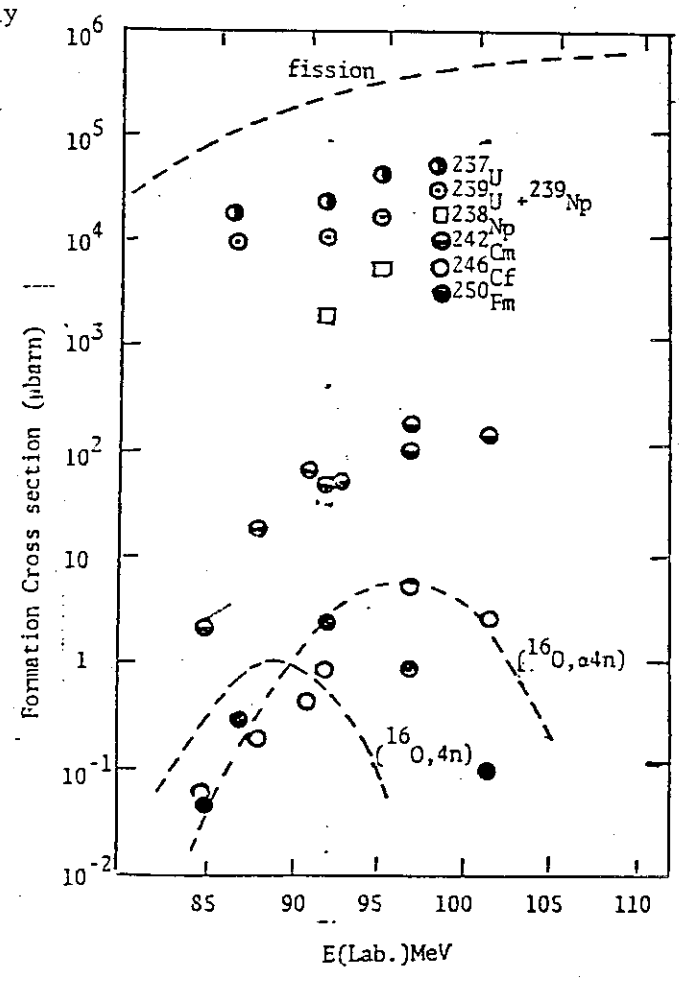

Fig. 1 Formation cross sections of ^{237}U, $^{239}U+^{239}Np$, ^{238}Np, ^{242}Cm, ^{246}Cf and ^{250}Fm, ---- computed cross section by ALICE code.

Superheavy Elements

Despite intensive researches in major laboratories in USA, USSR, Germany and France, no evidence for production of any superheavy element has been found in the proposed reactions. A wide variety of techniques has been developed and applied to the search for superheavy elements by accelerator. Table 1 shows the upper limits for production cross sections of heavy elements by accelerator experiments performed in the world for the time being. The assumed half-lives of superheavy elements cover from 10^{-9} sec to 1 year and the upper limits for the cross sections from 10^{-28} to 10^{-35} cm^2.

The $^{248}Cm(^{48}Ca, xn)^{296-x}116$ reaction has been studied most intensively since the nuclide produced by complete fusion provided the closest approach to double magic number Z=114 and N=184. Experiment with this reaction is difficult since the target is a rare artificial nuclide, ^{248}Cm, and the projectile is an enriched isotope of very low natural abundance. The results of experiments with $^{48}Ca + ^{248}Cm$ reaction are summarized in Fig. 2, where the upper limits for production cross section are plotted against the half-life range, which covers with the particular techniques; (SF)Spontaneous fission, (α) α-particle counting, (CHEM) Chemical procedure, (GAS) Volati-

Table 1 Attempts to synthesise superheavy elements by complete fusion reactions

System*	Compound nucleus	Upper limit for production cross-section (cm^2)	Half life range covered
$^{232}_{90}Th + ^{48}_{20}Ca$	$^{280}110^{170}$	3×10^{-35}	$\geq3\times10^{-3}$ s
$^{231}_{91}Pa + ^{48}_{20}Ca$	$^{279}111^{168}$	4×10^{-35}	$\geq3\times10^{-3}$ s
$^{233}_{92}U + ^{48}_{20}Ca$	$^{281}112^{169}$	7×10^{-35}	≥2 h†
$^{248}_{96}Cm + ^{40}_{18}Ar$	$^{288}114^{174}$	2×10^{-32}	10^{-9} s–1 d
$^{242}_{94}Pr + ^{48}_{20}Ca$	$^{290}114^{176}$	1×10^{-35}	2 h–1 yr†
$^{243}_{95}Am + ^{48}_{20}Ca$	$^{291}115^{176}$	2×10^{-35}	2 h–1 yr†
$^{246}_{96}Cm + ^{48}_{20}Ca$	$^{294}116^{178}$	2×10^{-35}	2 h–1 yr†
$^{248}_{96}Cm + ^{48}_{20}Ca$	$^{296}116^{180}$	See Fig. 2	
$^{208}_{82}Pb + ^{84}_{36}Kr$	$^{292}118^{174}$	1×10^{-30}	$\geq6\times10^{-7}$ s
$^{208}_{82}Pb + ^{86}_{36}Kr$	$^{294}118^{176}$	6×10^{-33}	3×10^{-3} s–100 d
		1.5×10^{-30}	2×10^{-9} s–5 h
$^{238}_{92}U + ^{59}_{27}Co$	$^{297}119^{178}$	4×10^{-33}	1 s–30 h†
$^{238}_{92}U + ^{(60)}_{28}Ni$	$^{298}120^{178}$	2×10^{-33}	1 s–30 h†
$^{238}_{92}U + ^{(65)}_{29}Cu$	$^{303}121^{182}$	8×10^{-33}	1 s–30 h†
		2×10^{-33}	2 h–1 yr†
$^{238}_{92}U + ^{65}_{29}Cu$	$^{303}121^{182}$	4×10^{-34}	2×10^{-6} s–10 h
$^{232}_{90}Th + ^{76}_{32}Ge$	$^{308}122^{186}$	1×10^{-34}	5×10^{-3} s–1 yr
$^{136}_{54}Xe + ^{170}_{68}Er$	$^{306}122^{184}$	1.5×10^{-33}	2×10^{-6} s–10 h
$^{238}_{92}U + ^{76}_{32}Ge$	$^{314}124^{190}$	1×10^{-34}	5×10^{-3} s–1 yr
$^{243}_{95}Am + ^{68}_{30}Zn$	$^{311}125^{186}$	5×10^{-32}	10^{-9} s–5 d
$^{232}_{90}Th + ^{84}_{36}Kr$	$^{316}126^{190}$	5×10^{-30}	$\geq6\times10^{-7}$ s
$^{238}_{92}U + ^{84}_{36}Kr$	$^{322}128^{194}$	8×10^{-29}	$\geq6\times10^{-7}$ s

lization of gas, (FOIL) Collection of recoiled product, (VW) Transport with gas jet, and (DIF) Spontaneous fission in flight. Since a fusion cross section was estimated theoretically to be at least 10^{-27} cm^2 for the ^{48}Ca – ^{248}Cm system, such negative results shown in Fig. 2 would be ascribed to the competition between fission and evaporation; the survival probability from fission is estimated less than 4 x 10^{-9}% in the most pessimistic case, which corresponds to the production cross section of the order of 10^{-38} cm^2.

An alternative pathway to synthesize the superheavy element is the reaction between two ^{238}U nuclides. The reaction was examined at the Darmstadt UNILAC. This study was initiated to demonstrate that the superheavy elements might be produced by exchange of nucleons in damped collision and that overall production cross section for the 114 element is estimated to be 10^{-35} cm^2 just exceeding the detection limit of the most sensitive method available at present.

If the superheavy element is found in nature, it should be a very useful target for the study of very heavy nuclides by accelerator. Most of search of nature for the superheavy element have produced negative results. In a hot spring at Cheleken Peninsula in the Caspian Sea, Flerov et al. observed some fissioning activity after chemical separations. It is only a positive evidence of the superheavy element in nature but not yet confirmed.

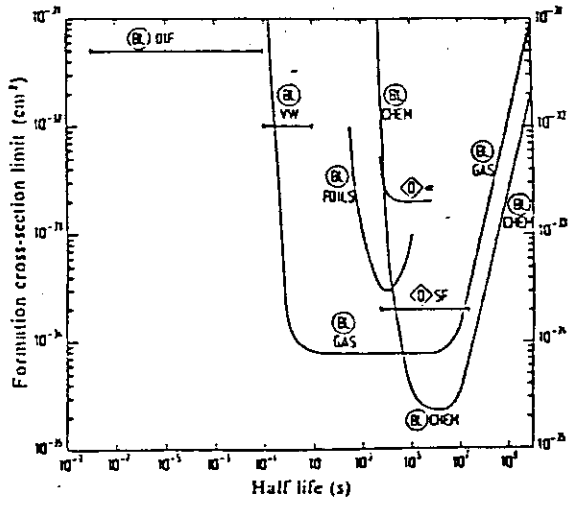

Fig. 2 Upper limits of the production cross-section for superheavy elements in the reaction of ^{248}Cu with ^{48}Ca versus the half-life range covered with different techniques. The data are from work of the Berkeley–Livermore group[91–93] (BL) and the Dubna group[41] (D); for details see text.

One of the authors of this paper observed spontaneous fission events in lead samples separated chemically from the filter dust obtained by calcination of the tin mineral dug out from Ikuno Mine in the west Japan. Although the phenomenon might be caused by contamination of such nuclides as ^{252}Cf, it is still one of the candidates for the superheavy element.

References

1) C. Keller: "The Chemistry of the Transuranium Elements", Verlag Chemie GMbH (1971).
2) G. Muezenberg, S. Hofmann, F. P. Hessberger, W. Reisdorf, K. H. Schmidt, J. H. R. Schneider, P. Armbruster, C. C. Sahm and B. Thuma: Z. Phys. A, Atoms and Nuclei, 300 (1981) 107.
3) G. Muenzenberg, P. Armbruster, F. P. Hessberger, S. Hofmann, K. Poppensieker, W. Reisdorf, J. H. R. Schneider, W. F. W. Schneider, K. H. Schmidt, C. C. Sahn and D. Vermeulen: Z. Phys. A, Atoms and Nuclei, 309 (1982) 89.
4) G. Herrmann: Nature 280 (1979) 534.
5) V. P. Perelygin, E. D. Donets and G. N. Flerov: J. Exptl. Theoret. Phys. 37 (1959) 1558 and Sov. Phys. JETP 10 (1960) 1106.
6) F. Plasil and M. Blann: Phys. Rev. C11 (1975) 508.
7) M. Blann: Report C00-3493-29 (1976).

II.4 Symmetric Fission in Relatively Light-Mass Reaction Systems

H.Nakahara, Y.Nagame*, K.Sueki, M.Yanokura** and I.Kohno**

Department of Chemistry,Tokyo Metropolitan University, *Japan Atomic Energy Research Institute, **Institute of Physical and Chemical Research.

1.Introduction

It has been predicted by the liquid drop model that the fission barrier height will reach the maximum of about 55MeV for the nucleus of mass number around 90.[1] This barrier height will decrease as the angular momenta brought into the system become larger, as in the case of heavy-ion reactions.[2] Up to now, no definite experimental evidence of nuclear fission has been presented for nuclei of mass number less than 140.[3] Most of the difficulties arise from the facts that fission products can not be distinguished from some of deeply inelastic events so long as their kinetic energies and angular distributions are compared. Besides, in relatively light-mass reaction systems, the region of symmetric fission products often overlap with that of deeply inelastic collision products. The present authors have attemped to seek some evidence of fission in those light-mass reaction systems by varying projectile energies and by using target isotopes of different Z^2/A.

2.Experimental

Reaction systems chosen are shown in Table 1 where projectile energies and some of experimental results on ℓ_{max}, ℓ_{cr} and σ_{ER}/σ_R are also given. Reaction products were detected by a ΔE-E gas proportional-solid state detector. Details of experiments are described in Refs.4) and 5).

Table 1. The reaction systems and some of experimental results.

Reaction system	Compound nucleus	Z^2/A	E_{lab}(MeV)	E_X^{CN}(MeV)	ℓ_{max}(ħ)	ℓ_{cr}(ħ)	σ_{ER}/σ_R	σ_{SY}(mb)	σ_f(mb)^{cal*}
$^{20}_{10}Ne+ ^{50}_{24}Cr$	^{70}Se	16.5	146	109	62±2	49±1	0.60±0.05	38±10	36
			120	90	53±1	43±1	0.62±0.04	12±5	7
$^{20}Ne+ ^{54}Cr$	^{74}Se	15.6	146	115	65±1	50±1	0.60±0.05	12±2	22
$^{14}_{7}N + ^{58}_{28}Ni$	^{72}Br	17.0	115	94	51±1	42	0.67	7.7±2.3	6
$^{14}N + ^{64}Ni$	^{78}Br	15.7	115	104	52±1	44	0.69	2.3±0.8	4
$^{20}_{10}Ne+ ^{92}_{42}Mo$	^{112}Te	24.1	146	104	72±1	54±3	0.56±0.03	22±5	21
$^{20}Ne+^{100}Mo$	^{120}Te	22.5	146	118	74±2	56±3	0.55±0.03	12±4	13

* ALICE code ; $B_f=0.5B_f$(RLDM), $a_f/a_\nu=1.05$,
ΔJ_ν; n 1ħ, p 1ħ, α 4ħ

3.Results and Discussion

Kinetic energies of the products with Z larger than that of the projectile by more than two were found completely damped whereas angular distributions in terms of $d\sigma/d\theta$ were found flat for the products with $Z \geq 14$ in both reaction systems of ^{14}N and ^{20}Ne projectiles. Symmetric product yields were found strongly dependent on target isotopes in all the combinations of ^{14}N+Ni, ^{20}Ne+Cr and ^{20}Ne+Mo as shown, for example, in Figs.1 and 2. In the case of ^{20}Ne+Mo reactions, the product yields exhibit clear dips at Z=16, indicating the existence of two kinds of reaction mechanisms(See Fig.2). The yield distributions are rather continuous, on the other hand, for the case of ^{20}Ne+Cr, and the target isotope effect is also observed for the products of Z=11, 12 and 13(See Fig.1) whose angular distributions are clearly forward peaking. The curves drawn in the figures are those predicted by the diffusion model of Agarwal[6] with a half life of the composite nucleus of 1×10^{-21}sec. (For more details of calculations, see Ref.7).) The calculations were normalized to the experimental cross section for Z=14 observed at $\theta_{cm}=40°$ in the 146MeV ^{20}Ne reaction on ^{50}Cr. It is clear that the effect of target isotopes can not be explained by the diffusion model although the projectile energy dependence of product yields for $Z \geq 11$ can be partly accounted for the the model as shown in Fig.3. In order to understand the target isotope dependence of symmetric yields, calculations of evaporation -fission competition were carried out by ALICE code[8] with reduction of fission barrier heights to one half of those predicted by the liquid drop model. Experimental symmetric yields σ_{SY} obtained by summing over the charge distribution and angular distribution are compared with calculated fission cross sections in the last two columns of Table 1. General agreement is satisfactory. For better understanding of the phenomena, some more experiments of Ghoshal type are in progress by varying the projectile energy in wider range.

References

1) W.Myers and W.J.Swiatecki, Nucl.Phys. 81,1(1966).
2) S.Cohen, F.Plasil and W.J.Swiatecki, Ann.Phys.(N.Y.), 82,557(1974).
3) H.H.Gutbrod, F.Plasil, H.C.Britt, B.H.Erkkila, R.H.Stokes, M.Blann, Physics and Chemistry of Fission 1973, Vol II, p309(IAEA).
4) M.Yanokura, H.Nakahara and I.Kohno, J.Phys.Soc.Japan, 50,369(1981).
5) Y.Nagame, H.Nakahara, K.Sueki, H.Kudo, I.Kohno and M.Yanokura,

accepted in Z.Phys.A(1984).

6) S.Agarwal, Z.Phys.A, 297,41(1980).

7) Y.Nagame, Ph.D.thesis, Tokyo Metropolitan University(1981).

8) M.Blann, U.S.ERDA No.COO-3494-29, 1976.

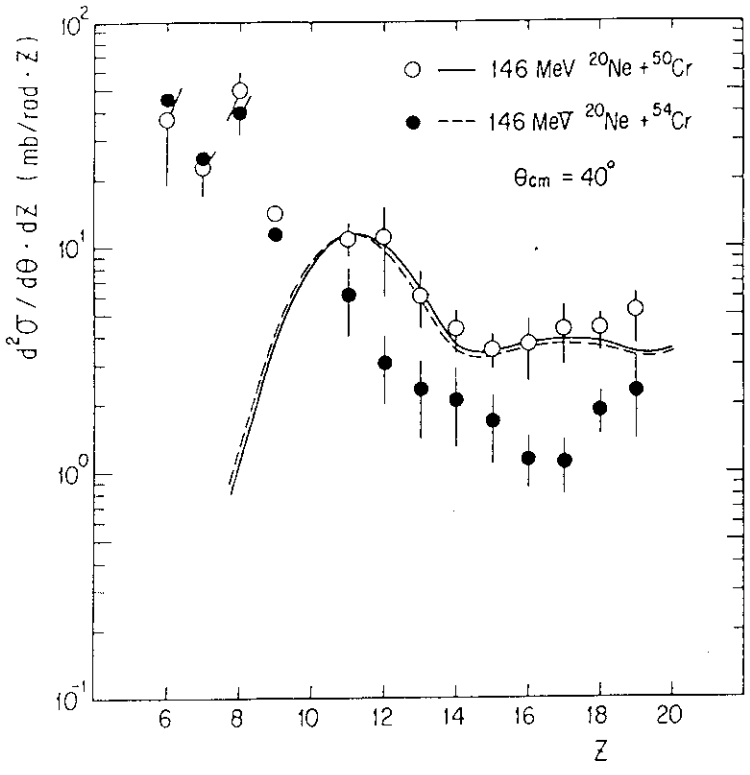

Fig.1. Charge distributions in two different systems; ^{20}Ne+^{50}Cr and ^{20}Ne+^{54}Cr at θ_{cm}=40°. The solid and dashed lines are calculated values(see text).

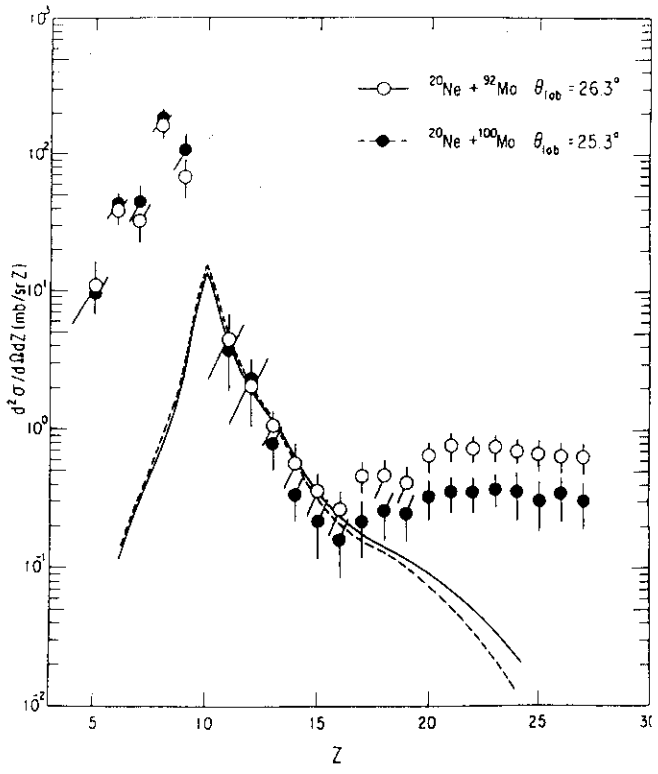

Fig.2. Charge distributions in two reaction systems; ^{20}Ne+^{92}Mo and ^{20}Ne+^{100}Mo. The solid and dashed lines are calculated charge distributions.

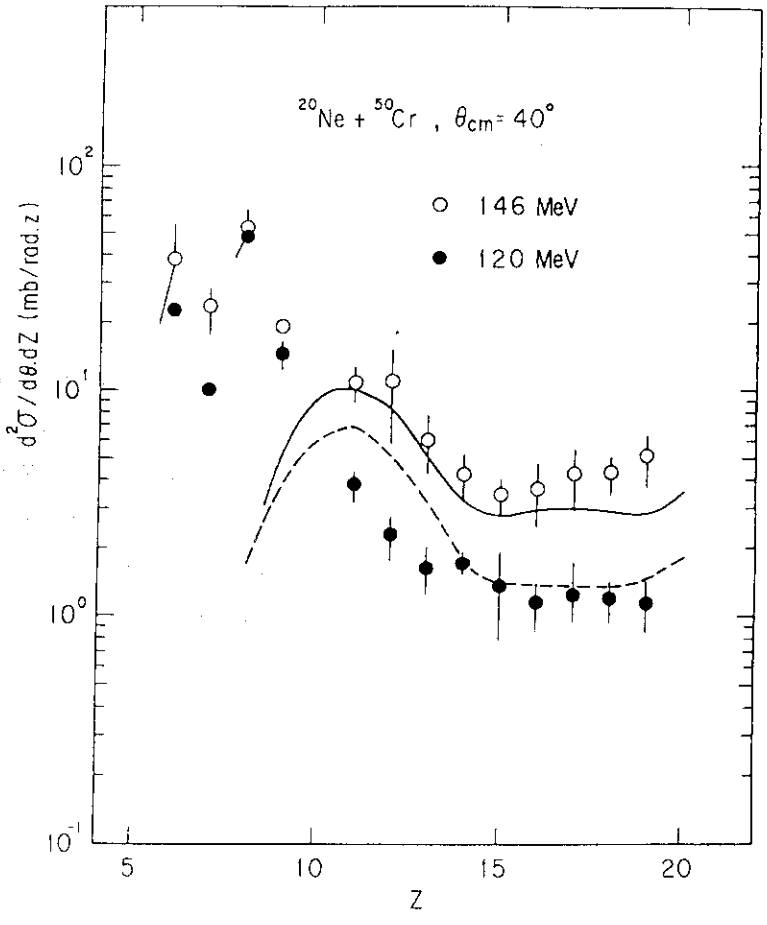

Fig.3. Charge distributions at two different bombarding energies at θ_{cm}=40°. The solid(E_{lab}=146MeV) and dashed (E_{lab}=120MeV) lines are calculated charge distributions.

II.5 Incomplete Fusion in the $^{12}C + ^{93}Nb$ Reaction

Toshiaki Sekine*, Sumiko Baba*, Kentaro Hata* and Shin-ichi Ichikawa**

*Production Development Division, Department of Radioisotope Production and **Nuclear Chemistry Laboratory, Department of Chemistry, Japan Atomic Energy Research Institute.

High angular momentum can be brought into the interaction between heavy ions. The highest angular momentum for the complete fusion is somewhat lower than the maximum angular momentum for the nuclear interaction. On the other hand, the lowest angular momentum for the complete fusion is usually postulated to be zero. Orsay group[1], however, has proposed a possibility of what is known "low-ℓ cutoff": the lowest angular momentum for the complete fusion is not always zero in analogy with two colliding water drops[2]. They found a possible evidence in the observation of reduced cross sections, as a straightfoward consequence of the low-ℓ cutoff, in some reactions of near-symmetric combination of projectile and target. The experimental results, however, are not so persuasive.

In order to test this possibility, isomer ratios offer some hope since they are expected to reflect the initial angular momentum distribution of the compound nucleus[3]. It is necessary to compare the isomer ratios between two initial channels leading to the same compound nucleus; the lowest ℓ waves in the formation of the compound nucleus are assumed to be cut off in one channel and not in the other.[§]

We have chosen as the initial channels $^{12}C + ^{93}Nb$ and $^{37}Cl + ^{68}Zn$ systems, and as the isomer pair $^{99m}Rh(9/2+, 4.7h)$ and $^{99g}(1/2-, 15d)$ induced by (HI,α2n) or (HI,2p4n) reaction. However, the isomer ratios should not be compared in a direct manner, since incomplete fusion mechanism[4] may occur intensively, in which "fast" light particles are emitted in the foward direction from the projectile and target system prior to the establishment of the statistical equilibrium. The foregoing isomers may be produced in the incomplete fusion by α-particle emission, which would be a significant part in various incomplete fusion channels, followed by two-neutron evaporation. The incomplete fusion is anticipated to contribute to the $^{12}C + ^{93}Nb$ system consisting of considerably asymmetric combination of projectile and target;

[§]In the present meeting, Nomura reports a possible evidence for the low-ℓ cutoff on the same principle as written here, independently with us.

the cross-section systematics of the incomplete fusion given by Tricoire et al.[5] predicts 56 MeV as a threshold at lab system for the $^{12}C + ^{93}Nb$ reaction, which is not so high compared with the Coulomb barrier of 38 MeV. Therefore, we must be well-informed as to the contribution of the incomplete fusion to the $^{12}C + ^{93}Nb$ reaction.

In this paper, we study mean recoil ranges of some nuclides produced in the $^{12}C + ^{93}Nb$ reaction as a function of bombarding energy, since the recoil range reflects the momentum transferred from the projectile to the target; the recoil range will be observed to be less than that for the complete fusion if the incomplete fusion occurs.

EXPERIMENTAL

We have irradiated foil stacks consisting of "thick" niobium targets with thickness of 3.4 mg/cm^2 separated by aluminum catcher foils in order to obtain average recoil ranges by means of thick target and thick catcher method[6]. Beam of ^{12}C of 6.4 or 7.5 MeV/a.m.u. was obtained at the JAERI tandem accelerator. The energy loss of the ions in the stack was calculated by the method described in Ref.7. The integrated beam current was monitored with a Faraday cup. The identification and measurement of the products were made with Ge(Li) detectors.

RESULTS AND DISCUSSION

We have calculated the recoil ranges theoretically with the formalism given by Delagrange et al.[8] on the assumption of the complete momentum transfer. This calculation gives the average recoil ranges projected on the beam direction, which is directly obtainable by experiment, taking into account the multiple scattering of heavy ions in the target. However, influence of particle evaporations is not considered; the values obtained may be underestimated by a few parcent.

Most of the nuclides regarded as products by particle evaporation of the compound nucleus show the recoil ranges, which increase with the beam energy, in accordance with the values calculated above. The formation mechanism of these nuclides is attributed to the complete fusion.

The recoil ranges of nuclides with a mass near that of the target nucleus decrease with the beam energy. From this behaviour, the formation mechanism of these nuclides is attributed to the transfer reaction[9].

The recoil ranges and excitation functions of ^{99m}Rh and ^{99g}Rh are plotted vs. the beam energy in Fig.1. The recoil ranges of both ^{99m}Rh and ^{99g}Rh, which considerably deviate from the two types mentioned above, almost stop increasing at 65 MeV and restart increasing around 75 MeV. This means that

the complete fusion is predominant at energies less than 65 MeV, while at energies above 65 MeV another reaction process takes place besides the complete fusion to reduce the mean recoil range. We consider this process to be the incomplete fusion expected before.

It is also interesting that in Fig.1 the recoil range is observed to differ appreciably from one isomer to the other at energies in which the incomplete fusion occurs. This phenomenon, which probably has been noticed for the first time, is interpreted as a consequence of coexistence of the two fusion mechanisms. We assume that both isomers have the same recoil range in each of the fusion processes. The observed value of the recoil range of one isomer is a mean, between the recoil range in the complete fusion and that in the incomplete fusion, weighted by a formation cross section of the isomer in each of the fusion processes. If one fusion process gives rise to an isomer ratio distinct from that of the other fusion process, some difference will be observed in the recoil range between the two isomers.

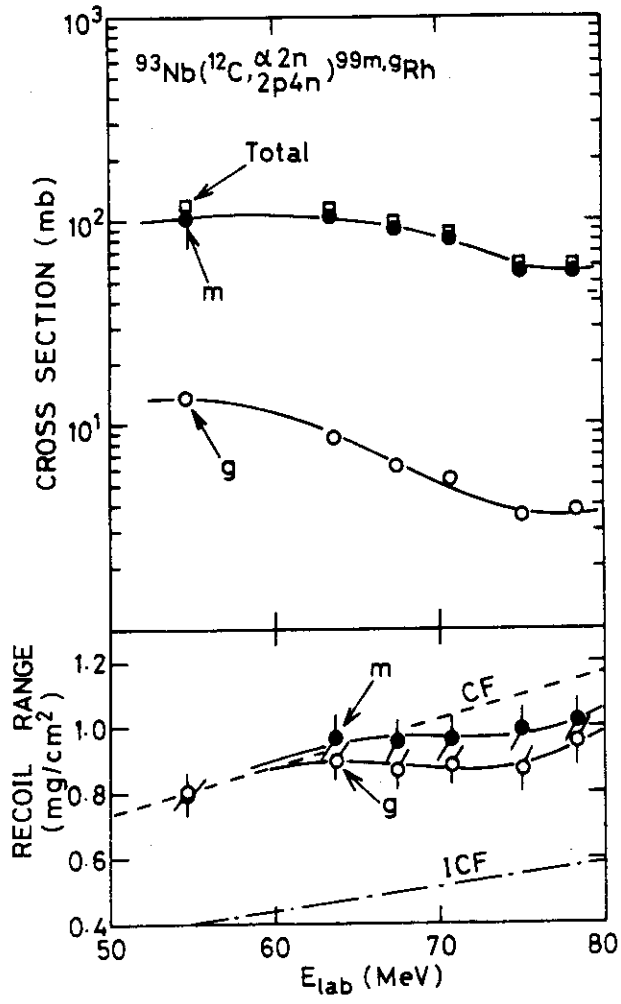

Fig.1 Excitation functions and mean recoil ranges. Broken lines with and without dots are calculated theoretically. See text.

In order to obtain quantitatively the contribution of the incomplete fusion to the formation of each of the isomers, the foregoing discussion enables us to write the follwing equations.

$$\sigma^i_{ICF} = \sigma^i_{obs}\, x^i \qquad (i = m \text{ or } g) \qquad (1)$$

$$x^i R_{ICF} + (1 - x^i) R_{CF} = R_{obs} \qquad (i = m \text{ or } g) \qquad (2)$$

Here, σ and R with various suffixes represent the corresponding values of cross sections and recoil ranges, respectively. Superscripts of m and g mean the meta-stable and the ground state, respectively. Subscripts of ICF,

CF, and obs are the contractions of incomplete fusion, complete fusion, and observed, respectively. To obtain x^i, the values of R_{ICF} are required. We have calculated R_{ICF} on a simple model that, after an α particle is separated from the projectile, a virtual fragment of ^{8}Be collides to the target nucleus with the same speed as that of the projectile and then forms a compound nucleus. This model is equivalent to the complete fusion between the ^{93}Nb target and the ^{8}Be projectile with three quarters of the ^{12}C beam energy. Therefore, the recoil range on this model is calculated in the same way as descibed above. The values of R_{ICF} obtained are also shown in Fig.1.

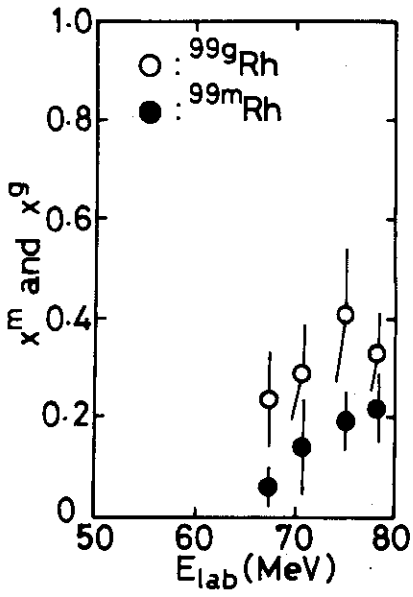

Fig.2 Contribution of the incomplete fusion to the formation of ^{99}Rh isomers in the $^{12}C + ^{93}Nb$ reaction.

The resulting values of x^m and x^g are plotted against the beam energy in Fig.2. The results indicate that a considerable number of the ^{99}Rh nuclei, especially low-spin isomer ^{99g}Rh, are produced in the incomplete fusion around 75 MeV.

REFERENCES

1) M. Lefort and Ch. Ngo: Ann. Phys. 3 (1978) 5.
2) J.R. Adam, N.R. Lindblad and C.D. Hendrics: J. Appl. Phys. 39 (1968) 5173.
3) G. Rudstam: Phys. Scripta 20 (1979) 165.
4) K.Siwek-Wilczynska, E.H. du Marchie van Voorthuysen, J. van Popta, R.H. Siemssen and J. Wilczynski: Nucl. Phys. A330 (1979) 150.
5) H. Tricoire, C. Gershel, N. Perrin, H. Sergolle, L. Valentin, D. Bachelier, H. Doubre and J. Gison: Z. Phys. A306 (1982) 127.
6) A. Ewart, C. Valentine and M. Blann: Nucl. Phys. 69 (1965) 625.
7) K. Hata and H. Baba: to be published.
8) H. Delagrange, F. Hubert and A. Fleury: Nucl. Phys. A228 (1974) 397.
9) P.M. Strudler, I.L. Preiss and R. Wolfgang: Phys. Rev. 154 (1967) 1126.

II.6 Stability of Unstable Nuclei

Kengo Ogawa

Institute for Nuclear Study
University of Tokyo
Tanashi, Tokyo 188

Search for the proton radioactivity, namely the discrete state which emit a proton, is one of the interesting subjects in nuclear physics.[1),2)] However, up to now, we know very few examples. Those are listed in Table 1.

Table 1. Observed Proton Radioactitivies

nucleus	$t_{1/2}$(ms)	E_p(MeV)	Ref.
$^{53}Co^*$	247	1.59	3)
^{147}Tm	420	1.06	4)
^{151}Lu	85	1.23	5)
^{113}Cs	$0.9 \cdot 10^{-3}$	0.98±0.08	6)
^{109}I	$25 \cdot 10^{-3}$	0.83±0.08	6)

In the table, $t_{1/2}$ and E_p are the half-life of the emitting states and the energy of the emitted proton respectively. It is notable that the last four examples are discovered by the heavy-ion experiments at GSI.

In order to know the possibility of the direct proton emission from the very proton-rich $1g_{9/2}$ shell nuclei, first we study the structure of nuclei near 100 Sn within the framework of shell model.[7)] From the calculated binding energies, nuclei like ^{97}In are predicted to exist beyond the proton-drip line. Therefore we can expect some proton radioactivities around this mass region.

Furthermore, as is shown schematically in Fig. 1, the predicted binding energy of ^{98}Sn, B(^{98}Sn), is larger than B(^{97}In), but smaller than B(^{96}Cd), i.e.

$$B(^{96}Cd) < B(^{98}Sn) < B(^{97}In). \quad (1)$$

This relation suggests that the ground state of ^{98}Sn cannot emit a proton, but emit two proton. Therefore the nucleus ^{98}Sn might be classified into so- called "two-proton radioactivity" predicted by Goldanskii.[8]

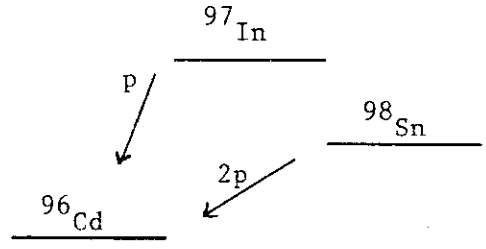

Fig. 1 Schematic Decay Modes of ^{97}In and ^{98}Sn.

In this case the total energy of the emitted two-proton is very small (it is predicted to be 0.8 MeV in the present calculation), the probability of two- proton emission might be hindered and the nucleus ^{98}Sn might be almost against the particle emission.

Besides the ground state discussed above, the high-spin isomers predicted by the shell-model are expected to exhibit peculiar property against particle emission. Thus the study of the very proton-rich $1g_{9/2}^{-}$ shell nuclei provides interesting subjects in nuclear physics.

References

1) V. I. Goldanskii, Ann. Rev. Nucl. Sci. 16 (1966) 1
2) J. Cerny and J. C. Hardy, Ann. Rev. Nucl. Sci. 27 (1977) 333
3) J. Cerny et al., Nucl. Phys. A188 (1972) 666
4) O. Klepper et al., Z. Phys. A305 (1982) 125
5) S. Hofmann et al., Z. Phys. A305 (1982) 111
6) T. Faestermann et al., to be published in Phys. Letters
7) K. Ogawa, Phys. Rev. C28 (1983) 958
8) V. I. Goldanskii, Usp. Fiz. Nauk, 87 (1965) 147

II.7 Multiple Coulomb Excitation of Odd-Mass Nuclei*

Takashi Inamura
Cyclotron Laboratory, RIKEN, Wako, Saitama 351

Multiple Coulomb-excitation experiments on ^{161,163}Dy, ^{167}Er, and ^{173}Yb have been carried out using 165-MeV ^{35}Cl and 250-MeV ^{58}Ni beams from the JEARI 20-UR tandem accelerator.

Multiple Coulomb excitation provides one of the best means to study the properties of the ground-state rotational band of a deformed nucleus: The band members are populated selectively and their lifetimes extracted enable absolute B(M1) and B(E2) values to be determined in a model-independent way when taken together with γ-ray branching and mixing ratios. In the present study special attention has been paid to the ground-state rotational band built on the $i_{13/2}$-neutron orbital, for instance, the case of ^{167}Er.

We measured γ-ray angular distributions, directional correlations, $\gamma\gamma$ coincidences, and nuclear lifetimes of the members of the ground-state band. γ rays were measured with an anti-Compton spectrometer consisting of Ge(Li) and NaI(Tl) detectors. Coincidences(and correlations) were recorded with three sets of anti-Compton spectrometers.

Figure 3 shows multiply Coulomb-excited states of the ground-state rotational band in ^{167}Er. States higher than the 19/2 member have newly been identified. Nuclear lifetimes of the excited states up to 23/2 have for the first time been determined from Doppler broadened γ-ray lineshapes. Multiply Coulomb-excited members of the ground-state rotational band in ^{163}Dy and ^{173}Yb are also shown in fig. 4. The members with spins higher than 17/2 in ^{163}Dy and those higher than 13/2 in ^{173}Yb have newly been identified. Extraction of lifetimes for ^{173}Yb is in progress.

For ^{161}Dy the band members up to 33/2 have been reported,

---

*This work has been made in collaboration with T. Ohshima, E. Minehara, M. Ishii, S. Kikuchi(JAERI), A. Hashizume (RIKEN), and H. Kumahora(Hiroshima University).

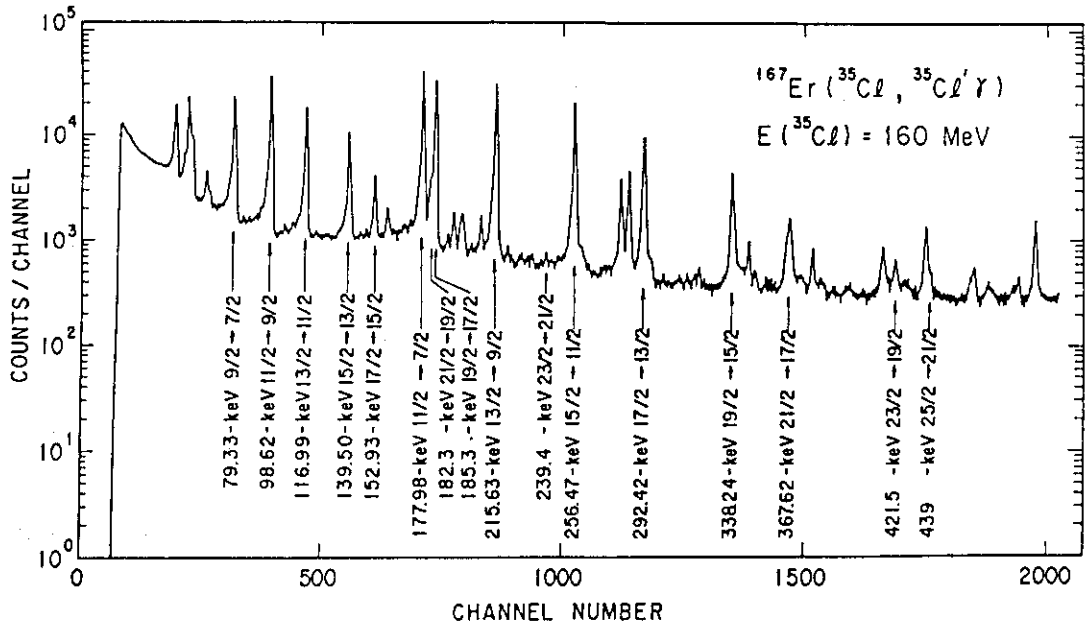

Fig. 1. A typical singles γ-ray spectrum observed in multiple Coulomb excitation: ^{167}Er(^{35}Cl,^{35}Cl'γ)^{167}Er at 160 MeV.

but those higher than the 13/2 state have for the first time been Coulomb-excited: the highest spin state observed here is the 29/2 state at 1692.7 keV. No information on lifetimes was available for the band members higher than 13/2.

An energy plot such that $[E(I)-E(I-1)]/2I$ vs I^2 for the ground-state rotational band built on the $i_{13/2}$ orbital is known to manifest a zigzag pattern which is classified by the signature $r = \exp(-i\pi\alpha)$, where we have $I = \alpha \bmod 2$: in the case of ^{167}Er,[1] the levels at peaks in the plot correspond to $r = +i$(unfavored) and those at valleys to $r = -i$(favored).

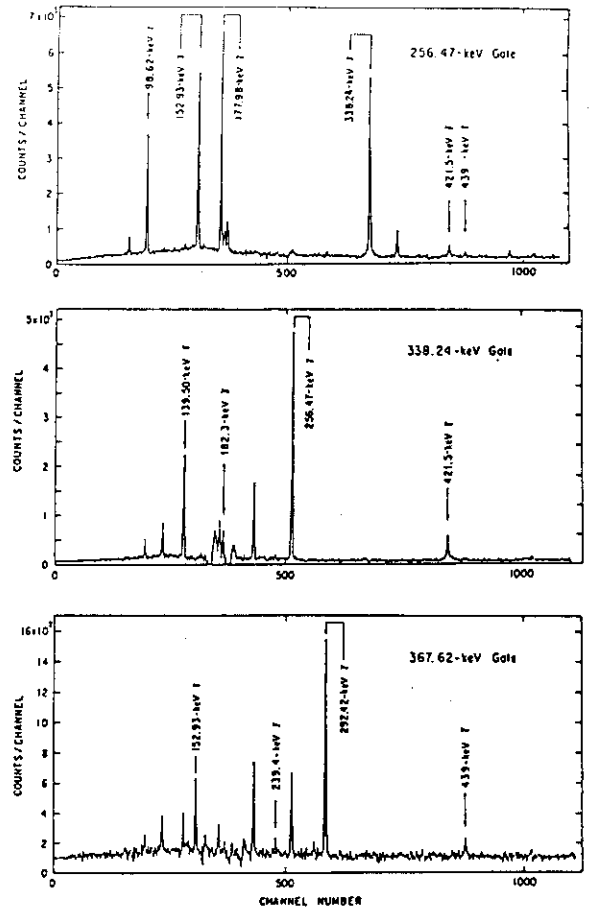

Fig. 2. An example of γγ coincidences to identify the new band members: ^{167}Er(^{35}Cl,^{35}Cl'γ)^{167}Er at 160 MeV.

^{163}Dy($\nu f_{7/2}$ orbital) and ^{173}Yb (νh9/2 orbital) do not show such behavior at all.

The signature dependence is also observed in reduced transition probabilities B(M1) and B(E2) as is shown in fig.5. It seems very hard to describe this behavior by a conventional Coriolis band-mixing calculation although it can reproduce the level energies satisfactorily. Recently, Hamamoto[2] and Marshalek[3] have pointed out a possibility of such signature dependent B(M1) and B(E2) in the rotational band built on the $i_{13/2}$ orbital.(See Fig. 5.) A microscopic calculation(CHFB) with quantum number projection[4] is presented for comparison, too. For B(M1) values which show a remarkably large signature dependence, Marshalek's prediction seems best except for the 11/2→9/2 transition. Quantitatively speaking, however, we need to further investigation of this problem. It would be very much desirable to accurately measure B(M1) values for

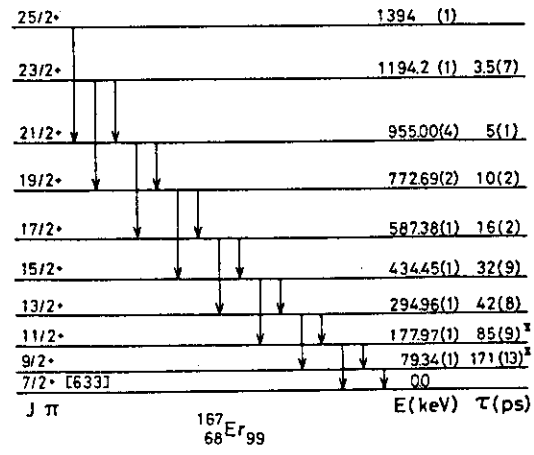

Fig. 3. The ground-state rotational band in ^{167}Er. Measured lifetimes τ are given in units of ps. Numbers in parentheses indicates the uncertainties in the least significant figure.

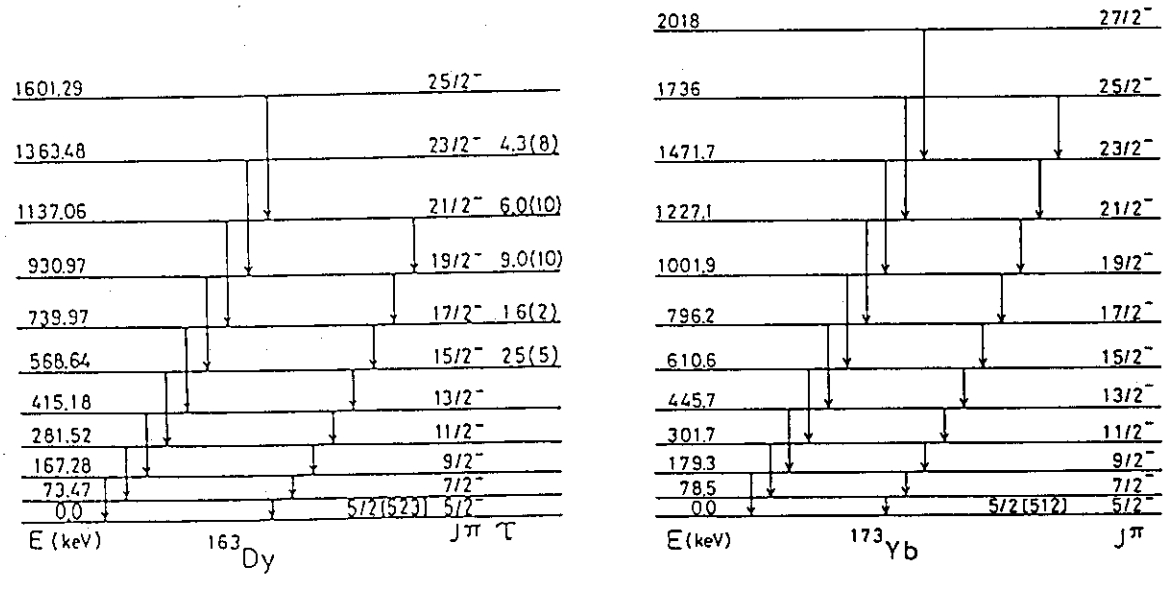

Fig. 4. The ground-state rotational bands in ^{163}Dy and ^{173}Yb.

relatively low-spin members of the ground-state rotational band in order to see the adequacy of a model calculation.

It is also important to study how B(E2) values change with spin in the deformed nuclei. If we do this systematically up to, say, I = 16 (or 27/2), the result will give us much insight into the nuclear structure of the rotating nuclei, for instance, such a long-standing problem as the interplay of the centrifugal distortion and the Coriolis anti-pairing effect. In this sense multiple Coulomb excitation with heavy ions should be still very much informative. The advent of heavy-ion tandem accelerator will cause a sort of renaissance of Coulomb excitation.

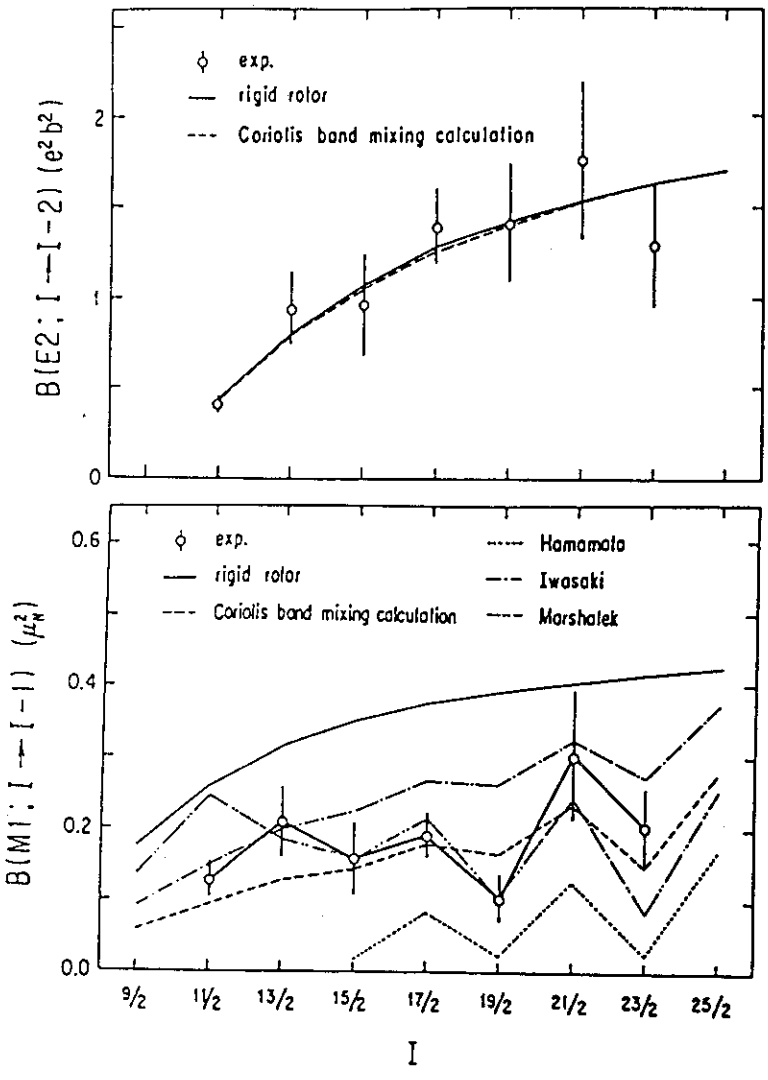

Fig. 5. B(E2;I→I-2) and B(M1;I→I-1) values observed for ^{167}Er. The open circles indicate experimental values, which are compared with theories.

References

1) M. Ohshima, E. Minehara, M. Ishii, T. Inamura, and A. Hashizume, J. Phys. Soc. Japan 52 (1983) 2959.
2) I. Hamamoto, Phys. Lett. 102B (1981) 225; 106B (1981) 281.
3) E.R. Marshalek, Phys. Rev. C26 (1982) 1678.
4) S. Iwasaki, private communication.

II.8 In-Beam Gamma-Ray Spectroscopy Through Heavy-Ion Induced Fusion Reaction

Mitsuhiko Ishii and Akiyasu Makishima*

Division of Physics, Japan Atomic Energy Research Institute, Tokai-mura, Ibaraki-ken, * Department of Applied Physics, Tokyo Institute of Technology, Meguro-ku, Tokyo

Fusion reactions induced by heavy ions can excite nuclei in high spin states and produce more proton-rich nuclides than those induced by light ions such as alpha-particles, carbon-12 and oxigen-16. So they are very attractive in the field of in-beam gamma-ray spectroscopy. In these reactions, however, the excitation energy is so high that protons and alpha-particles are emitted from compound nuclei and that many nuclides are produced. This makes it difficult to identify nuclides emitting individual gamma-rays and to obtain clear coincidence spectra between gamma-rays.

In order to solve this problem, we have developed the charged particle multiplicity filter (CPM filter) which can discriminate protons and alpha-particles emitted in the nuclear reactions. It consists of ten Si detectors; two of them are of an annular type with a size of 35 mm x 35 mm x 0.5 mm and eight side detectors rectangular of 30 mm x 35 mm. They surround the target as shown in fig. 1 so that 90 % or more of the emitted charged particles can be counted. Each of them is covered with a Cu foil of 20 mg/cm^2 so that scattered projectiles and low energy delta-rays can be stopped therein.

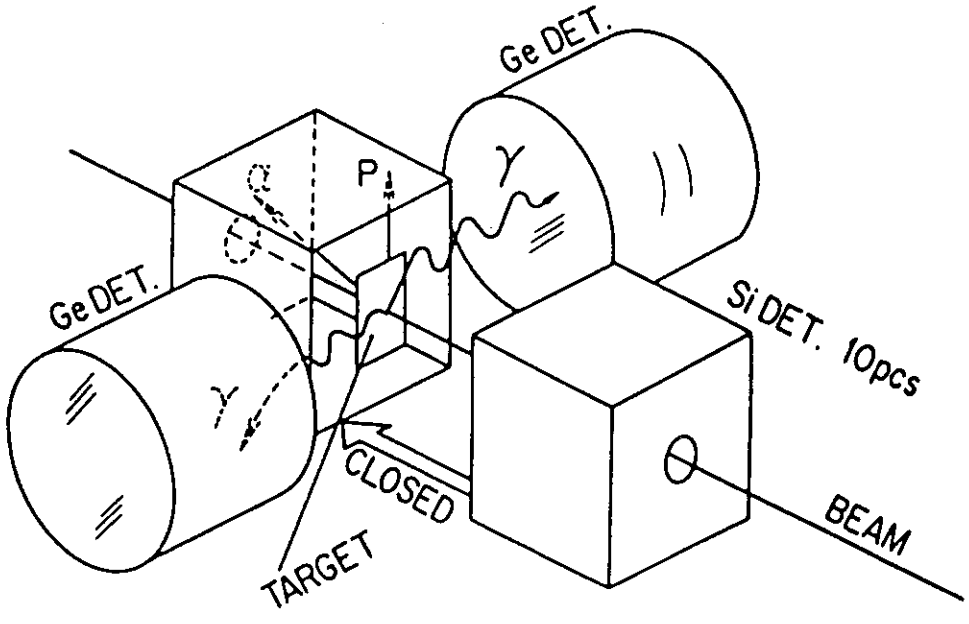

Fig. 1. A schematic drawing of the charged particle multiplicity filter.

We have employed the CPM filter to study high spin states in samarium-138 by bombarding Ag-107 with a Cl-35 beam of 155 MeV. Gamma-gamma coincidence, gamma-ray angular distribution and Doppler shift measurements have been carried out with a gate set on the reaction channel emitting two protons.

Some of preliminary results are shown in fig. 2. Excited states up to spins 12^+ have been established; members of the ground band up to the 8^+ state and some members of another band joining it. An isomeric transition from the 10^+ to the 8^+ states was found and turned out to have almost the same value of the reduced E2 transition probability as the one in samariun-140. This indicates that the 10^+ isomer is ascribed to a broken pair of neutrons in the $h\text{-}11/2^-$ orbital. On the whole the transition energies and the lifetimes of other excited states imply the increase of collectivity with the decrease of neutron number in light samarium isotopes.

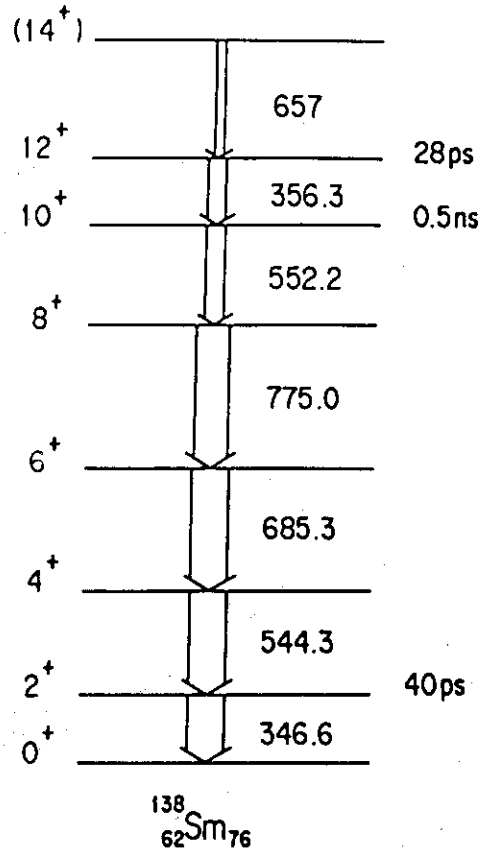

Fig. 2. A level scheme of Sm-138.

II.9 Deformed Ground Band States in $^{152}_{66}Dy_{86}$

Y. Nagai

Department of Physics, Osaka University

It is generally accepted that in the nuclei of many nucleons outside of closed shells a large number of $J^{\pi}=0^{+}$ pairs (quanta) exist in the ground state. An assembly of these identical quanta (called condensate[1]) can be described by the static deformation of the field that creates these quanta. In other words the pair field causes the deformation in the gauge space and thus breakes the rotational invariance giving rise the rotational motion in the space[1]. Analogous situation occurs in the ordinary space when the quadrupole field breakes the rotational invariance. Forthermore as the rotational ground band state involves many single particle configurations, enhanced E2 transition strength is observed. Similarly the pair transition strength was firstly predicted by S. Yoshida[2] to be enhanced and later experiments confirmed the enhancement.

Thus an angular momentum (I) is equivalent to the particle number (N) in the gauge space. Consequently the rotational frequency (ω) of the nucleus in the ordinary space, defined as $\omega=\frac{1}{\hbar}\cdot\frac{\partial E}{\partial I}$, is also equivalent to the Fermi energy (λ) in the gauge space, which is defined as $\lambda=\frac{1}{\hbar}\cdot\frac{\partial E}{\partial N}$ [1].

Backbending plot (I vs ω) in the ordinary space reveals a crucial role of the rotational frequency on the alignment of the quasiparticles[3]. Thus it is quite interesting to see what can be learned from backbending plot (N vs λ) in the gauge space[4].

The yrast states of ^{152}Dy up to spin 38 were studied by (HI, xn) and (α, xn) reactions[5] and they are interpreted as aligned multiparticle configurations. The present work of (α, 4n) reaction on ^{152}Gd identified ground band non yrast states up to $I^{\pi}=18^{+}$[6].

The dependence of the Fermi energy λ on the neutron number N is plotted in Fig. 1. The curves N(λ) for lower- and higher-branches indicate the two different states of the spherical and deformed shapes. (The backbending in gauge space can only appear when a rapid change in deformation of the nucleus occurs). The present result indicates that deformed shapes persist down to lower N for higher spins, or equivalently the deformation increases smoothly when going up to the ground band. Measured B(E2) values on N=88 nucleus of

^{152}Dy show a more pronounced spin dependence on the deformation. It is of course highly desirable to get an information on E2 transition strengths at these higher spin states in order to confirm the present result. As mentioned before, however, the ground band higher spin states of ^{152}Dy were nonyrast states and consequently it is quite difficult to measure the transition strengths at these higher spin states.

In conclusion ground band states of ^{152}Dy were identified up to spin 18^+ for the first time and the backbending plot in the gauge space demonstrates that at high spin states of $I^{\pi}=10^+$ the N=86 nucleus of ^{152}Dy gets well deformed shape as that of the nucleus with more than 90 neutrons. The reason why the deformation persists down to lower neutron number for higher spin states may be explained as the less energy consumption for a deformed nucleus to form the higher spin states compared to the case of a spherical nucleus.

References

1) A. Bohr and B.R. Mottelson: Nuclear Structure, Vol. II (Benjamin, New York, 1975).
2) S. Yoshida: Nucl. Phys. 33 (1962) 685.
3) A. Johnson et al.: Phys. Lett. 34B (1971) 605.
4) R. Bengtsson et al.: Phys. Lett. 105B (1981) 5.
5) T.L. Khoo et al.: Phys. Rev. Lett. 41 (1978) 1027
Y. Nagai et al.: Z. Phys. A296 (1980) 91.
6) J. Styczen, Y. Nagai, M. Piiparinen, A. Ercan and P. Kleinheinz: Phys. Rev. Lett. 50 (1983) 1752.
7) D. schwalm: Nucl. Phys. A396 (1983) 339C.

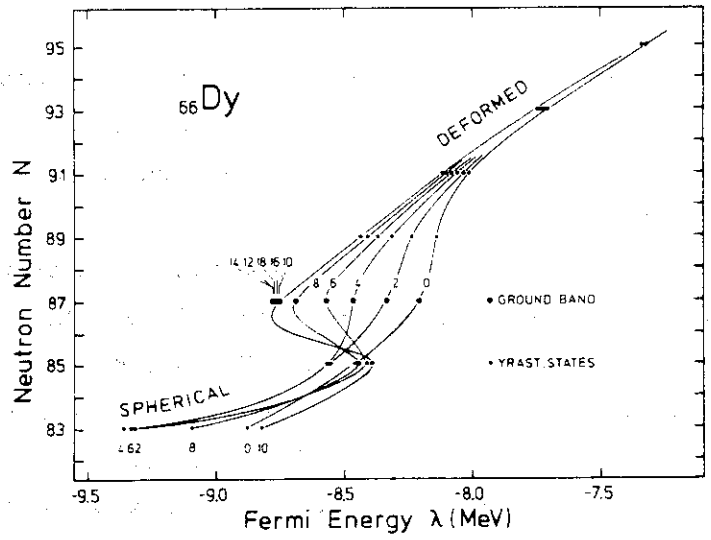

Fig.1
Backbending plot for the even Dy isotopes, showing the neutron number(N) vs the Fermi energy(λ).

II.10 Nuclear Spectroscopy of Radioisotopes Produced by Heavy-Ion Reactions

T. Tamura

Nuclear Engineering School, Japan Atomic Energy Research Institute

Since the installation of JAERI tandem van de Graaf accelerator, radioactivity group[1] of JAERI has started α, β, γ spectroscopy. A mass separator was introduced from Danfysik Denmark (Fig. 1), and was successfully operated off line supplying pure radioactivities of iodine 118-121 for the detailed spectroscopy of these nuclides.

For on-line use of the mass separator, target-ion source assembly of Fig. 2 was developed by S. Ichikawa et al.[4] Radioactivities of short-lived Cs in the mass range of 119-121 were produced via $^{93}Nb(^{32}S,X)$ reactions. A 150- to 165-MeV ^{32}S beam was directed on a 4-μm thick Nb target which was used as an entrance window for the ion source. The recoiled product was stopped on the graphite catcher and freed by heating. Ionizer made of tungsten cylinder at 1500°C ionizes the Cs atoms quite efficiently. The activities are mass separated and was transported to the collector tape situated in the measurement room.

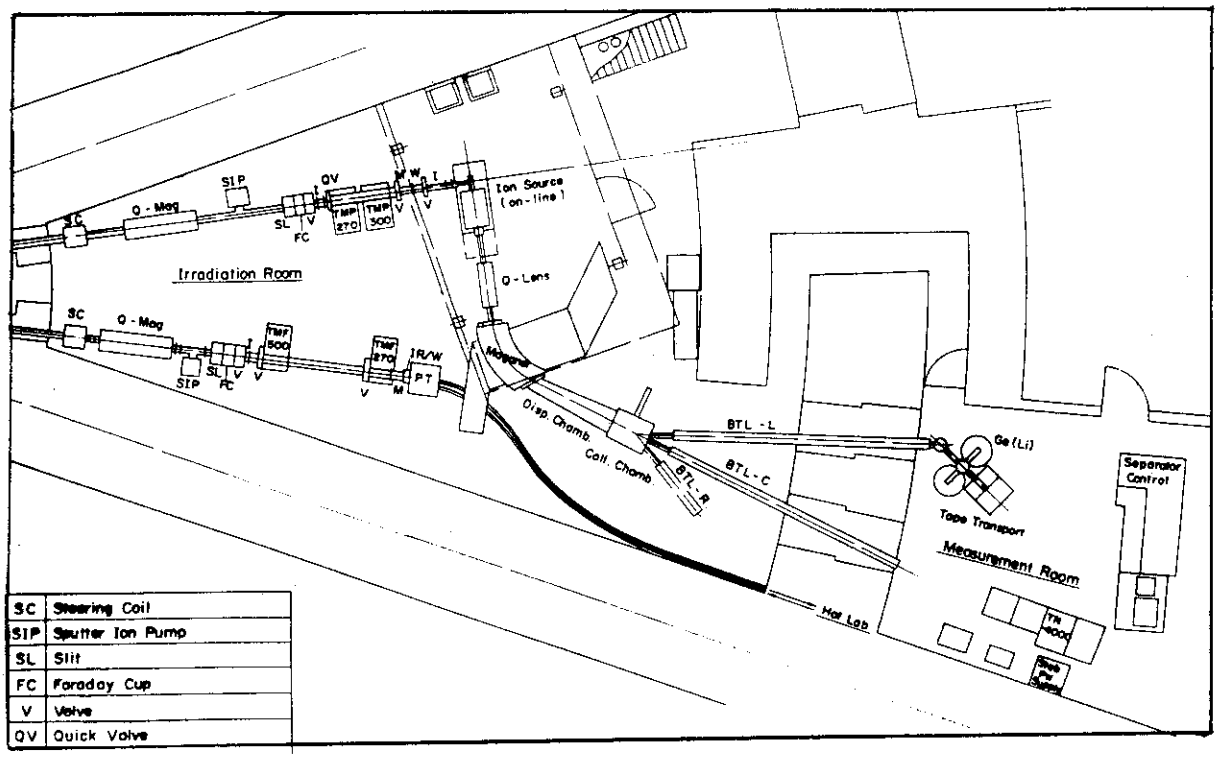

Fig. 1 JAERI on-line mass separator.

Fig. 3 shows an example of γ-ray spectrum for the mass 119 observed with HP Ge detector in multiscaling mode during 1 min collection time for 3 hours. The efficiencies of each stage of the separator was estimated off line[4]:

(1) rate of recoil out of the target (4μm thick Nb) with a 165-MeV ^{32}S beam	80%
(2) ionization efficiency	50%
(3) transport in the mass separator	30%
overall efficiency	12%

Fig. 2
Ion source for on-line mass separator

1. Beam
2. Target
3. Carbon catcher
4. Vaporizer
5. Ionizer
6. Inner heat-shield
7. Outer heat-shield

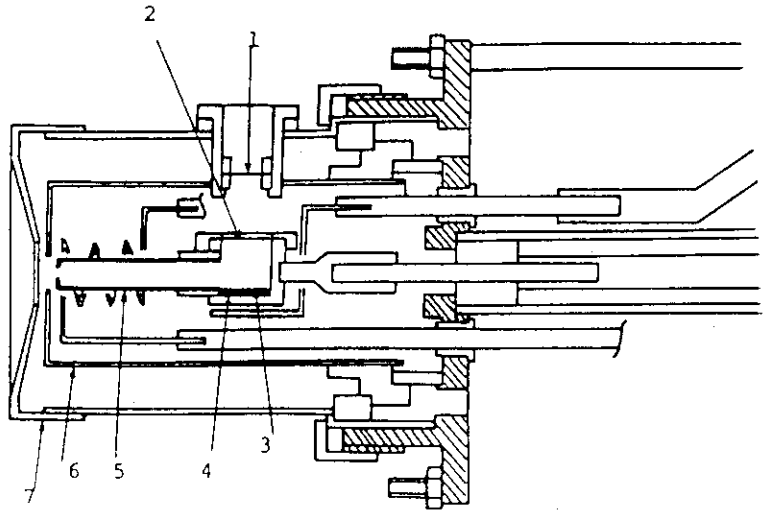

Fig. 3
Gamma-ray spectrum of ^{119}Cs

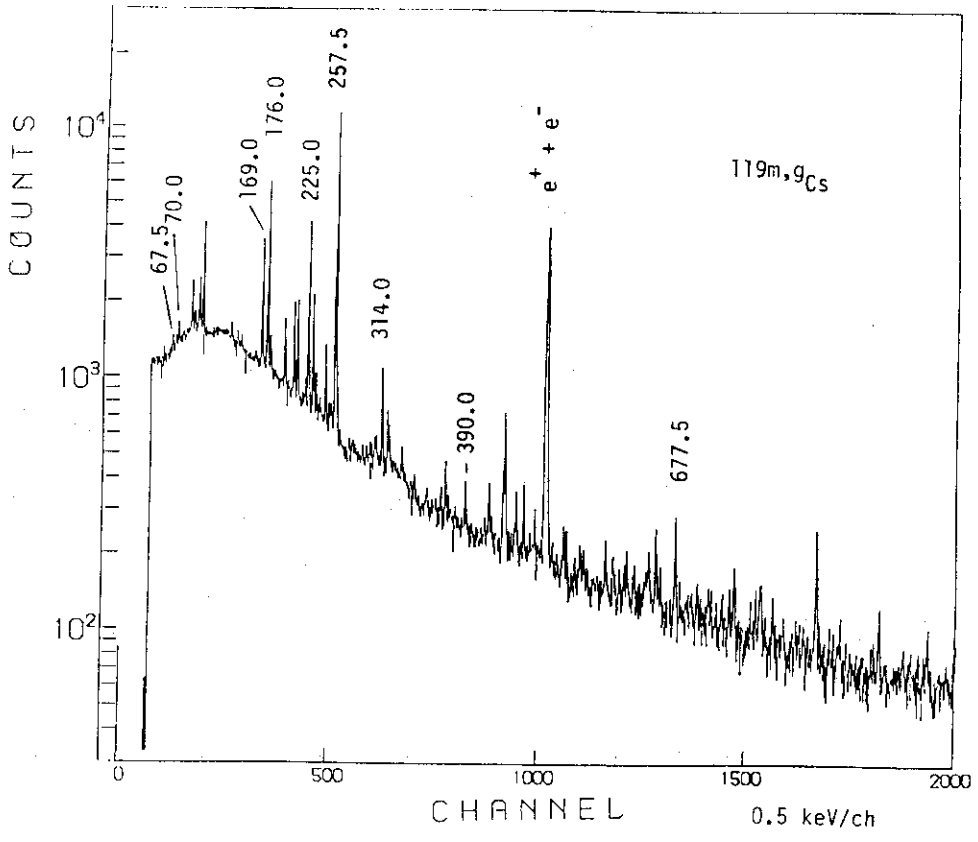

From the analysis of γ-ray spectra, we obtained a tentative decay scheme of $^{119\,g}$Cs. The spins, magnetic moments and isotope shifts of Cs isotopes for A = 118 - 145 have been determined by the ISOLDE collabolation and were considered as an indication of the change of deformation in this region of nuclide[5]. The Nilsson orbit $9/2^+(404)$ was assigned to the ground state of ^{119}Cs. The level scheme of ^{119}Xe fed from $9/2^+$ state is consistent with the result of in-beam experiments[6,7].

Fig. 4 Tentative decay scheme of ^{119}Cs

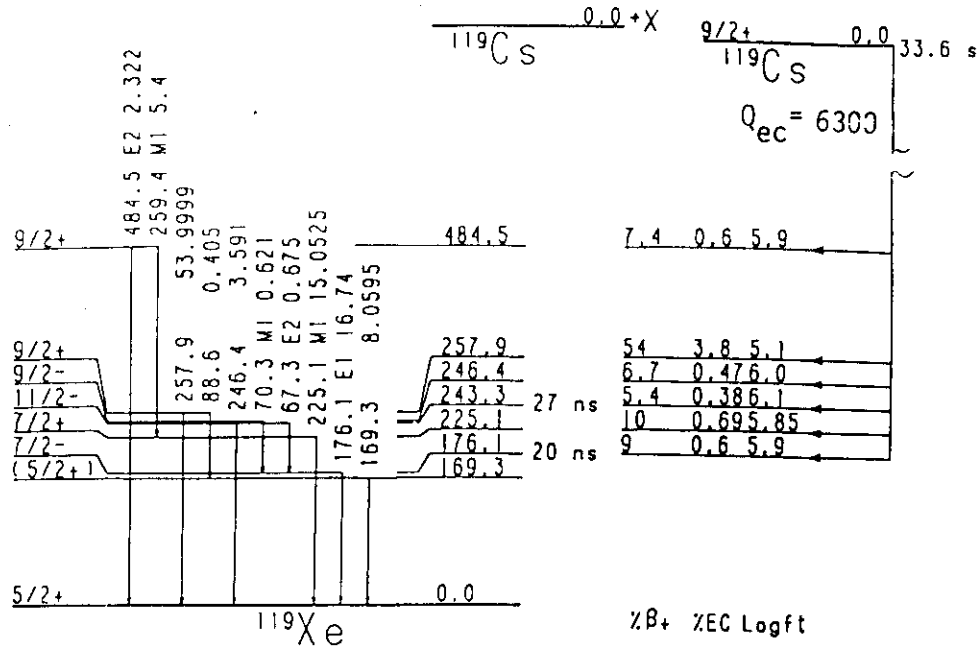

We are planning to extend our field of nuclear spectroscopy to Ba and rare earth nuclides in the far neutron deficient side.

1) Radioactivity study group:
T. Tamura: Nuclear Engineering School; M. Ohshima, E. Minehara: Department of Physics, T. Sekine, K. Hata: Department of Radioisotope Production, S. Ichikawa: Department of Chemistry; Japan Atomic Energy Research Institute; O. Nakamura, S. Ohya, K. Nishimura, N. Mutsuro: Niigata University; N. Takahashi: Osaka University; N. Imanishi: Kyoto University; T. Horiguchi: Hiroshima University.

2) T. Tamura, M. Ohshima, E. Minehara, T. Sekine, K. Hata, S. Ichikawa, O. Nakamura, S. Ohya, N. Mutsuro: JAERI Tandem Annual Report 1982 P.58

3) T. Tamura, M. Ohshima, T. Sekine, S. Ichikawa, K. Nishimura, S. Ohya, N. Mutsuro: JAERI Tandem Annual Report 1982 P.61

4) S. Ichi kawa, T. Sekine, K. Hata, N. Imanishi, T. Horiguchi, N. Takahashi: The XXVII Symposium on Radiochemistry at Nagoya; October 1983 P.28

5) C. Thibault et al.: Nuclear Physics A367 (1981) 1

6) V. Barci et al.: Nuclear Physics A383 (1982) 309

7) P. Chowdhury et al.: Phys. Rev. C23 (1981) 733

II.11 Difference Between Renormalization Factors for Unique First Forbidden AXIAL-β Transitions and Those for Analogous M2-γ Transitions

Hiroyasu Ejiri

Dept. of Physics, Osaka University, Toyonaka, Osaka 560, Japan

Unique first forbidden β-decays ($B_{ij}(\beta)$) and analogous magnetic-quadrupole γ-decays (M2(γ)) are studied precisely for semi-magic nuclei with Z=50 or N=82. Experimental studies have been mainly made by Ejiri, et.al.[1] Theoretical analyses in terms of the spin isospin polarization have been extensively carried out by Ejiri and Fujita.[1] The transition matrix elements are reduced largely due to the uniform quenching effect of the spin isospin polarization.[1] Finite difference between the renormalization factors for the β and γ transitions are indicated, being suggestive of the exchange current contribution of an order of 5% to the γ-transition. Transitions studied are simple stretched transitions[1] of $(1h11/2)_p \overset{\gamma}{\rightarrow} (1g7/2)_p$, $(1h11/2)_n \overset{\gamma}{\rightarrow} (1g7/2)_n$ and $(1h11/2)_n \overset{\beta}{\leftrightarrow} (1g7/2)_p$. Multipole assignments and the γ transition rates were obtained by means of the precise inbeam e-γ spectroscopy with the TESS[2] (Triple-Focussing Electron Spectrum Selector).

The transition operator for the M2(γ) transition is given by

$$\frac{e\hbar}{2MC}(J(2J+1))^{1/2} r^{J-1} \cdot i^{J-1} \left[\frac{1}{2}\left(g_s - \frac{2g_l}{J+1}\right)(Y_{J-1}\times\sigma)_J + \frac{2g_l}{J+1}(Y_{J-1}\times j)_J\right]. \quad (1)$$

The second term is proportional to $\langle J_i \| \mathbf{j} \| j_i \rangle \langle j_f \| Y_{J-1} \| j_i \rangle$, and vanishes for the stretched single quasi-particle transitions of $|j_i - j_f| = J$. Therefore the stretched M2(γ) and $B_{ij}(\beta)$ transitions have similar terms of the spin and isospin operators,

$$T_\gamma(M2) = g_1 \tau_3 ir[Y_1 \times \sigma]_2 + g_0 ir[Y_1 \times \sigma]_2, \quad (2)$$

$$T_\beta(B_{ij}) = g_A \tau_\pm r[Y_1 \times \sigma]_2, \quad (3)$$

where $g_1 = (e\hbar/2MC)(\sqrt{6}/2)(\mu_- - g_{\ell-}/3)$, $g_0 = (e\hbar/2MC)(\sqrt{6}/2)(\mu_+ - g_{\ell+}/3)$, $\mu_- = \mu_n - \mu_p$,

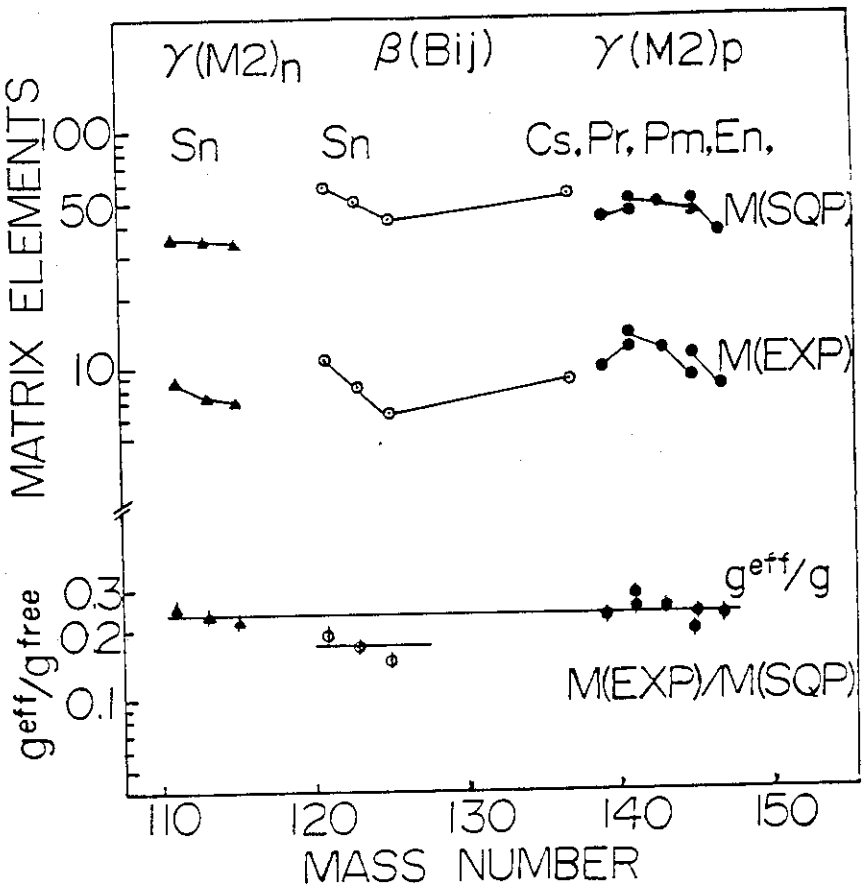

Fig. 1. Matrix elements for the (1h11/2 → 1g7/2) M2 γ transitions and the (1h11/2 ↔ 1g7/2) β transitions in nuclei with Z=50 or N=82. $\gamma(M2)_n$ and $\gamma(M2)_p$ stand for the odd-neutron and odd-proton γ transitions, respectively. B_{ij} is the unique first forbidden transitions. The γ and β transition matrix elements are given in units of $e\hbar/2MC$ and 10^{-14}cm, respectively. M(EXP) and M(SQP) are the experimental value and the shell-model calculation. The M(EXP)/M(SQP) ≡ g^{eff}/g is the renormalization factor .

$\mu_+=\mu_n+\mu_p$, $g_{\ell-}=g_{\ell n}-g_{\ell p}$ and $g_{\ell+}=g_{\ell n}+g_{\ell p}$. Note that the isovector term dominates the M2γ transition operator, and is analogous to the $B_{ij}(\beta)$ operator. The observed transition matrix elements $\langle M\rangle_{exp}$ are reduced uniformly over the simple model calculations $\langle M\rangle_{sqp}$, as shown in Fig. 1. Here $\langle M\rangle_{sqp}=_0\langle f|T|i\rangle_0$, and $|k\rangle_0$ is the eigen function for the model Hamiltonian without the spin-isospin interaction,

$$H_0 = H_{shell} + H_{pair} + H_{QQ} + H_{OO}. \qquad (4)$$

The quadrupole and octupole interactions in the eq.(4) have minor effects in the semi-magic nuclei of the present concerns. It is interesting to note that the renormalization factors $g^{eff}/g=<M>_{exp}/<M>_{sqp}$ are $\simeq 0.22 \sim 0.24$ for both the odd-proton and odd-neutron γ-decays, while the values $0.15 \sim 0.19$ for the β transitions are smaller than those for the γ transitions, as shown in Fig. 1. The renormalization factors for the γ-transitions are given by

$$g_p^{eff}/g_p = 0.89\ g_1^{eff}/g_1 + 0.11\ g_0^{eff}/g_0 , \tag{5}$$

$$g_n^{eff}/g_n = 1.14\ g_1^{eff}/g_1 - 0.14\ g_0^{eff}/g_0 , \tag{6}$$

where g_1^{eff}/g_1 and g_0^{eff}/g_0 are the renormalization factors for the isovector and isoscalar terms. The isoscalar term is small, and change of the g_0^{eff}/g_0 within the errors of the g_p^{eff}/g_p and g_n^{eff}/g_n affects little the values g_1^{eff}/g_1. Thus $g_1^{eff}/g_1 \simeq 0.22 \sim 0.24$ exceeds the values $g_A^{eff}/g_A \simeq 0.15 \sim 0.19$, as shown in Fig. 2.

Now lets introduce the spin isospin polarization interaction,

$$H_I = (M\omega/A\hbar)\chi_{\tau\sigma}\boldsymbol{\tau}\,\boldsymbol{\tau}\,(Y_1\times\boldsymbol{\sigma}).(Y_1\times\boldsymbol{\sigma}) \tag{7}$$

Then the renormalization factor is given by

$$g_1^{eff}/g = 1/[1+\chi_{\tau\sigma}G^2+h] . \tag{8}$$

$G^2=\Sigma|<j\|\tau\sigma\, Y_1\|i>|^2/(E_1\pm E_{ij})$, and the term h stands for the contribution of the higher excitation strength (effects of tensor interaction, isobar etc.). We use the value[3] $h\simeq 0.45$ and $\chi_{\tau\sigma}=\chi'_{\tau\sigma}/A^{1/3}$. The result of the PPA calculation for the H_I is shown in Fig. 2. The H_I interaction reduces uniformely both the β and isovector γ-transition matrix elements because of the symmetry in the isospin space. Consequestly use of such $\chi'_{\tau\sigma}$ as to reproduce the g_p^{eff}/g_p and g_n^{eff}/g_n overestimates the g_A^{eff}/g_A, while use of such $\chi_{\tau\sigma}$ as to reproduce the g_A^{eff}/g_A underestimates the value g_p^{eff}/g_p and g_n^{eff}/g_n.

In short the g^{eff}/g for the $B_{ij}(\beta)$ is smaller than those for the isovector M2γ, and this is not explained by the spin isospin polarization interaction. As for the $(Y_1\times j)$ term configuration mixing introduced by the H_I is considered to contribute little to the $(Y_1\times j)$ term in the γ-transition because the phase is random. The difference between the β and γ renormalization factors suggests the contribution of the exchange

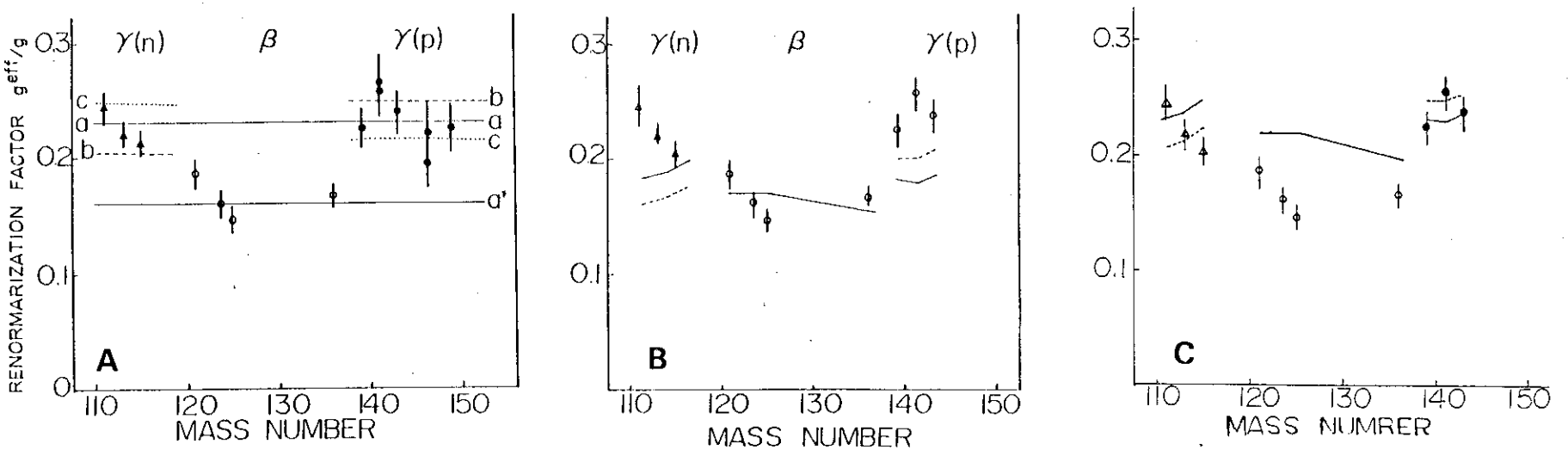

Fig. 2. Renormalization factors for the 1h11/2 → 1g7/2 M2γ transitions and the 1h11/2 → 1g7/2 β transitions.

A. Lines a,a' b and c are the values corresponding to the $(g_1^{eff}/g_1, g_0^{eff}/g_0)$ = (0.23, 0.23), (0.16,0.16), (0.23, 0.4), and (0.23, 0.1), respectively.

B. RPA calculations for the spin isospin polarization interactions with $\chi_{\tau\sigma}$= 1.5χ_τ and h=0.45 (sec,text).
Solid lines: The isoscalar term g_0^{eff}/g_0 is taken to be the same as the isovector term g_1^{eff}/g_1
Dashed lines: g_0^{eff}/g_o = 0.4 is used.

C. RPA calculations with $\chi_{\tau\sigma}$= 1.1χ_τ and h=0.45. Solid lines and dashed lines are the same as given in the caption B.

current. Qualitative evaluations of the exchange current and the $(Y_1 \times j)$ term contribution are under progress.

1. H. Ejiri and J.I. Fujita, Phys. Rep. 38C (1978) 85,
   H. Ejiri, Phys. Rev. C26 (1982) 2628
2. H. Ejiri, et.al., Nucl. Inst. Meth. 134 (1976) 107
3. H. Ejiri, Nucl. Phys. A396 (1983) 181

II.12 Nuclear-Spin Polarization of Heavy Ions Produced by Tilted Foils and Detected by Coulomb Excitation

Kenzo Sugimoto

Institute for Nuclear Study, Univ. of Tokyo

Production of nuclear-spin polarization by means of the tilted-foil method has been studied for 40-MeV ^{23}Na ions. To detect the nuclear polarization, the left-right asymmetry in inelastic scatterings was measured for the projectile Coulomb excitation of ^{23}Na-ions. The detected polarization of ^{23}Na($3/2^+$) was $\gtrsim(2.5\pm1.4)$%, with three carbon foils in the tilted angle of 60° for 40-MeV ^{23}Na ions.

The tilted-foil method seems to be a promising way to produce nuclear-spin polarized heavy ions, even in deeply ionized states of heavy elements. We have, therefore, planned to study the method systematically, by utilizing the left-right asymmetry in inelastic scattering through the projectile Coulomb excitation by incidence of spin-polarized projectiles.

The basic principle of the present experiment is as shown in Fig. 1: The tilted foils act as a polarizer of incident heavy ions, i.e., surface interactions in the out-going surfaces of the tilted foils produce polarization of electronic angular momenta (J) of ions in the direction parallel to $\hat{n}\times\vec{k}_i$, where $\hat{n}$ is the unit vector normal to the foil surface and $\vec{k}_i$ is the wave vector of incident heavy ions.[1] And the electronic (J) polarization partially transfers to the nuclear-spin (I) polarization through the hyperfine interactions in ions in flight in free space.[2-4] The nuclear polarization thus produced are analyzed by detecting the left-right asymmetry of inelastically scattered ions through the projectile Coulomb excitation. In the E2 Coulomb excitation, the predominant contribution comes from the component with the magnetic substate of M=+2, being $Z/\!/\vec{k}_f\times\vec{k}_i$, where $\vec{k}_f$ and $\vec{k}_i$ are the wave vectors of scattered and incident ions, respectively. This is true especially in the forward scattering angles and in the excitations when the adiabaticity parameter η is not too small, $\eta \gtrsim 0.1$.[5] The analyzing power of polarization,

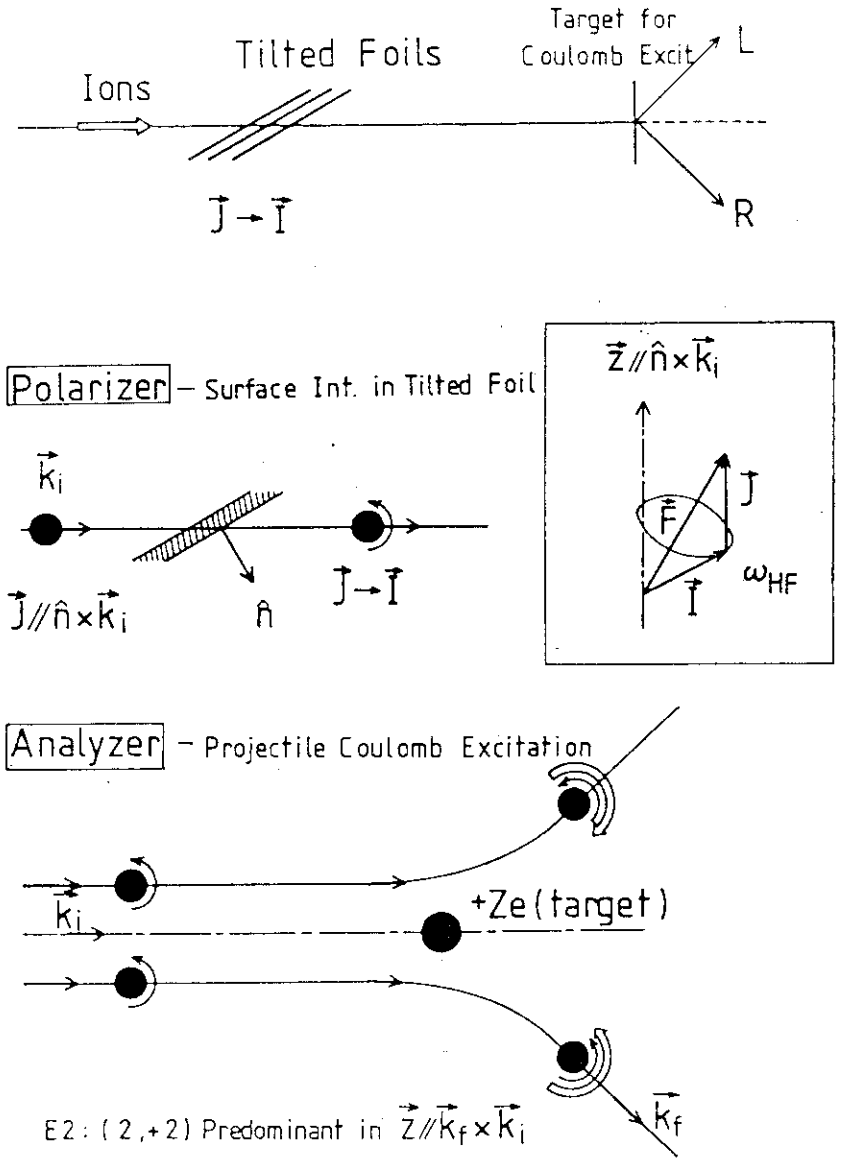

Fig. 1

therefore, can be made large and be unambiguously calculated. This sort of experiment has firstly tried by using ^{23}Na ions.

The experimental setup is schematically shown in Fig. 2. The $^{23}Na^{4+}$ ions, accelerated by the INS-SF cyclotron up to 40.1 MeV, went through three layers of tilted carbon foils with $\sim$10 $\mu g/cm^2$ in each thickness. The foils were mounted in a frame with the tilt angle of $\theta(\hat{n},\vec{k}_i)=60$, and the frame was rotatable as a whole so that the tilt angle could be changed from +60° to -60°. The ^{23}Na ions after passing through the tilted foils hit

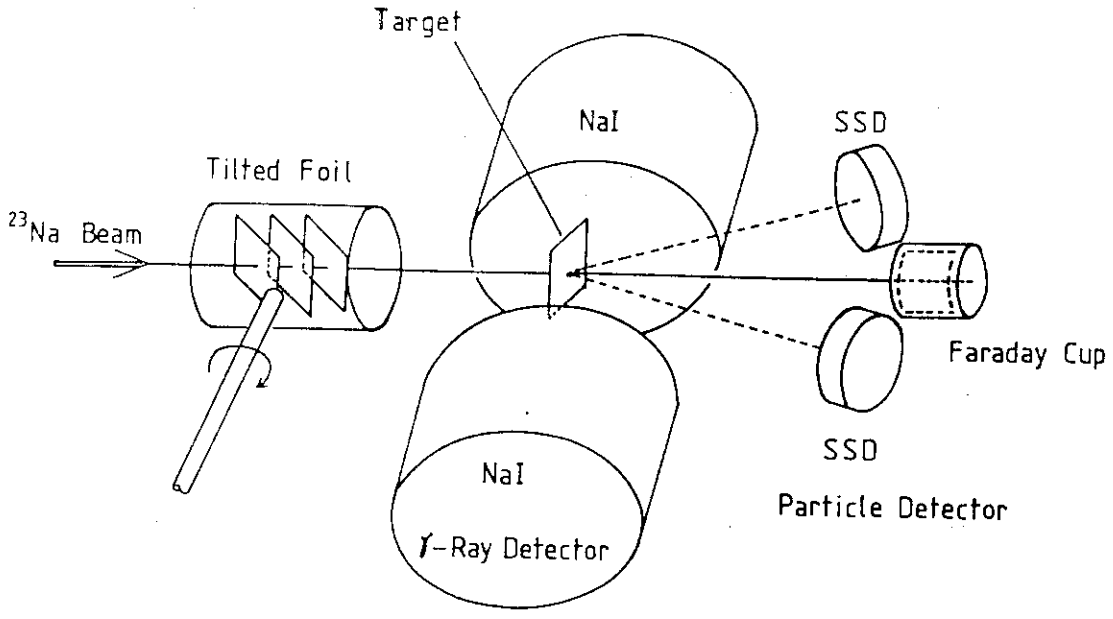
Target
NaI
SSD
Tilted Foil
^{23}Na Beam
Faraday Cup
SSD
Particle Detector
NaI
γ-Ray Detector

Fig. 2

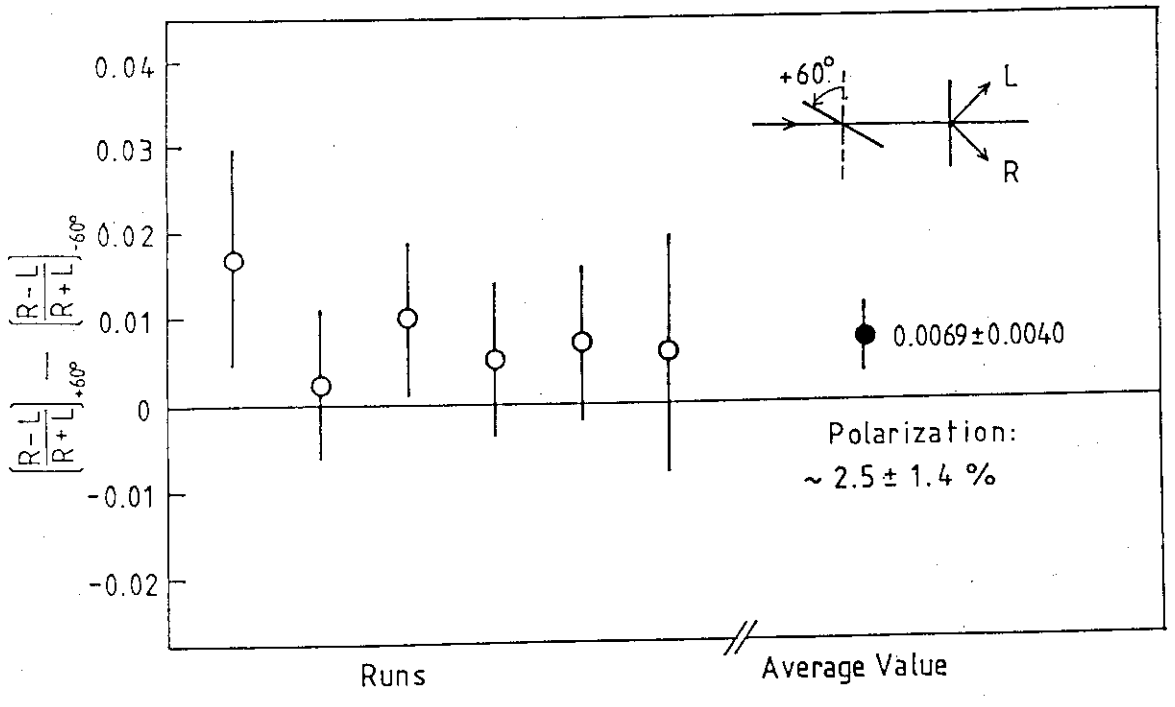
0.04
0.03
0.02
0.01
0
-0.01
-0.02
+60°
L
R
0.0069±0.0040
Polarization:
~ 2.5 ± 1.4 %
Runs
Average Value

Fig. 3

the ^{58}Ni target of ~350 $\mu g/cm^2$ in thickness. A pair of Si detectors, located at the scattering angle of $\pm(45^\circ \pm 15^\circ)$, detected the scattered ions. Inelastic components with excitation of the 440-keV first-excited state ($5/2^+$) were tagged by detecting the de-excitation gamma rays in coincidence with the particle detection. In order to eliminate possible instrumental asymmetry, the left-right asymmetries in counting rates, (R-L)/(R+L), were measured at the tilted-foil angles with $+60^\circ$ and -60°, and the genuine effect was determined from their difference.

The results at present on the left-right asymmetry measurments are shown in Fig. 3. The averaged asymmetry observed was (0.35 ± 0.20) %. The nuclear-spin polarization of ^{23}Na ($3/2^+$) was decuced to be $\gtrsim(2.5 \pm 1.4)$ %, for three carbon foils with the tilt angle of 60° at 40 MeV of ^{23}Na-ion energy. This value was not yet corrected for some systematic errors such as due to multiple Coulomb scatterings in the tilted foils, which might increase the value. The Coulomb excitation of ^{23}Na ($3/2^+$, ground $\rightarrow$ $5/2^+$, 440keV) transition exhibits a reasonably large cross section, however, the analyzing power of polarization is unfortunately small, since the excitation by E2 process is neither the stretched nor the jack-knife ones in vector adition of angular momenta.

Nevertheless, the left-right asymmetry of inelastic scatterings, through projectile Coulomb-excitation by incidence of polarized projectiles, provides a useful tool to analyze the heavy-ion polarization, produced by the tilted-foil method, in the high-energy region ($\gtrsim$ 1 MeV/nucleon) where no experimental investigation has been made so far.

The experimental work presented here has been done in collaboration with T. Tanabe, T. Hattori, K. Haga, N. Shikazono and J. Ichimura. Thanks are due to I. Sugai for his skillful target and foil preparation.

References

1) H. G. Berry et al., Phys. Rev. Lett. 32 (1974) 751
2) H. J. Andrä et al., Z. Phys. A281 (1977) 15
3) F. Q. Lu et al., Phys. Rev. 25 (1982) 25
4) Y. Nojiri and B. I. Deutch, Phys. Rev. Lett. 51 (1983) 180
5) K. Alder et al., Rev. Mod. Phys. 28 (1956) 432

SESSION III. RELATED TOPICS

(Jan. 11, Wednesday 1984)

Chairmans

Kichinosuke Harada
Japan Atomic Energy Research Institute

Kunio Nagatani*
Institute for Nuclear Study, The University of Tokyo

---

* Professor Kunio Nagatani died on 19 March 1984. He was 48 years old. The organizing committee and all of the participants bless a his memory.

III.1 Refinement of Brink Model†

---Application to massive transfers---

Atsushi Ichimura* and Munetake Ichimura**

*The institute of Space and Astronautical Science, Tokyo

**Institute of Physics, Univ. of Tokyo, Komaba, Tokyo

1. Introduction

Let us consider the direct transfer reaction between heavy ions

$$A\ (a,\ b)\ B, \quad a = b + x, \quad B = A + x. \tag{1}$$

The Brink model[1] tells in what situation the transfer strongly occurs and how the transition strength distributes among many final states.

The Brink's matching conditions

(i) in-plane condition $l_1 + \lambda_1 = \text{even}, \quad l_2 + \lambda_2 = \text{even}$

(ii) angular momentum matching $\Delta L = (L^i_{gr} + \lambda_1) - (L^f_{gr} + \lambda_2) = 0$

(iii) momentum matching $\Delta k_x = p^i_x - p^f_x = 0$

specify the optimum situation, and the factorized strength distribution

$$|T|^2 = |T_0|^2 \exp(-(\Delta L/\sigma_L)^2 - (\Delta k_x/\sigma_k)^2) \tag{2}$$

is assumed in the model. The conditions are obtained from assumptions;

(a) the transfer strongly occurs only in the localized region near the distance of the closest approach of both the initial and final channel grazing tragectories.

(b) the clusters A, x and b lie on the straight line perpendicular to those trajectories at the moment of the transfer,

(c) the impact on the cluster x is very small for the direction of the relative motion at this moment, and

(d) the mass relation $m_x \ll m_b, m_a$ holds.

The (semi)classical arguments[1,2,3] lead to the conditions but to reach them from the quantum mechanical DWBA expression is not apparent. The condition $\Delta L=0$ is rather easily understood[4] from DWBA because the grazing partial waves dominantly contribute to the DWBA integral, while the condition $\Delta k_x = 0$ and the factorization (2) are not easily understood.

Recently, massive transfer reactions are of a great interest, but no DWBA code is available for them. It is very desirable to develop any method for analysing them even if it is rather crude. For this purpose, the extended Brink model[5] has been introduced with the same assumptions except for the condition $m_x \ll m_b, m_A$, but their validity is more questionable.

---

† The talk is presented by M. Ichimura.

We comment that the optimum situation given by $\Delta L = 0$, and $\Delta k_x = 0$ can also be obtained from the momentum matchings of the clusters b and A, i.e.

(iv) $\Delta k_b = p_b^i - p_b^f = 0$, (v) $\Delta k_A = p_A^i - p_A^f = 0$.

Actually any two of the four conditions, (ii)~(v), give the same optimum situation (the spin and excitation energy of the residual nucleus B for the given incident energy E_i and projectile spin). Thus the priority of $\Delta L = 0$ and $\Delta k_x = 0$ is missing and so the factorized form (2) becomes questionable.

To answer those questions, we derive the extended Brink model from DWBA with several assumptions and approximations. In the course of this procedure, we obtain an approximate expression of the T-matrix, which is more easily calculated than DWBA, but more reliable than the extended Brink model. Let us call it the refined Brink model, by which we numerically study the validity of the assumptions and approximations used here.

2. From DWBA to the Brink model ---Approximate expressions of the T-matrix

Let us now proceed the above program. The DWBA amplitude of the reaction (1) is written as

$$T_{\beta\alpha}(\vec{k}_\beta, \vec{k}_\alpha) = C_{\beta\alpha} \int \chi_\beta^{(-)*}(\vec{k}_\beta, \vec{r}_\beta)\, \psi^*_{n_2 l_2 \lambda_2}(\vec{s}_2) V(\vec{s}_2, \vec{s}_1)\, \psi_{n_1 l_1 \lambda_1}(\vec{s}_1) \times \chi_\alpha^{(+)}(\vec{k}_\alpha, \vec{r}_\alpha)\, dx \qquad (3)$$

where the bound state wave functions $\psi_{nl\lambda}(\vec{s})$ is of the form

$$\psi_{nl\lambda}(\vec{s}) = R_{nl}(s) Y_{l\lambda}(\theta, \phi) \qquad (4)$$

and $V(\vec{s}_2, \vec{s}_1) = V_{bx} + V_{bA} - U_{bB}$ (or $V_{bA} + V_{xA} - U_{aA}$), and $C_{\beta\alpha}$ is the spectroscopic coefficient which will be set unity in the present argument. The coordinate system is shown in Fig.1 and x represent the 6-dimensional coordinates $(\vec{s}_1, \vec{r}_\alpha)$ or $(\vec{s}_1, \vec{s}_2)$ etc. and $dx = d\vec{s}_1 d\vec{r}_\alpha = J d\vec{s}_1 d\vec{s}_2 =$ etc.

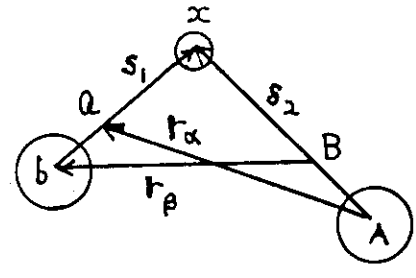

Fig. 1

Firstly, the distorted waves are evaluated by the 3-dimensional WKB approximation as[3]

$$\chi^{(+)}(\vec{k}, \vec{r}) = \sum_j A_j(\vec{k}, \vec{r}) D_j(\vec{k}, \vec{r}) \exp(-i(S_j(\vec{k}, \vec{r}) - \nu_j(\vec{k}, \vec{r})\pi/2)) \qquad (5)$$

where $S_j(\vec{k}, \vec{r}) = \int_{C_j}^{\vec{r}} \vec{p}_j(\vec{k}, \vec{r}) \cdot d\vec{r}$ is the action from the incident point to the point $\vec{r}$ through the j-th classical trajectory C_j and $\nu_j(\vec{k}, \vec{r})$ is the index given by how often C_j hits the caustics on this path. The amplitude $A_j(\vec{k}, \vec{r})$ is determined by the cross section of the flux tube around C_j at $\vec{r}$,

and $D_j(\vec{k}, \vec{r})$ is the damping factor due to the absorption. For simplicity, we take only the outermost trajectory and hence drop the sum over j and set = 0. This would be justified in practice due to the strong absorption.

Insert (4) into (3) and decompose the integrand into the modulus and the phase as

$$T_{\beta\alpha}(\vec{k}_\beta, \vec{k}_\alpha) \equiv T(q) = \int \exp(-f(x,q))\exp(ig(x,q))dx \tag{6}$$

where q represents the set of all quantum numbers specifiying the initial and final states, $q = (\vec{k}_\alpha n_1 l_1 \lambda_1 , \vec{k}_\beta n_2 l_2 \lambda_2)$. The modulus is

$$\exp(-f(x,q)) = A(-\vec{k}_\beta, \vec{r}_\beta)D(-\vec{k}_\beta, \vec{r}_\beta)\psi^*_{n_2 l_2 \lambda_2}(\vec{s}_2)V(\vec{s}_2, \vec{s}_1) \times \psi_{n_1 l_1 \lambda_1}(\vec{s}_1)A(\vec{k}_\alpha, \vec{r}_\alpha)\, D(\vec{k}_\alpha, \vec{r}_\alpha) , \tag{7}$$

and the phase is

$$g(x,q) = S(-\vec{k}_\beta, \vec{r}_\beta) + S(\vec{k}_\alpha, \vec{r}_\alpha) - \lambda_2\phi_2 + \lambda_1\phi_1 . \tag{8}$$

Secondly expecting the modulus is well localized for every q, we approximate it by a Gauss function around its peak at $x = \bar{x}(q)$ as

$$\exp(-f(x,q)) = F(q)\exp(-(\Sigma_{\mu\nu} a_{\mu\nu}(q)\xi_\mu\xi_\nu)/2) \tag{9}$$

with $\xi_\mu = x_\mu - \bar{x}_\mu(q)$. Assuming the localization is so well that the integration is evaluated by expanding g(x,q) up to the first order of , one can carry out the integral analytically. The result is written as

$$T(q) = T_0(q)\exp(-(\Sigma_\mu(\Delta p_\mu(q)/a_\mu(q))^2/2), \tag{10}$$

where $M(a_{\mu\nu})M^t = (a_\mu\delta_{\mu\nu})$ by the orthogonal matrix M and

$$\Delta p_\mu(q) = \Sigma_\nu (M^t)_{\mu\nu} \partial g/\partial x_\nu \Big|_{x = \bar{x}(q)} . \tag{11}$$

The expression (10) is obtained neither assuming the localized position nor the linear chain configuration apriori as the Brink model did. It does not usually have the factorized form of ΔL and Δk_x. It is calculable even for the massive transfer and should have wider applicability than the extended Brink model. Therefore let us call it the refined Brink model.

To reach the extended Brink model, one needs further assumptions. If the q-dependence of $T_0(q)$ is weak, one obtains the generalized matching conditions $\Delta p_\mu(q) = 0$, or equivalently

$$\partial g(\bar{x}(q), q)/\partial x_\mu = 0 . \tag{12}$$

Assuming further that $\bar{x}(q)$ represents the straight line configuration

perpendicular to the relative motion, one finds

$$\partial g(\bar{x}(q),\ q)/\partial \vec{s}_1 = -\Delta\vec{k}_b, \qquad \partial g(x(q),\ q)/\partial \vec{s}_2 = -\Delta\vec{k}_A. \tag{13}$$

Therefore the generalized matching conditions turn out to be the conditions (iv) and (v) in sect. 1. Thus the matching conditions of the extend Brink model are obtained.

3. Numerical study of the Brink's assumptions

To make the argument simple, we consider the two dimensional problem in the reaction plane. We take a spinless projectile a ($\lambda_1 = 0$) and assume that only the tails of the bound state wave functions contribute to the DWBA integral. Then, we can set $x = (s_1\phi_1, s_2\phi_2)$ and $q = (E_i,\ Q,\ \lambda_2,\ \theta)$ with the Q-value Q, and the scattering angle θ.

Two examples involving two ^{16}O's and α are investigated; the symmetric case , $^{16}O(^{20}Ne,\ ^{16}O)^{20}Ne^*$ (α-transfer), and the asymmetric case, $^{16}O(^{20}Ne, \alpha)^{32}S^*$ (^{16}O-transfer).

To see the localization and straight line configuration assumptions, the cluster distributions given by the DWBA integrand (9) are shown in Fig.2 where spreading widths are denoted by the thick lines. For the symmetric case, the reaction regions are well localized and the clusters place almost on the straight line, while for the asymmetric case, the straight line configuration does not realize and the reaction region of the lighter cluster (α particle in this case) rather widely spreads.

Fig. 2

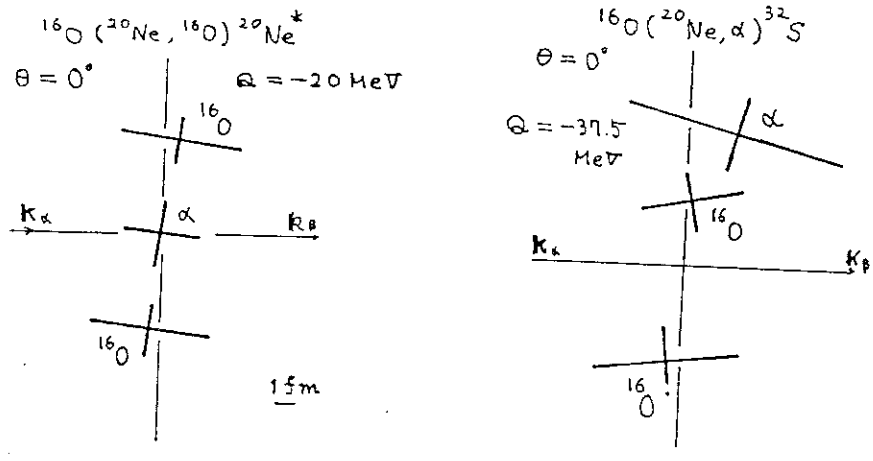

Next, let us see the strength distribution. Noting that the q-dependence of $T_0(q)$ of eq.(10) was found very weak in these cases, we drew in Fig.3 the equi-strength contours of the exponent part $T(q)/T_0(q)$ on the $(Q,\ \lambda_2)$ plane for the fixed $E_i^{lab} = 100$ MeV and $\theta = 0°$. The curves of $\Delta L = 0$,

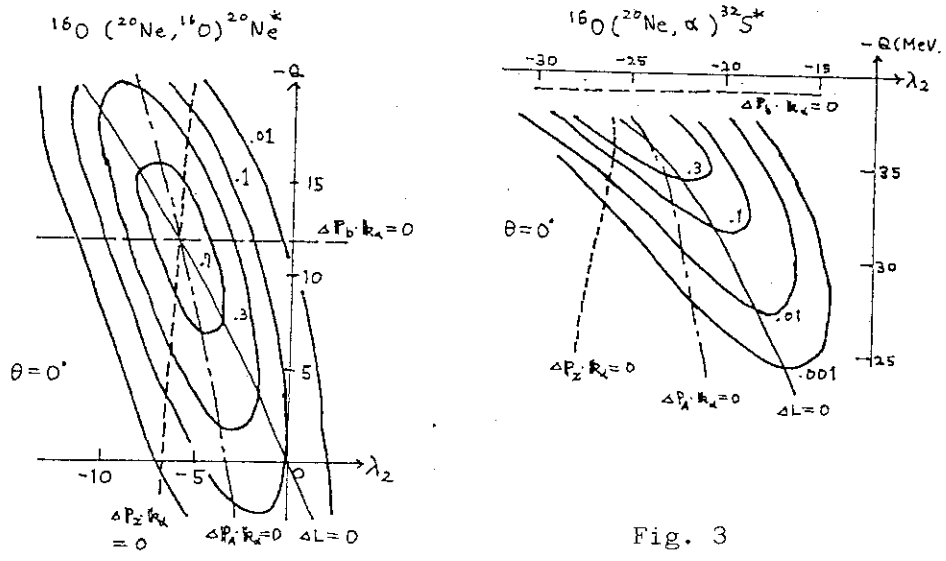

Fig. 3

$\vec{k}_z \cdot \vec{k}_\alpha = 0$, $\Delta\vec{k}_b \cdot \vec{k}_\alpha = 0$ and $\Delta\vec{k}_A \cdot \vec{k}_\alpha = 0$, which correspond to the matching conditions (ii), (iii), (iv) and (v) respectively, are also drawn. The curves of $\Delta L = 0$ and $\Delta\vec{k}_z \cdot \vec{k}_\alpha = 0$ do not necessarily run to the direction of the principal axes (the steepest and the gentlest slopes). Thus the factorization of the form (2) does not hold. However, the curves of $\Delta L = 0$ lie rather close to the ridges for both the symmetric and asymmetric cases. This indicates wider validity of the argument for $\Delta L = 0$ given in sec. 1.

The formula (9) which includes the phase can express the far- and near-side interference. The angular distribution with this interference is shown in Fig.4 for $^{16}O(^{20}Ne,^{16}O)^{20}Ne^*$.

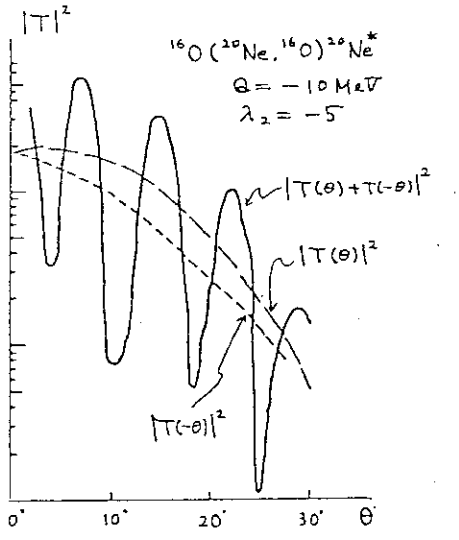

Fig. 4

References

1) D. M. Brink, Phys. Lett. 40B(1972)37.
2) H. Hasan and D. M. Brink, J. Phys, G4(1978)1573, G5(1979)771.
   T. Kammuri and K. Matsuoka, Nucl. Phys. A366(1981)171.
3) D. H. E. Gross, Phys. Lett. 43B(1973)371, 'Heavy-ion, High Spin States and Nuclear Structure' vol.1 (IAEA, Vienna, 1975) p.27.
4) K. Nagatani, M. Ichimura and A. Arima, Physica Scripta 6(1972)289.
5) M. Ichimura, E. Takada, T. Yamaya and K. Nagatani, Phys. Lett. 101B(1981) 289.

III.2 TDHF calculations of Heavy-Ion Collisions

Shuhei Yamaji

Cyclotron Laboratory, The Institute of Physical and Chemical Research

The time-dependent Hartree-Fock (TDHF) method is the only fully microscopic description of heavy-ion collisions and has been extensively applied to analysis of heavy ion collisions[1]. Since the first schematic calculation by Bonche et al in 1976, realistic calculations with effective interactions have been directly compared with the experimental observables.

In the first part of this report, I give the summary of TDHF calculations for fusion cross sections, scatterings and non-equilibrium emissions.

(1) Fusion

Fusion is the dominant process at a few MeV per nucleon above the interaction barrier in light systems. It can be explained fairly well by TDHF. The existence of a dynamic lower angular momentum limit in TDHF calculations, which can be qualitatively understood in terms of the long mean free path assumption, is an open subject and the experimental results are as yet inconclusive.

Fusion in heavy systems is not so dominant process that it can be represented by TDHF with the same degree of accuracy as it is in light systems. Fusion region is split as a function of energy in some of heavy systems. The lowest region, which just above the Coulomb barrier, is like a molecular resonance phenomenon with long collision time $\sim 10^{-20}$ sec. TDHF study of formation of long-lived superheavy molecules for the investigation of supercritical positron emission was carried out for head-on symmetric collisions of two isomeric uranium.

(2) Scattering

The deflection and energy loss in TDHF calculations can be divided into three region of interest: peripheral scattering for large angular momentum L, fusion or orbiting for intermediate L, and highly inelastic scattering for small L.

Double differential cross sections in TDHF are in good agreement with the experimental ones.

The mean mass and charge of the scattered projectile-like ion are very close to the initial projectile, in accord with the experimental DI

behavior.

The calculated charge and mass distribution width are always much smaller than the experimental values.

(3) Non-equilibrium emission

The emission of α-like fragments occurs from the neck of the composite system at a time comparable to the heavy-ion collision time. The three-body nature of the final stste has been found in some TDHF calculations, yielding low energy α-particles with a multiplicity of a few times 10^{-2}.

The emission of fast nucleons in mass asymmetric collisions also occors with a small multiplicity. The nucleons emerge promptly as a low density jet of matter in TDHF calculations, on time scales comparable to the time during which the projeclile transmits the target.

In the remaining part, I introduce our work which intends to solve one open problem that the variances of mass distribution calculated in TDHF are always an order of magnitude smaller than the observed values. For that purpose, we use the method of the time-dependent coupled-cluster approximation(TDCCA), which includes the effect of two-body collisions.

The equations to be solved numerically are derived by taking the lowest-order terms in TDCCA[2] :

$$i\frac{\partial}{\partial t}\varphi_\nu(t)=h(t)\varphi_\nu(t) \qquad (1)$$

$$i\frac{d}{dt}\langle\rho_1\rho_2|S_2|\nu_1\nu_2\rangle_A=\langle\rho_1\rho_2|V|\nu_1\nu_2\rangle_A \qquad (2)$$

The first equation determines the time-evolution of the single-particle basis , where h(t) is the Hartree-Fock(HF) Hamiltonian. The second equation specifies the time-evolution of the two particle-two hole amplitude $\langle\rho_1\rho_2|S_2|\nu_1\nu_2\rangle_A$. The indices ν and ρ denote hole and particle states, respectively.

Then, the mean number $\bar{N}_R$ of particles and the variance σ_R^2 of the mass distribution in the right fragment can be expressed in terms of the right-hand overlap integrals of single particle wave functions and two particle-two hole amplitudes at the time when two fragments are well seperated in the final stage of the collision.

We have performed numerical TDCCA calculations for the collision 320 MeV $^{16}O+^{40}Ca$ on the basis of the Skyrme force TDHF-code with axial symmetry. The initial particle states are restricted to 0d and 1s orbitals for ^{16}O and to 0f and 1p orbitals for ^{40}Ca. We use the δ-function $V(\vec{r},\vec{r}')=V_0\delta(\vec{r}-\vec{r}')$ as the residual interaction. The strength V_0 is dtermined to be -400 ~ -530 MeV

fm^3 from the condition that the depth of one-body potential obtained by folding the residual interaction with the density reproduces approximately that of the HF potential.

In Fig.1, the variances σ_R^2 of mass distribution for the 320 MeV $^{16}O+^{40}Ca$ reaction are shown as a function of angular momentum l. The TDCCA results indicated by shaded area with two boundary curves corresponding to V_0=-400 MeV fm^3 and V_0=-530 MeV fm^3 are very much enhanced as compared with the TDHF results.

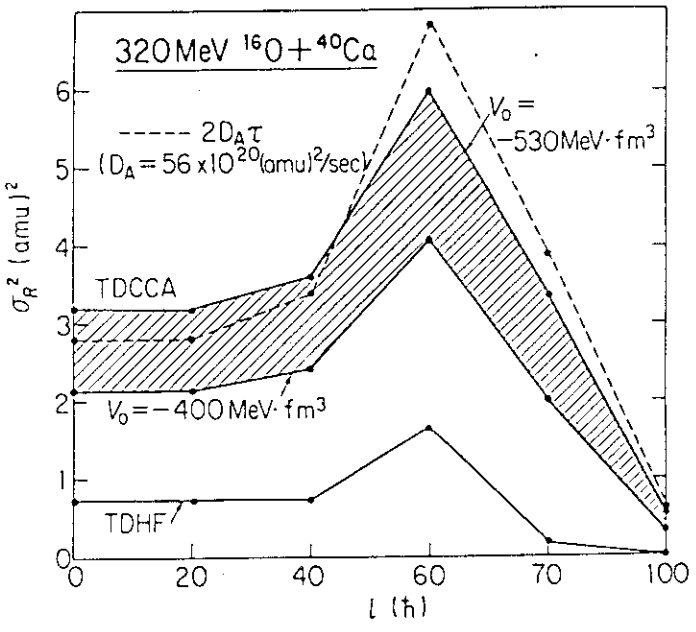

Fig.1

The variance σ_R^2 versus the initial angular momentum l for the 320 MeV $^{16}O+^{40}Ca$ reaction.

For lack of observed values for this reaction, the calculated values are compared with the empirical values of σ_R^2 estimated by the use of the relation $\sigma_R^2 = 2D_A\tau$, which can well reproduce observed mass distributions for heavy systems with the mass difusion coefficient $D_A \sim A\times10^{20}$ $(amu)^2/sec$, where A is the total mass number of the composite system. The collision time τ is calculated by TDHF, defining it as the interval during which the minimum density along the symmetry axis between the fragments exceeds 1/4 of nuclear matter density. The TDCCA results are slightly smaller than the empirical one shown by the dashed line in Fig.1. Considering V_0 to be an adjustable parameter, small increase of V_0 from the values used here yields the empirical values.

To summarize, the realistic calculation with two-body collisions reproduces the order of magnitude of empirical values of σ_R^2 for the 320 MeV $^{16}O+^{40}Ca$ reaction.

References

1) J.W.Negele: Rev. Mod. Phys. 54(1982)913.

2) M.Tohyama, and S.Yamaji: Phys.Lett.123B(1983)16.

III.3 Preequilibrium Light Particle Emission in ^{14}N Induced Reactions

Tomokazu Fukuda

Department of Physics, Osaka University

(1) Preequilibrium (PEQ) light particle emissions (p, d, t and α) have been investigated by measuring inclusive differential cross sections in the reaction of $^{93}Nb + ^{14}N$ at 132, 159 and 208 MeV[1]. The experimental data of inclusive spectra are analyzed in terms of two model: an extended exciton model[2], and a modified coalescence model[3].

The angle integrated energy spectra of proton at 132 and 208 MeV are well described by the extended exciton model which takes into account the finite collision time for heavy-ion fusion process. A calculation neglecting the finite collision time does not agree with the data. Such a calculation corresponds to the conventional exciton model with the initial exciton number n_o equal to projectile nucleon number A_p. In the conventional exciton model, n_o is regarded as a parameter to fit the data and found to be usually larger than A_p. However the physical meaning of n_o obtained in such a way is ambiguous. In the present model, the collision time $T = \Delta t \times A_p$ is a parameter and a good fit is obtained with $\Delta t = 1 \times 10^{-23}$ sec for both incident energies. In principle, the time T can be predicted theoretically, if we know the details of heavy-ion fusion process. Recently Niita have developed an exciton model[4] to describe the fusion process as well by incorporating with the transport theory[5]. This model gives the collision time to be about 10^{-22} sec, which is comparable to the value T of $1 \times 10^{-23} \times 14$ sec in the present case.

For composite particles, the present exciton model fails to reproduce both absolute values and spectral shapes of the data. The discrepancy between the calculation and the data is more pronounced as the mass of the

---

This work was performed in collaboration with M. Ishihara*, H. Ogata**, I. Miura**, T. Shimoda***, K. Katori***, S. Shimoura****, M.-K. Tanaka****, E. Takada+, T. Otsuka++, T. Nomura*, and K. Sueki+++. *IPCR, **RCNP, ***Lab. of Nucl. Studies, Osaka Univ., ****Dept. of Phys. Kyoto Univ., +MPI and Tokyo Univ., ++JAERI, +++Dept. of Chem. Tokyo Metro. Univ.

light particle and incident energy increase. The particle emission probability in the exciton model is calculated by using the detailed balance argument. However the PEQ process in heavy ion reactions may not proceed in completely statistical way and it may be necessary to take into account some correlation effects for composite particle production.

The coalescence model takes into account such an effect, where composite particles are assumed to be synthesized by the coalescence of free nucleons which happen to occupy the same momentum space P_0. The analysis in terms of the modified coalescence model can describe composite particle spectra quite well except for α at forward angles. Extracted coalescence radii P_0 are about 140 MeV/c for d and t and about 220 MeV/c for α or equivalently root-mean-square radii R_{rms} of the highly excited zone are 4-5 fm for d and t and about 2 fm for α.

Because the coalescence model makes no specific assumption about the dynamics of the reaction, source spectra of nucleons (proton or neutron) are not predicted by the model and usually taken from the experimental data. However we note that the proton and neutron spectra are well described by the extended exciton model. Thus we could reproduce light particle spectra fairly well by the coalescence model incorporating with the exciton model.

We note a distinctive aspect of alpha production; larger coalescence radii P_0 (or equivalently smaller radii R_{rms} of the highly excited zone) than those of d and t are observed, implying abnormally large cross section for α emission. This feature of large cross section of α is commonly observed in light heavy-ion ($A \lesssim 20$) induced reactions with the energy between just above the Coulomb barrier and 20 MeV/A, but not in relativistic energies. The large cross section is not totally attributed to the decay of ^{8}Be and excited projectile-like fragment, because its contribution is estimated to be at most 30% at forward angles where the effect is most significant. If we consider the particle emission from a single highly excited zone, R_{rms} for each composite particle should be the same, implying much smaller cross section of α than the experimental data. Therefore the large cross section of α may suggest another mechanism of production rather than that considered until now. One possibility is strong α-clusterization in preequilibrium process, which may be related to the α-cluster structure of light heavy ions or to the liquid-gas phase transition discussed in Ref. 6.

(2) We have also measured the longitudinal momentum transferred to the target (Δp) in the light particle emission of ^{14}N on ^{232}Th reaction at 208 MeV[7]. The transferred momentum was deduced by measuring the folding angle between the two fission fragments resulting from the sequential decay of the target-like nucleus. One of the most remarkable facts is the observation that the average values of fraction $f = (\langle\Delta p\rangle + P_{out}^{//})/P_{beam}$ are about 0.68 almost independently of light particle species and the detection angles (10°-55°), where $P_{out}^{//}$ is the momentum component parallel to the beam carried away by the observed light particles. This indicates that all the observed particles, protons, deuterons, tritons and α particles, are emitted from the same system that is produced in a reaction with around 70% momentum transfer. This suggests a possible mechanism to describe the phenomena in the following. Firstly some part (about 30% in this case) of the beam momentum is carried away by unobserved ejectiles and then the remainder of the projectile interacts with the target strongly and forms the preequilibrium system, and finally the PEQ system decays by the preequilibrium light particle emission. The decay process may be described by the exciton model[2]. The mechanism discussed above may be related to the recent theoretical work[8] of breakup in deep-peripheral region followed by fusion. More complete theory taking into account both first process (breakup) and the preequilibrium emission should be needed in order to see whether the above mechanism is really respondible for the experimental results or not.

References

1. T. Fukuda et al.: submitted to Nucl. Phys.
2. T. Otsuka and K. Harada: Phys. Lett. 121B (1983) 106
3. T.C. Awes et al.: Phys. Rev. C24 (1981) 89
4. K. Niita: submitted to Nucl. Phys.
5. K. Niita and N. Takigawa: Nucl. Phys. A397
6. M.W. Curtin et al.: Phys. Lett. 123B (1983) 289
7. T. Fukuda et al.: submitted to Nucl. Phys.
8. T. Udagawa et al.: Phys. Lett. 116B (1982) 311

III.4 Pre-Equilibrium Light Particle Emission in Heavy Ion Induced Reactions

Koji Niita

Department of Physics, Tohoku University

We have presented a model to describe the pre-equilibrium process in heavy-ion induced reactions. It is an extention of the time dependent statistical theory[1], which we have developed to analyze the energy transport in deep inelastic heavy-ion collisions. The basic idea of our model is as follows. We simultaneously take into account two different kinds of processes. The one is the relaxation of the relative motion between the colliding nuclei, and the other is the equilibration process of the excited nuclei. As for the relaxation of the relative motion, we assume the one-body dissipation mechanism similarly to deep inelastic heavy-ion collisions. Namely, we assume that one particle-hole pair is successively created by a collision with the moving wall of the other nucleous. The kinetic energy of the relative motion is thus converted into intrinsic excitation energy. The excitation energy is then spread over many particle-hole pairs through the two-body residual interaction. During the equilibration process, the light particles are emitted by the two-body residual interaction. We neglect the particle emission due to the one-body interaction, and also the multi-particle emission processes.

Based on this idea, we have deribed a coarse grained master equation which determines the time evolution of occupation probability of different intrinsic states. As stressed above, it describes not only the equilibration and the particle emission process as in the usual exciton model, but also the energy supply from the relative motion. The coarse graining cell is specified by the combined index (E,m), E being the excitation energy and m the exciton number. Once the occupation probability is known, the energy spectrum of the emitted particles is calculated in the same way as in the usual exciton model. We consider only nucleon emissions, and neglect the emission of complex particles such as d, t, ^{3}He and α. We have proposed also a simple prescription to calculate the angular distribution of emitted nucleons. We cosider the phase-space only, and introduce the level density which takes into account the total linear momentum of exciton gas.

The study of ^{14}N and ^{16}O induced reactions has shown that our model is

a useful model to elucidate the pre-equilibrium effects in heavy-ion induced reactions.(see Figs.1 and 2) For example, the systematics of the moving source parameters[2] can be understood by the present model by considering the moving exciton gas, i.e. the exciton gas with a finite linear momentum. The test of our model for heavier projectiles is, however, still necessary. Another interesting information can be obtained from the study of the emission rate. It suggests that the light particle emission process can be roughly devided into two stages. The one is the pre-equilibrium stage and the other the equilibrium stage.

References

1) N. Takigawa, K. Niita, Y. Okuhara and S. Yoshida, Nucl. Phys. A371(1981) 130; K. Niita and N. Takigawa, Nucl. Phys. A397(1983)141

2) T. C. Awes, et.al., Phys. Rev. C25(1982)2361

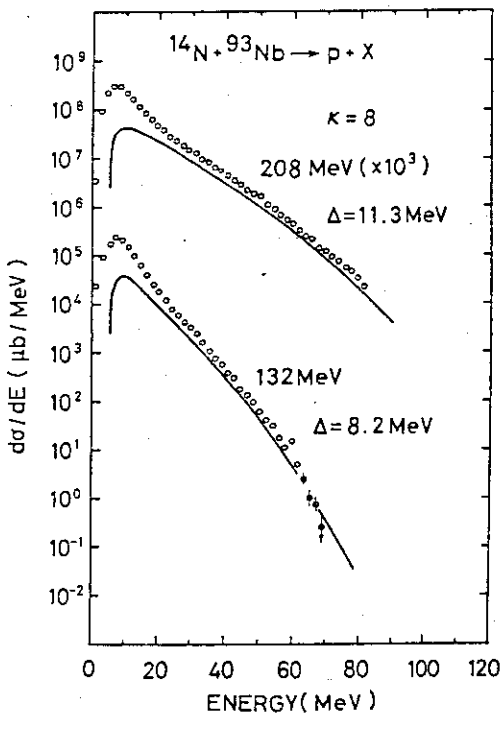

Fig.1

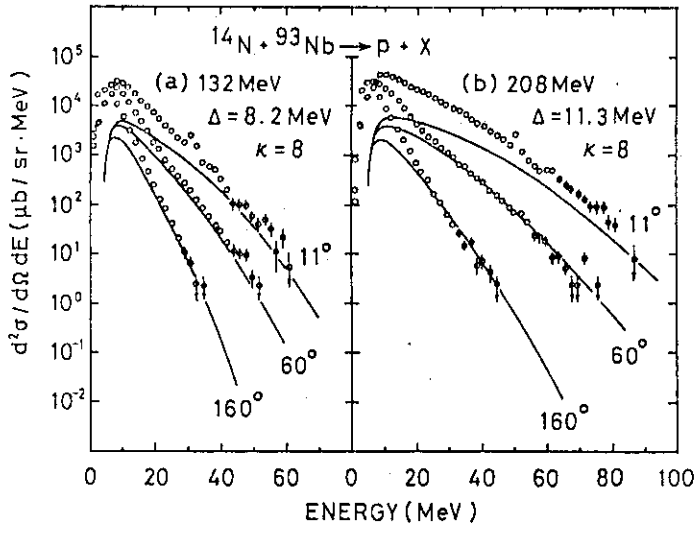

Fig.2

Energy spectra of protons in the $^{93}Nb(^{14}N, p)$ reaction at three different angles for (a) E=132MeV and (b) E=208MeV. The solid lines represent the result of our calculation.

Angle-integrated energy spectra of protons in the $^{93}Nb(^{14}N,p)$ reaction at 208MeV and 132MeV incident energies. The solid lines represent the results of our calculation.

III.5 Evidence for Lower Angular-Momentum Cutoff in Heavy-Ion Fusion Reactions

T. Nomura

Cyclotron Laboratory, The Institute of Physical and Chemical Research

The existence of a lower cutoff in angular momentum that limits the complete fusion cross section in a heavy-ion reaction has been predicted by the time-dependent Hartree-Fock calculation as well as by the semi-classical coupled-channels model calculation. However, no clear experimental evidence for this effect has so far been found. A main difficulty in the experimental search for the effect lies in the fact that the expected magnitude of the effect influences only a small fraction of the reaction cross section. We should therefore look for observables that are sensitive to the exsistence of the low-spin cutoff.

It is well known that high-spin states in a highly excited light nucleus preferentially decay by the evaporation of α-particles, and that low-spin states deexcite mainly by the emission of nucleons. When the evporation residues resulting from the fusion reaction are classified by the number of α-particles evaporated in the decay chain of the compound nucleus, those nuclei produced without the emission of α-particles originate mainly from lowest-spin states in the compound nucleus. The yield of such residual nuclei is therefore considered to have high sensitivity to test the possible existence of the low spin cutoff in fusion reactions.

We have measured cross sections of some residual nuclei produced in the $^{16}O+^{12}C$ and $\alpha+^{24}Mg$ reactions by using the technique of γ-ray spectroscopy. The low spin cutoff is predicted to occur at $E_{c.m.} \simeq 29$ MeV in the $^{16}O+^{12}C$ system, which corresponds to the excitaion energy of about 46 MeV in the compound nucleus, whereas no such effect is expected to exist in the $\alpha+^{24}Mg$ system at the similar excitation energy. An advantage of using the γ-ray spectroscopy is that it is often possible to discriminate low-spin yield from high-spin yield in the same residual nucleus. For instance, the nuclei ^{22}Na and ^{24}Na are known to have 1^+ isomeric states at the first excited levels, while the ground state in ^{24}Na is 4^+, and that for ^{22}Na is 3^+. Therefore, the yields of the $1^+ \rightarrow 4^+$ and $1^+ \rightarrow 3^+$ γ-transitions in ^{24}Na

and ^{22}Na respectively roughly represents low-spin population in these nuclei, which should be sensitive to the existence of the low spin cutoff especially for the case of the $1^+ \rightarrow 4^+$ transition in ^{24}Na because this nucleus is produced without the emission of α-particles.

A part of the present experimental results is shown in fig. 1. It should be noted that the product cross sections in the α+^{24}Mg system have been multiplied by a factor of $(\lambda\!\!\!^{-}_0/\lambda\!\!\!^{-}_\alpha)^2$, where $\lambda\!\!\!^{-}_0$ and $\lambda\!\!\!^{-}_\alpha$ are the relative wavelengths in the ^{16}O- and α-induced reactions, respectively. Therefore, the values of the product cross sections (σ) must be equal to each other, if the residual nuclei are produced from the decay of the compound nuclei having the same distribution of angular momenta. It is clear that the values of σ for the $1^+ \rightarrow 4^+$ transition in ^{24}Na are by 2-4 times smaller in the ^{16}O+^{12}C reaction than those in the α+^{24}Mg system, while the values of σ for the high-spin yield ($4^+ \rightarrow 3^+$ and $5^+ \rightarrow 3^+$ γ rays) in ^{22}Na are nearly the same in both reaction systems. The σ values for the $1^+ \rightarrow 3^+$ transition in ^{22}Na in the ^{16}O+^{12}C system are about 50 % smaller than those in the α+^{24}Mg system. These facts clearly indicate the effect of the low-spin cutoff in the case of the heavy-ion fusion reaction. The product cross sections of other residual nuclei (not shown in the figure) are also consistent with the existence of the effect.

Fig. 1
The measured product cross sections of ^{22}Na and ^{24}Na. The open circles are those in the α+^{24}Mg system, while closed circles indicate those measured in the ^{16}O+^{12}C system.